(12)

ESD-TR-86-241, Volume I

MTR-9622, Volume 1

MONOPOLE ELEMENT AT THE CENTER OF A CIRCULAR GROUNDPLANE OF ARBITRARY RADIUS

VOLUME 1: THEORY AND RESULTS

By

M. M. WEINER
S. P. CRUZE
C. C. LI
W. J. WILSON

MARCH 1986

Prepared for

DEPUTY COMMANDER FOR TACTICAL SYSTEMS
ELECTRONIC SYSTEMS DIVISION
AIR FORCE SYSTEMS COMMAND
UNITED STATES AIR FORCE
Hanscom Air Force Base, Massachusetts

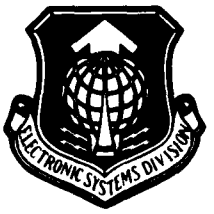

Project No. 6480
Prepared by
THE MITRE CORPORATION
Bedford, Massachusetts
Contract No. F19628-84-C-0001

When U.S. Government drawings, specifications or other data are used for any purpose other than a definitely related government procurement operation, the government thereby incurs no responsibility nor any obligation whatsoever; and the fact that the government may have formulated, furnished, or in any way supplied the said drawings, specifications, or other data is not to be regarded by implication or otherwise as in any manner licensing the holder or any other person or conveying any rights or permission to manufacture, use, or sell any patented invention that may in any way be related thereto.

Do not return this copy. Retain or destroy.

REVIEW AND APPROVAL

This technical report has been reviewed and is approved for publication.

Michael A Villareal

MICHAEL A. VILLAREAL, Capt, USAF
Deputy Program Manager, Engineering
AF Airborne SINCGARS

R Randall Sutter

R. RANDALL SUTTER, Maj, USAF
Program Manager
AF Airborne SINCGARS

FOR THE COMMANDER

Charles P Winters

CHARLES P. WINTERS, Brig Gen, USAF
Deputy Commander for Tactical
Systems, JTIDS and AWACS

UNCLASSIFIED

SECURITY CLASSIFICATION OF THIS PAGE

AD-A166 991

REPORT DOCUMENTATION PAGE

1a. REPORT SECURITY CLASSIFICATION Unclassified	1b. RESTRICTIVE MARKINGS
2a. SECURITY CLASSIFICATION AUTHORITY	3. DISTRIBUTION/AVAILABILITY OF REPORT Approved for public release, distribution unlimited.
2b. DECLASSIFICATION/DOWNGRADING SCHEDULE	
4. PERFORMING ORGANIZATION REPORT NUMBER(S) MTR-9622, V.1 ESD-TR-86-241, V.I	5. MONITORING ORGANIZATION REPORT NUMBER(S)
6a. NAME OF PERFORMING ORGANIZATION The MITRE Corporation 6b. OFFICE SYMBOL (If applicable)	7a. NAME OF MONITORING ORGANIZATION
6c. ADDRESS (City, State and ZIP Code) Burlington Road Bedford, MA 01730	7b. ADDRESS (City, State and ZIP Code)
8a. NAME OF FUNDING/SPONSORING ORGANIZATION Deputy Commander for (cont.) 8b. OFFICE SYMBOL (If applicable) TCVS	9. PROCUREMENT INSTRUMENT IDENTIFICATION NUMBER F19628-84-C-0001
8c. ADDRESS (City, State and ZIP Code) Electronic Systems Division, AFSC Hanscom AFB, MA 01731-5000	10. SOURCE OF FUNDING NOS. PROGRAM ELEMENT NO. / PROJECT NO. 6480 / TASK NO. / WORK UNIT NO.
11. TITLE (Include Security Classification) MONOPOLE ELEMENT AT THE CENTER (continued)	
12. PERSONAL AUTHOR(S) Weiner, M.M.; Cruze, S.P.; Li, C.C.; Wilson, W.J.	
13a. TYPE OF REPORT Final 13b. TIME COVERED FROM _____ TO _____	14. DATE OF REPORT (Yr., Mo., Day) 1986 March 31 15. PAGE COUNT 136
16. SUPPLEMENTARY NOTATION	
17. COSATI CODES FIELD / GROUP / SUB. GR.	18. SUBJECT TERMS (Continue on reverse if necessary and identify by block number) Circular Groundplane Geometric Theory of Diffraction Diffraction (Awadalla) Directive Gain (continued)

19. ABSTRACT (Continue on reverse if necessary and identify by block number)

The input impedance, field strengths, and directive gain of a monopole element at the center of a circular groundplane in free space are determined for arbitrary groundplane radius, element length, and element radius. Numerical results are obtained by using various models and are compared with measurements. Particular emphasis is given to groundplane radii that are small or comparable to a wavelength.

The models include the induced EMF method, integral equation method, method of moments, oblate spheroidal wave functions, variational method, the method of moments combined with the geometric theory of diffraction, and the method of images.

This report is in two volumes. Volume 1 contains the theory and results. Volume 2 contains the computer printouts of directive gain and the listings of the computer programs for the various models.

20. DISTRIBUTION/AVAILABILITY OF ABSTRACT UNCLASSIFIED/UNLIMITED ☐ SAME AS RPT. ☒ DTIC USERS ☐	21. ABSTRACT SECURITY CLASSIFICATION Unclassified
22a. NAME OF RESPONSIBLE INDIVIDUAL Diana F. Arimento	22b TELEPHONE NUMBER (Include Area Code) (617)271-7454 22c. OFFICE SYMBOL Mail Stop D230

DD FORM 1473, 83 APR EDITION OF 1 JAN 73 IS OBSOLETE.

UNCLASSIFIED

SECURITY CLASSIFICATION OF THIS PAGE

8a. Tactical Systems.

11. OF A CIRCULAR GROUNDPLANE OF ARBITRARY RADIUS. VOLUME: THEORY AND RESULTS.

18. Groundplane of Zero Extent
Induced EMF Method (Brillouin)
Input Impedance
Integral Equation Method (Bardeen)
Method of Moments (Richmond)
Method of Images
Monopole Antenna
Monopole Element
Oblate Spheroidal Wave Functions (Leitner and Spence)
Radiation Pattern
Radiation Resistance
Scalar Diffraction Theory (Tang)

PREFACE

The Air Force SINCGARS VHF-FM radio is a frequency-hopping anti-jam radio which utilizes an electrically short antenna to minimize aerodynamic drag on airborne platforms. The development of optimally efficient, electronically tuneable antennas for this radio is of interest. Although the antenna groundplane is platform-dependent, it is usually small compared to an rf wavelength. A circular groundplane provides a standardized groundplane geometry with which to model and evaluate candidate antennas. Accordingly, a VHF antenna range with an 8 ft. diameter circular groundplane has been constructed at The MITRE Corporation to evaluate candidate antennas.

The electrical properties of a monopole element at the center of a circular groundplane of finite radius are of interest to this program for (a) qualifying the antenna range; (b) establishing antenna standards with which to measure test antennas; and (c) modeling candidate antennas. Our survey of the literature revealed that although this antenna has the simplest geometry of any monopole antenna, its properties are neither well understood nor standardized, particularly for groundplane radii which are small or comparable to a wavelength. The present paper attempts to address this deficiency.

FOREWORD

M. Weiner wrote Sections 1 - 5. S. Cruze contributed to Section 3.5 and wrote program MONOPL in Appendix B3. C. Li contributed to Section 3.4; edited program RICHMD1 in Appendix B2 and program AWADALLA in Appendix B5; and wrote program BARDEEN in Appendix B1, program RICHMD2 in Appendix B2, and program MONOSTOR in Appendix B4. W. Wilson contributed to Sections 2.3 and 3.3. J. E. Kriegel of The MITRE Corporation derived the correct form of the continued fractions given in Eqs. 3.5-4 and 3.5-5 and contributed to the evaluation of the limits in Eqs. 3.3-22--3.3-24. W. C. Corrieri skillfully performed the measurements discussed in Section 5. K. Pamidi contributed to the development of Eq. 3.3-16.

The authors are grateful to Prof. Alfred Leitner of Rensselaer Polytechnic Institute for helpful conversations regarding his method of oblate spheroidal wave functions; Prof. Jack Richmond of Ohio State University for helpful conversations and a magnetic tape of his method of moments program; and Prof. Kamal Awadalla of Menoufia University (Egypt) for helpful correspondence including a listing of his program for the method of moments combined with the geometric theory of diffraction.

After the authors had obtained results using the integral equation method and the method of oblate spheroidal functions, it was possible to confirm the correctness of Prof. Richmond's method of moment results which were subsequently published in the open literature (see Ref. [2]).

This document has been prepared by The MITRE Corporation under Project No. 6480, Contract F19628-84-C-0001. The contract is sponsored by the Electronic Systems Division, Air Force Systems Command, Hanscom Air Force Base, Massachusetts 01731.

TABLE OF CONTENTS

TABLE OF CONTENTS (CONT.)

LIST OF ILLUSTRATIONS

LIST OF ILLUSTRATIONS (CONT.)

LIST OF ILLUSTRATIONS (CONCLUDED)

LIST OF TABLES

SECTION 1

INTRODUCTION

Monopole antennas are commonly employed in airborne and ground-based communication systems at a wide range of frequencies. The electrical properties of such antennas are dependent upon the geometry of both the monopole element and the groundplane. Typically, the monopole element may be electrically-short (length much less than a quarterwave) or near-resonant (length approximately a quarterwave) and may be thin (length to radius ratio much greater than 10^4) or relatively thick (length to radius ratio of 10^1 to 10^4). In addition, the groundplane dimensions may vary from a fraction of a wavelength to many wavelengths. Therefore it is desirable to know how the input impedance and radiation pattern of the antenna change as the dimensions of the monopole element and the groundplane vary. The directional gain on or near the radio horizon (the groundplane is assumed to be horizontal) is of particular interest since the maximum operational range of a communications system often depends upon the directivity on the radio horizon.

This study is restricted to a monopole geometry consisting of a vertical cylindrical element at the center of a perfectly conducting, infinitely thin, circular groundplane in free space. This geometry is of interest because its radiation pattern is uniform in the azimuthal direction and because its electrical characteristics are a function of primarily only three parameters, namely, the element length, the element radius, and the groundplane radius, when each is normalized to the excitation wavelength. For these reasons this geometry is conducive to analysis, experimental verification, and standardization.

A typical feed for the monopole antenna is a coaxial line whose inner conductor is connected through a hole in the groundplane to the vertical monopole element and whose outer conductor is connected by means of a flange to the groundplane. Typically, the inner conductor diameter is equal to the monopole element diameter and the outer conductor diameter is equal to the groundplane hole diameter. Unless stated otherwise, such a feed will be assumed in this study. The ratio of the coaxial line's outer to inner conductor diameters affects the antenna's input impedance, but only significantly for a relatively thick monopole element on a very small groundplane.

For the idealized case of a groundplane of infinite extent and of infinite conductivity, the monopole antenna may be modeled by the method of images as a dipole with one-half the input impedance and double the peak directivity of the dipole. The infinite groundplane prevents monopole radiation into the hemisphere below the groundplane but allows a radiation pattern identical to that of the dipole in the upper hemisphere. However, for a monopole element mounted on a groundplane of finite extent, the outer edge of the groundplane diffracts incident radiation in all directions and consequently modifies the currents on the groundplane and vertical element from those of an infinite groundplane. At the outer edge of the groundplane, the currents on the top and bottom faces of the groundplane are equal in magnitude but opposite in direction because the net current must be zero at the edge. Outer edge diffraction becomes increasingly significant with decreasing size of the groundplane because of increasing magnitude of the currents on the groundplane faces at the outer edge. Edge diffraction can alter the input impedance by more than 100% and directive gain in the plane of the groundplane by more than 6 dB from the values for a groundplane of infinite extent.

Theoretical models exist for predicting the effects of diffraction by the outer edge of the groundplane. The existing models may be classified into two categories distinguished by whether the current distribution on the monopole element is initially known or is unknown.

When the monopole element is very thin and not too long, its current distribution is approximately sinusoidal and independent of the radius of the groundplane. Consequently, the element's current distribution can be initially specified and only the groundplane's current distribution need be determined. For this category of monopoles, the theoretical models reported in the literature consist essentially of Bardeen's integral equation method for the groundplane radius small compared to a wavelength[1], Richmond's method of moments (groundplane only) for the groundplane radius not too large compared to a wavelength[2], Leitner and Spence's method of oblate spheroidal wave functions for the groundplane radius comparable to a wavelength[3]-[5], Tang's scalar theory of diffraction[6] and the geometric theory of diffraction (GTD) for the groundplane radius large compared to a wavelength, and Storer's variational method for the groundplane radius very large compared to a wavelength[7],[8].

When the monopole element is relatively thick, its current distribution is no longer sinusoidal and consequently the current distribution on both the monopole element and the groundplane need to be determined as a function of the groundplane radius. For this category of monopoles, the theoretical models reported in the literature consist essentially of Richmond's method of moments for the groundplane radius not too large compared to a wavelength[2] and Awadalla-Maclean's method of moments (monopole element only) combined with the geometric theory of diffraction for the groundplane radius large or comparable to a wavelength[9],[10]. Thiele and Newhouse have also reported a model which combines the method of moments with the geometric theory of diffraction but their computer program is unavailable[11].

Each of the existing models is valid for different and sometimes overlapping sets of limited values of groundplane radii. Some of the models require extensive numerical computation. For these reasons, the collection of models taken as a whole has several deficiencies. In the open literature, results for input impedance and directive gain have never been assembled as a continuous function of groundplane radius for the entire range of values from zero to infinite wavenumbers. In regions where models overlap, it is sometimes unclear which models are more accurate. In some models, numerical results have been reported for only a few values of groundplane radius. In one model (Bardeen's integral equation) the base of the monopole element has not been allowed to be in the same plane as the groundplane which is the present case of interest. Computer programs are not available for some of the older models because the models were developed before the advent of computers. One of the most versatile of the models (Richmond's method of moments) gives only the input impedance but not the radiation pattern. In one model (Leitner and Spence's oblate spheroidal wave functions), one of the published algorithms for computing the eigenvalues is incorrect. Finally, extensive numerical results for small groundplanes and for resonant monopoles with finite groundplanes are not found in the open literature.

This paper attempts to correct these deficiencies. Computer programs and numerical results are presented for all of the models. The induced emf method is utilized to determine the input impedance of a thin idealized monopole element in the absence of a groundplane. In Bardeen's integral equation method, the excitation function for the groundplane currents is extended to include the singularity which occurs when the base of the monopole element is in the same plane as the groundplane. Richmond's method of moments is extended to give the far-field radiation pattern. In Leitner and Spence's method of oblate spheroidal wave functions, the published continued-fraction algorithm for computing the eigenvalues is

corrected. Numerical results for input impedance and directive gain are presented as a continuous function of groundplane radius for arbitrary radius. Numerical results of various models are compared and the suspected best available results are identified. Extensive numerical results are given for small groundplanes and for resonant monopoles on finite groundplanes. New experimental data is presented and compared with numerical results.

Circuit representations of the monopole antenna are developed in Section 2. Theoretical models and numerical results are presented in Section 3 for the case in which the current distribution on the monopole element is initially known. In Section 4, theoretical models and numerical results are presented for the case in which the current distribution on both the monopole element and groundplane are initially unknown. The theoretical models are compared with experimental data in Section 5. Computer printouts of directive gain and the far-field elevation pattern are given in Appendix A. Computer programs of the theoretical models are given in Appendix B.

SECTION 2

CIRCUIT REPRESENTATION

2.1 Geometry and Coordinate Systems

Consider a monopole element of length h and radius b which is located in free space at the center of an infinitely thin circular groundplane of radius a and of infinite conductivity (see figure 1). The groundplane radius, when expressed in wavenumbers, is given by

$$\epsilon \equiv ka \tag{2.1-1}$$

where

$k = 2\pi/\lambda$ = wavenumber (m^{-1})

λ = excitation wavelength (m)

The monopole element and groundplane have current distributions in real time given by

$$I(z,t) = \mathrm{Re}[I(z)e^{j\omega t}],\ I(\rho,t) = \mathrm{Re}[I(\rho)e^{j\omega t}] \tag{2.1-2}$$

where

ω = radian frequency of the excitation = $2\pi c/\lambda$ (rad/sec)

c = wave velocity in free space = 2.9979×10^8 m/s

$I(z), I(\rho)$ = element and groundplane current amplitude distributions, respectively (amp)

A field point P(r, θ, ϕ), expressed in spherical coordinates, is shown in figure 1. The field is uniform in the azimuthal direction ϕ. The relationships between spherical, cylindrical , and oblate spheroidal coordinate systems are shown in table 1. In the far-field, the elevation angle θ is related to the oblate spheriodal angular coordinate η by $\eta \longrightarrow \cos\theta$ as the spheriodal radial coordinate $\xi \longrightarrow \infty$.

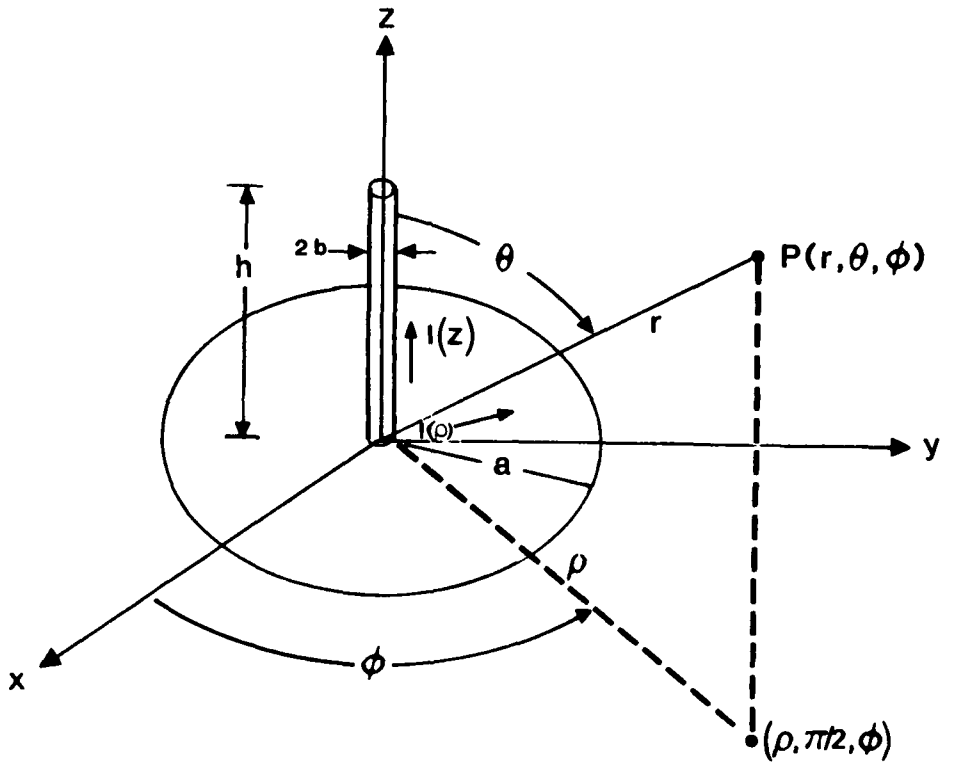

Figure 1. Monopole Element at the Center of a Circular Groundplane

TABLE 1

Spherical, Cylindrical, and Oblate Spheroidal Coordinates

SPHERICAL (r,θ,ϕ)		CYLINDRICAL (ρ, z, ϕ)	OBLATE SPHEROIDAL (ξ,η,ϕ)
radius	r	$\rho = r \sin\theta$	$\rho = a[(1-\eta^2)(1+\xi^2)]^{1/2}$
elevation	θ	$z = r \cos\theta$	$z = a\,\eta\,\xi$
azimuth	ϕ	ϕ	ϕ

Note 1: In Table 1, the notation ξ, η is that of Leitner and Spence (L+S), Franklin Institute Journal, Vol. 249, No. 4, pp. 299-321, April 1950. This notation is related to that of Abramowitz and Stegun (A+S), "Handbook of Mathematical Functions", National Bureau of Standards, Applied Mathematical Series, No. 55, p. 752, June 1964 by

$$\xi_{L+S} = (\xi^2_{A+S} - 1)^{1/2}$$

$$\eta_{L+S} = (1 - \eta^2_{A+S})^{1/2}$$

Note 2: The cylindrical coordinates (ρ, z, ϕ) are related to the rectangular coordinates (x, y, z) by

$$x = \rho \cos\phi$$
$$y = \rho \sin\phi$$
$$z = z$$

2.2 Directive Gain and Input Impedance

At a far-field observation point P(r, θ, ϕ), the numeric directive gain $d(\theta,\phi)$ of the antenna is defined as the ratio of its radiated power density $s(\theta,\phi)$ to its radiated power density averaged over all directions. The radiated power density averaged over all directions is equivalent to the power density radiated by a hypothetical "isotropic" antenna. Accordingly, the directive gain $d(\theta,\phi)$ expressed in spherical coordinates with the origin at the antenna, is given by

$$d(\theta,\phi) = \frac{s(\theta,\phi)}{(1/4\pi)\int_0^{2\pi}\int_0^{\pi} s(\theta,\phi)\,\sin\theta\,d\theta\,d\phi} \qquad (2.2\text{-}3)$$

For antenna patterns which are uniform in the azimuthal direction, such as for the antenna geometry of figure 1, Eq. (2.2-3) reduces to

$$d(\theta) = \frac{2\,s(\theta)}{\int_0^{\pi} s(\theta)\,\sin\theta\,d\theta} = \frac{2\,s'(\eta)}{\int_{-1}^{1} s'(\eta)\,d\eta} = d'(\eta) \qquad (2.2\text{-}4)$$

where

$s(\theta) = (1/2)\sqrt{\mu_o/\epsilon_o}\,|H_\phi|^2 = (1/2\sqrt{\epsilon_o/\mu_o}\,|E_\theta|^2$

H_ϕ, E_θ = far-field magnetic and electric field intensities, respectively

$s'(\eta)$, $d'(\eta)$ = radiation power density and directive gain, respectively, in oblate spheroidal coordinates

$\sqrt{\mu_o/\epsilon_o}$ = wave impedance in free space

The numeric directive gain $d(\theta,\phi)$ is related to the directive gain $D(\theta,\phi)$ expressed in dBi by

$$D(\theta,\phi) = 10\,\log_{10}\,d(\theta,\phi)\ (\text{dBi}) \qquad (2.2\text{-}5)$$

The total time-averaged radiated power P_{total} of the antenna is given by

$$P_{total} = \int_0^{2\pi} \int_0^{\pi} s(\theta,\phi)\, r^2 \sin\theta \, d\theta \, d\phi$$

$$= 2\pi r^2 \int_0^{\pi} s(\theta) \sin\theta \, d\theta = 2\pi r^2 \int_{-1}^{1} s'(\eta) \, d\eta \qquad (2.2\text{-}6)$$

The antenna radiation resistance R, referred to the complex amplitude I(z=0) of the antenna base current, is defined by

$$R \equiv 2P_{total}/|I(z=0)|^2 \qquad (2.2\text{-}7)$$

Substituting Eqs. (2.2-6) and (2.2-7) into Eq. (2.2-4),

$$d(\theta) = s(\theta)\, 8\pi r^2/[R|I(z=0)|^2] = s'(\eta)\, 8\pi r^2/[R|I(z=0)|^2] = d'(\eta) \qquad (2.2\text{-}8)$$

The antenna input impedance, Z_{in}, is given by

$$Z_{in} = V(z=0)/I(z=0) = R_{in} + j\, X_{in} \qquad (2.2\text{-}9)$$

where

$V(z=0)$ = complex amplitude of the excitation voltage across the aperture of the coaxial line feed to the antenna (volts)

R_{in} = input resistance (ohms)

X_{in} = input reactance (ohms)

The input resistance R_{in} is related to the radiation resistance R by

$$R_{in} = R + R_{ohmic} \qquad (2.2\text{-}10)$$

where R_{ohmic} is the ohmic loss resistance of the antenna for finite conductivity of either the monopole element or the groundplane. In the present paper, $R_{ohmic} = 0$ because the monopole element and groundplane are assumed to be of infinite conductivity. Accordingly,

$$R_{in} = R \quad , \; R_{ohmic} = 0 \qquad (2.2\text{-}11)$$

Equation (2.2-11) is a statement that the antenna is assumed to have an efficiency of unity.

2.3 Relationship Between Radiation Resistance and Directive Gain on the Horizon

For a vertical monopole element with a finite groundplane, the far-field radiated power density on the radio horizon, $s(\theta = \pi/2)$, is determined only by the current distribution on the monopole element (and not the groundplane current) since only the vertical monopole element has a component of electron acceleration which is normal to the radio horizon. (This statement is not true for a groundplane of infinite extent since then a far-field point on the radio horizon is on the groundplane.) Identical monopole elements with identical current distributions, but mounted on groundplanes of different finite radii, will consequently have identical far-field radiated power densities on the radio horizon. Accordingly,

$$s_{\epsilon}(\theta = \pi/2) = s_{0}(\theta = \pi/2); \text{ identical monopole element, identical element current distribution, groundplane of finite extent} \qquad (2.3\text{-}1)$$

where the subscript ϵ denotes the radius in wavenumbers of the groundplane of arbitrary but finite extent ($\epsilon < \infty$) and the subscript 0 denotes a groundplane of zero extent ($\epsilon = 0$).

If Eq. (2.2-8) is substituted into Eq. (2.3-1) and the quantity $s(\theta = \pi/2)|I(z=0)|^2/8\pi r^2$ is computed, one obtains the following relationship between radiation resistance R and numeric directive gain on the horizon $d(\theta = \pi/2)$:

$$d_{\epsilon}(\theta = \pi/2)\, R_{\epsilon} = d_{0}(\theta = \pi/2)\, R_{0} = \text{constant}; \text{ identical monopole elements, identical element current distributions, groundplane of finite extent} \qquad (2.3\text{-}2)$$

In Eqs. (2.3-1) and (2.3-2) the condition of identical element current distributions for groundplanes of different radii is generally not satisfied by monopole antennas. The element current distribution I(z) is generally dependent upon the groundplane current $I(\rho)$ which in turn is a function of the groundplane radius. However, for monopole elements which are sufficiently thin electrically and not too long, the element current distribution I(z) is approximately sinusoidal and independent of the groundplane current $I(\rho)$ (see Section 3.1). Expressions for $d_o(\theta = \pi/2)$ and R_o, for elements with a sinusoidal current distribution, are determined in Section 3.2. Substitution of those expressions into Eq. (2.3-2), for the case of an infinitely thin monopole element (b=0), yields

$$d(\theta = \pi/2)\, R = (\eta/4\pi)\, [1 - \cos(kh)]^2/\sin^2(kh); \quad b=0,$$

sinusoidal element current distribution, groundplanes of finite extent (2.3-3)

where

η = wave impedance of free space = 376.73 ohms

h = length of the monopole element

The condition b=0 may be removed from Eq. (2.3-3) without substantially altering the result since the radiation pattern and radiation resistance of electrically thin elements, which are not too long, are weakly dependent upon the element radius (see Section 3.2).

2.4 Characterization of Currents

The characterization of the currents on the monopole element, groundplane, and coaxial line feed is illustrated in figure 2. The physical realization, circuit representation, and two circuit idealizations of the currents are shown in figures 2(a), 2(b), 2(c), and 2(d), respectively. In Fig. 2(b), the coaxial line excitation of Fig. 2(a) is replaced by equivalent electric and magnetic currents on a conductor completely enclosing the coaxial line. In Fig. 2(c), the normalized ferrite attenuation distance $h_1/\lambda \ll 1$ is idealized to be zero. In Fig. 2(d), the magnetic frill M_ϕ is assumed to be negligible.

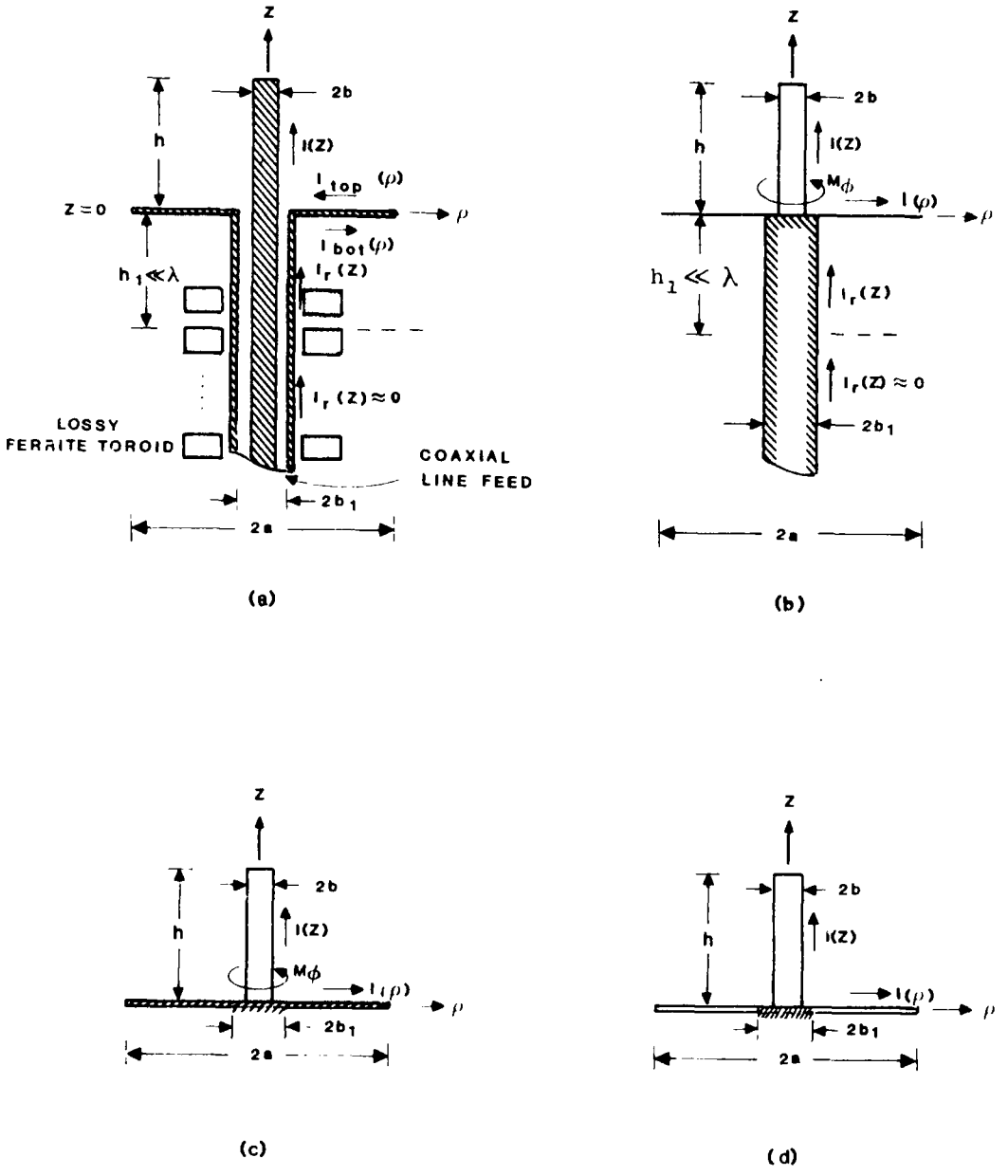

Figure 2. Characterization of Currents on Monopole Element, Groundplane and Coaxial Line Feed
(a) Physical realization
(b) Circuit representation
(c) Idealization of circuit ($h_1/\lambda=0$)
(d) Idealization of circuit ($h_1/\lambda=0$, $kb_1 \ll 1$, I(z) or $I(\rho)$ is initially known)

The currents of interest are the element current I(z) (positive in the + z direction), the return current $I_r(z)$ on the outside of the coaxial line outer conductor (positive in the + z direction), the current $I_{bot}(\rho)$ on the bottom face of the groundplane (positive in the + ρ direction, and the current $I_{top}(\rho)$ on the top face of the groundplane (positive in the negative ρ direction). A net groundplane current $I(\rho)$ (positive in the positive ρ direction) is defined as

$$I(\rho) = I_{bot}(\rho) - I_{top}(\rho) \tag{2.4-1}$$

In the physical realization of the currents [figure 2(a)], lossy ferrite toriods are mounted along the outside of the coaxial line outer conductor. Such a procedure is commonly utilized on antenna ranges to reduce the radiation or pickup of unwanted signals from currents induced on the outside of the transmitter or receiver coaxial cables. For a sufficient number of ferrite toroids near the termination end of the coaxial line, the return current $I_r(z)$ is approximately zero at distance greater than the 1/e attenuation distance h_1 from the termination end of the line. In this paper, the ferrite toroids are assumed to be sufficiently lossy so that

$$h_1 \ll \lambda \tag{2.4-2}$$

where λ is the excitation wavelength.

The radii of the outer and inner conductors of the coaxial line are b_1 and b, respectively, where b is also the radius of the monopole element. The wall thickness of the coaxial line outer conductor is assumed to be much less than its diameter. Consequently, the return current $I_r(z)$ occurs at the radial coordinate $\rho \approx b_1$.

The constraints on the various currents are:

element	$I(z=h) = 0$	(2.4-3)
groundplane	$I(\rho=a) = 0$	(2.4-4)
coaxial line	$I_r(z) \approx 0, \quad -\infty < z < -h_1$	(2.4-5)
element-groundplane	$I(z=0) = -I(\rho=b)$	(2.4-6)
groundplane-coaxial line	$I_{bot}(\rho=b_1) = I_r(z=0)$	(2.4-7)

The element and groundplane constraints are a consequence of an open circuit at the end of the element and the groundplane. The coaxial line constraint is a consequence of the lossy ferrites. The element-groundplane constraint is a consequence of conservation of charge (Kirchhoff's current law) at a node. The groundplane-coaxial line constraint is a consequence of conservation of charge along a conductor.

By the use of the equivalence principle[12] the coaxial line feed excitation may be replaced by equivalent tangential field excitations defined along a surface completely enclosing the coaxial line. At field points external to this surface the equivalent field excitations will give the same field as the original source excitation. In the circuit representation of the monopole antenna currents [figure 2(b)], the coaxial aperture excitation is replaced by an equivalent surface magnetic current density (magnetic frill) M_ϕ which sits on top of a thick groundplane of radius b_1. The magnetic frill M_ϕ is defined to be positive in the positive azimuthal direction and is given by

$$M_\phi = \begin{cases} -V(0)/[\rho \ln(b_1/b)], & b \leq \rho \leq b_1 \\ 0, & \rho < b, \quad \rho > b_1 \end{cases} \qquad (2.4\text{-}8)$$

Eq. (2.4-8) is derived as follows. The radial field E of the coaxial line aperture, assuming a TEM mode excitation, is given by

$$E_\rho = \begin{cases} V(0)/\rho \ln(b_1/b), & b \leq \rho \leq b_1 \\ 0, & \rho < b \end{cases} \tag{2.4-9}$$

where V(0) is the positive voltage at z=0 across the aperture with the coaxial outer conductor at zero potential. By the equivalence principle[12], an aperture field may be replaced by a magnetic frill $\vec{M}$ which sits on top of a groundplane congruent with the aperture surface and which is defined as

$$\vec{M} = \vec{E}_{\text{tangential}} \times \vec{n} \tag{2.4-10}$$

where $\vec{n}$ is the outward normal to the aperture surface and $\vec{E}_{\text{tangential}}$ is the tangential field at the aperture surface. Substituting Eq. (2.4-9) into Eq. (2.4-10),

$$\vec{M} = (\hat{u}_\rho E_\rho) \times \hat{u}_z = - E_\rho \hat{u}_\phi = \hat{u}_\phi M_\phi \tag{2.4-11}$$

where M_ϕ is given by Eq. (2.4-8). Eq. (2.4-8) agrees with the result obtained by Richmond[2].

In the circuit representation of figure 2(b), the net groundplane current $I(\rho)$ is the same as defined by Eq. (2.4-1) with the additional current constraint

$$I_{bot}(\rho) = 0, \quad 0 \leq \rho < b_1 \tag{2.4-12}$$

If the circuit representation of the monopole antenna in figure 2 is now idealized by setting the ferrite 1/e attenuation distance $h_1/\lambda = 0$, then

$$I_r(z) \approx 0 \text{ for } z < 0, \quad h_1/\lambda = 0 \tag{2.4-13}$$

Consequently, the coaxial line outer conductor may be removed from the circuit as shown in figure 2(c). The groundplane - coaxial line current constraint of Eq. (2.3-7) is not disturbed by such an idealization. Since it has already been assumed that $h_1 \ll \lambda$, the idealization $h_1 = 0$ does not appreciably alter either the radiation pattern or the input impedance of the monopole antenna provided that the monopole length $h \gg h_1$. Finite currents, on an aperture which is small compared to the excitation wavelength, contribute little to the far-field and input impedance (compare with the results for an electrically-small dipole). Experimental radiation patterns and measurements of input impedance (see Section 5) confirm that the use of lossy ferrite toroids along the coaxial line outer conductor yields results which are in close agreement with theoretical results for the circuit idealization condition of Eq. (2.4-13) -- even for electrically-small groundplanes.

In the idealization of the monopole antenna circuit, the magnetic frill M_ϕ may be removed [figure 2(d)] without appreciably altering the radiation pattern or input impedance, provided that

$$\left.\begin{array}{l} kb_1 \ll 1 \\ I(z) \text{ or } I(\rho) \text{ is initially known} \end{array}\right\} \text{conditions for neglecting magnetic frill} \tag{2.4-14}$$

The condition $kb_1 << 1$ corresponds to the condition for TEM mode excitation of the coaxial line and for negligible power being radiated from the coaxial line aperture. If either $I(z)$ or $I(\rho)$ is initially known then the one which is not known may be determined from the other without requiring a knowledge of the original coaxial line excitation or its equivalent -- provided that the field radiated by the known current distribution is the predominant field incident on the conductor whose current distribution is unknown. When neither $I(z)$ nor $I(\rho)$ is known, then the original source excitation or its equivalent (in this case, the magnetic frill M_ϕ) must be specified to determined the unknown radiated fields.

SECTION 3

MODELS IN WHICH THE CURRENT DISTRIBUTION ON THE MONOPOLE ELEMENT IS INITIALLY KNOWN

3.1 Boundary Conditions

The current amplitudes, $I(z)$ and $I(\rho)$, on the monopole element and groundplane, respectively, are generally complex and initially unknown quantities (see figure 1). Consider now the case where the current distribution on the monopole element is assumed to be sinusoidal. For such a case and for the waveform dependence given in Eq. (2.1-2),

$$I(z) = \frac{I(0)}{\sin(kh)} \sin[k(h-z)], \quad 0 \leq z \leq h \tag{3.1-1}$$

where

h = monopole length (m)

$k = 2\pi / \lambda$ = wavenumber (m^{-1})

$I(0)$ = current amplitude of the monopole base current at z=0 (amp)

From Eq. (3.1-1)

$$\arg I(z) = \text{constant}, \quad 0 \leq z \leq h \tag{3.1-2}$$

Although a sinusoidal distribution of current is not possible even for an infinitely thin antenna, Eq. (3.1-1) is most likely a fair approximation to the current if the monopole element is sufficiently thin electrically

and not too long.[13] For a center-fed dipole of radius b and total length 2h, Elliot[14] gives examples where the current distribution is approximately sinusoidal and is of approximately constant argument for $b/\lambda = 1.0 \times 10^{-4}$ and $h/\lambda = 0.125, 0.25$. However for $b/\lambda = 1.0 \times 10^{-4}$ and $h/\lambda = 0.375, 0.5$ Elliot demonstrates that the current distribution is no longer sinusoidal near the center of the dipole nor is arg z approximately constant. Balanis[15] shows that for $b/\lambda = 2.0 \times 10^{-4}$ and $h/\lambda = 0.25, 0.5$ the current distribution is not sinusoidal near the center of the dipole. Elliot and Balanis also demonstrate that for $b/\lambda = 1.0 \times 10^{-2}$ and $h/\lambda = 0.125, 0.25, 0.375, 0.50$ the current distribution is neither sinusoidal nor of constant phase and that the deviations from Eqs. (3.1-1) and (3.1-2) increase with increasing values of h/λ and b/λ. On the basis of the above results, it appears that Eqs. (3.1-1) and (3.1-2) are approximately valid for the conditions

$$b/\lambda < 10^{-4}, \; h/\lambda \lesssim 0.25 \tag{3.1-3}$$

In addition to the constraint on I(z) given by Eq. (3.1-1), assume that the return current $I_r(z)$ on the outside of the coaxial line outer conductor (see figure 2) is given by

$$I_r(z) \approx 0 \;, \; z < 0 \tag{3.1-4}$$

The constraint of Eq. (3.1-4) corresponds to the idealized condition that the ferrite toroids have a 1/e current attenuation distance h_1 given by

$$h_1/\lambda = 0 \tag{3.1-5}$$

It should be noted that Eqs. (3.1-4) and (3.1-5) do not alter the constraint $I_r(z=0) = I_{bot}(\rho = b_1)$ given by Eq. (2.3-7) nor do they impose any constraints on $I_{bot}(\rho = b_1)$ where $I_{bot}(\rho = b_1)$ is the current on the bottom of the groundplane at a radius equal to that of the outer conductor.

Combining the current constraints given by Eqs. (3.1-1) and (3.1-4) with those given by Eqs. (2.4-3) - (2.4-7) and Eq. (2.4-12), the current constraints on the monopole antenna are given by

element	$I(z) = [I(0)/\sin(kh)]\sin[k(h-z)],\ 0 \leq z \leq h$	(3.1-6)
groundplane	$I(\rho=a) = 0$	(3.1-7)
	$I_{bot}(\rho) = 0,\ 0 \leq \rho \leq b_1$	(3.1-8)
coaxial line	$I_r(z) \approx 0,\ z < 0$	(3.1-9)
element-groundplane	$I(z=0) = -I(\rho=b)$	(3.1-10)
groundplane-coaxial line	$I_{bot}(\rho) = I_r(z=0)$	(3.1-11)

In Section 3, it will be assumed that all models satisfy the current constraints given by Eqs. (3.1-6) - (3.1-11). The results are expected to be approximately correct if the monopole element is electrically sufficiently thin and not too long [Conditions (3.1-3)] and if the ferrite toroids are sufficiently lossy [$h_1/\lambda \ll 1$, idealized by Condition (3.1-5)]. For these conditions, the circuit representation of the monopole antenna is shown in figure 2(d).

For the current constraints of Eqs. (3.1-6)-(3.1-11), the total magnetic and electric field intensities $\vec{H}^{(total)}, \vec{E}^{(total)}$ at an arbitrary field point P(x,y,z) external to the element excitation source points are simply the vector sum of the fields resulting from the element current and the current induced on the groundplane by the fields incident from the element.

Accordingly,

$$\left.\begin{aligned} \vec{H}^{(total)} &= \vec{H}^{(e)} + \vec{H}^{(g)}[\vec{E}^{(e)}, \vec{H}^{(e)}] \\ \vec{E}^{(total)} &= \vec{E}^{(e)} + \vec{E}^{(g)}[\vec{E}^{(e)}, \vec{H}^{(e)}] \end{aligned}\right\} \text{, current constraints of Eqs. (3.1-6)-(3.1-11)} \qquad (3.1\text{-}12)$$

where

$\vec{H}^{(e)}, \vec{E}^{(e)}$ = magnetic, electric field intensities, respectively, generated by the element current

$\vec{H}^{(g)}, \vec{E}^{(g)}$ = magnetic, electric field intensities, respectively, generated by the groundplane current induced by the element incident fields.

The element fields $\vec{H}^{(e)}, \vec{E}^{(e)}$ are determined in Section 3.2. The groundplane fields $\vec{H}^{(g)}, \vec{E}^{(g)}$ are determined in Sections 3.3 - 3.8 for groundplane radii of various extents.

3.2 Induced EMF Method, Groundplane of Zero Extent

Concept of a groundplane of zero extent

Consider a monopole antenna excited by a coaxial line whose outer conductor of radius b_1 is terminated by free space rather than by a groundplane [figure 3(a)]. The groundplane for such an antenna is denoted as being of "zero extent". As was shown in Section 2.4, the coaxial line excitation may be replaced by an equivalent magnetic current (frill) M_ϕ sitting on top of a thick groundplane of radius $\rho = b_1$ [figure 3(b)]. For sufficiently lossy ferrite toroids along the outside of the coaxial line, the current on the exterior of the coaxial line outer conductor may be neglected [figure 3(c)]. The magnetic frill may be removed from the circuit without appreciably affecting the results since $kb_1 << 1$ for the assumed sinusoidal current distribution on the monopole element [see Eq. (3.1-3) and the discussion concerning the circuit idealization of figure 2(d)]. Finally, the groundplane of radius b_1 may be removed from the circuit without appreciably affecting the results since a finite current on an electrically-small conductor does not radiate appreciable power compared to the power radiated by a monopole element of length $h >> b_1$. The circuit idealization of a monopole antenna with a groundplane of zero extent is therefore an electrically thin monopole element with no groundplane [figure 3(d)].

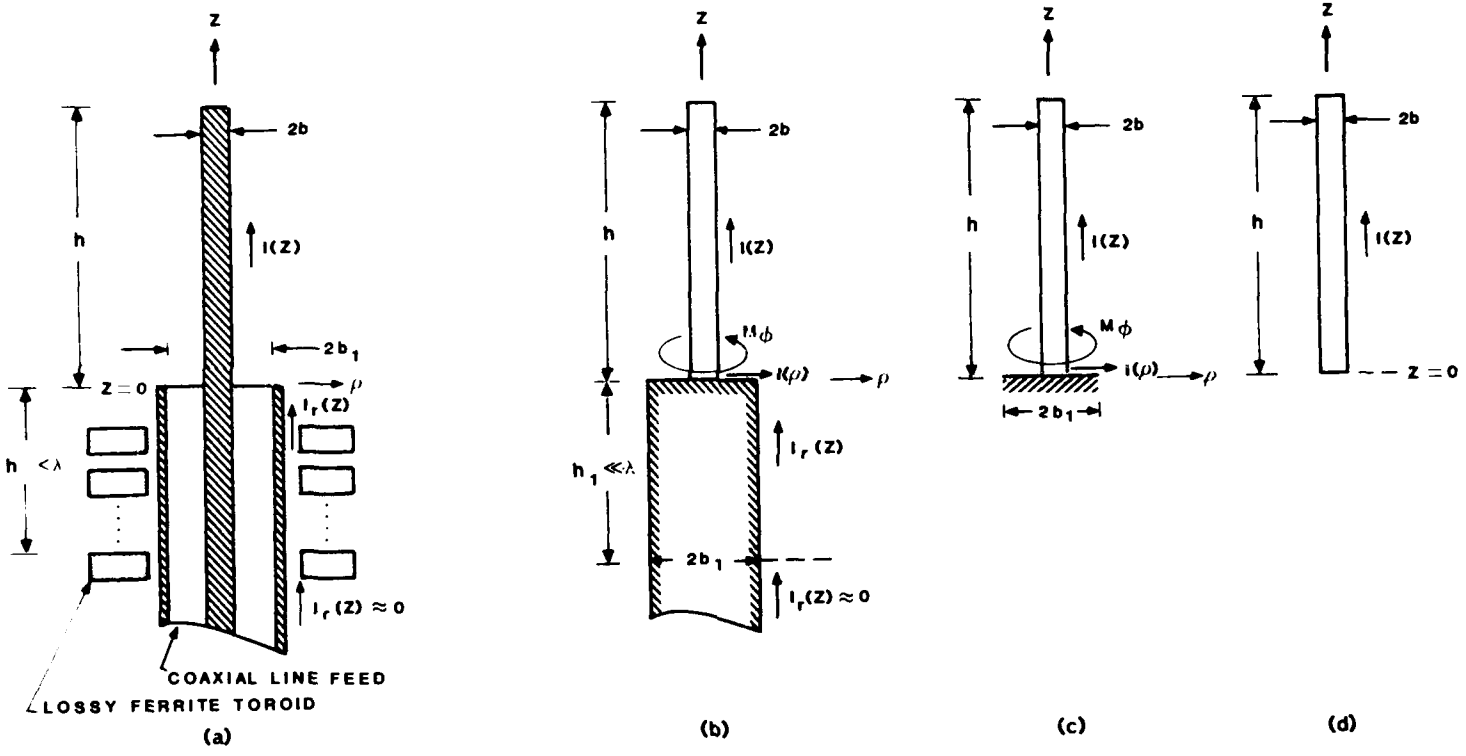

Figure 3. Characterization of Currents for Monopole Antenna with Groundplane of Zero Extent
(a) Physical realization
(b) Circuit representation
(c) Idealization of circuit ($h_1/\lambda=0$)
(d) Idealization of circuit ($h_1/\lambda=0$, $kb_1 \ll 1$, I(z) or $I(\rho)$ is initially known)

The near-fields, far-fields, and input impedance of an electrically thin monopole element are derived and summarized in the remainder of Section 3.2. The input impedance is derived by the induced emf method.

Near-fields

Consider a monopole element of length h with a sinusoidal current distribution $I(z') = [I(0)/\sin(kh)] \sin [k(h-z')]$. $0 \leq z' \leq h$, at points $Q(x', y', z')$ on the surface of the element (figure 4). For an electrically-thin element with a known current distribution, the fields at arbitrary points $P(x, y, z)$ external to the element may be determined almost exactly be approximating the source points to lie on the element axis, i.e., $Q(x', y', z') \approx Q(0, 0, z')$. For the current waveform of Eq. (2.1-2), the magnetic vector potential $\vec{A}$ is given by[16]

$$\vec{A}(x,y,z) = \hat{u}_z A_z = \hat{u}_z \frac{\mu_o I(0)}{4\pi \sin(kh)} \int_0^h \frac{\sin[k(h-z')] \exp(-jk\overline{PQ})}{\overline{PQ}} dz' \qquad (3.2\text{-}1)$$

where

μ_o = permeability of free space = $4\pi \times 10^{-7}$ henries/m

$\overline{PQ} = [(x-x')^2 + (y-y')^2 + (z-z')^2]^{1/2}$

$[x^2 + y^2 + (z-z')^2]^{1/2} = [\rho^2 + (z-z')^2]^{1/2}$

$\hat{u}_\rho, \hat{u}_\phi, \hat{u}_z$ = unit vectors in the radial, azimuthal, and axial cylindrical directions, respectively.

The magnetic and electric field intensities, $\vec{H}$ and $\vec{E}$, respectively, are given by

$$\vec{H} = \frac{1}{\mu_o} (\nabla \times \vec{A}) = -\hat{u}_\phi \frac{1}{\mu_o} \frac{\partial A_z}{\partial \rho} \qquad (3.2\text{-}2)$$

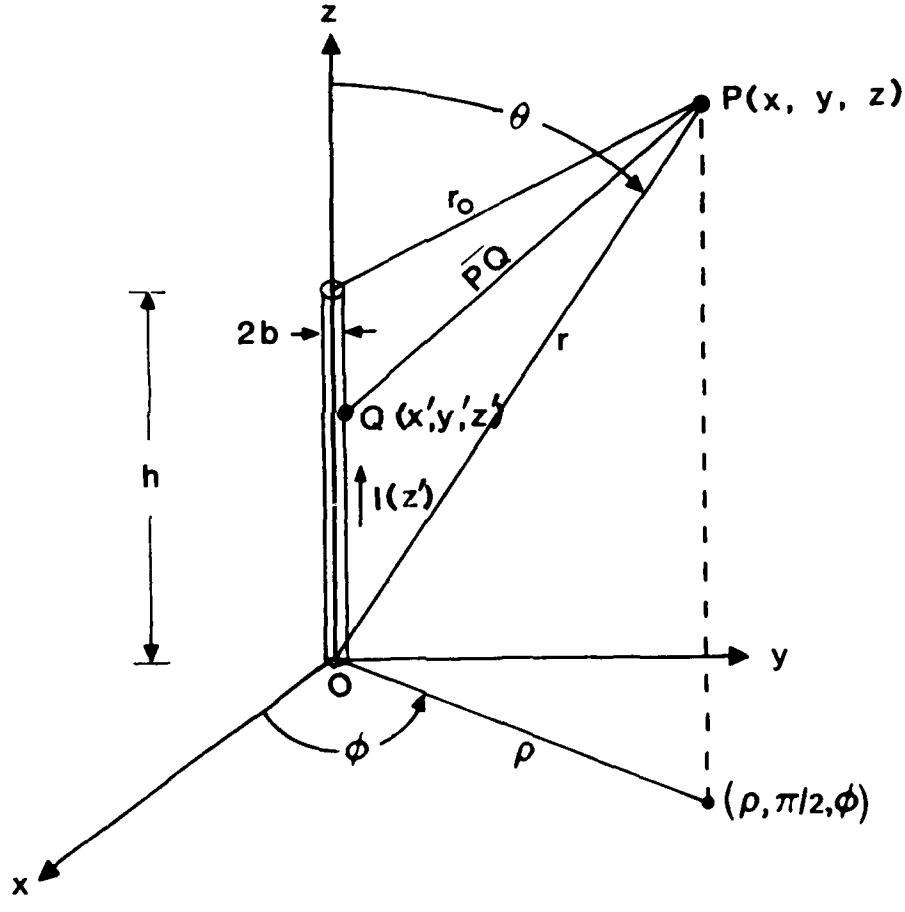

Figure 4. Monopole Element Geometry

$$\vec{E} = \frac{1}{j\omega\epsilon_o}(\nabla \times \vec{H}) = -\hat{u}_\rho \frac{1}{j\omega\epsilon_o}\frac{\partial H_\phi}{\partial z} + \hat{u}_z \frac{1}{j\omega\epsilon_o}\frac{1}{\rho}\frac{\partial}{\partial \rho}(\rho H_\phi) \tag{3.2-3}$$

where ϵ_o = permittivity of free space = 8.854×10^{-12} farad/m

Exact closed form expressions of $\vec{A}$, $\vec{H}$, $\vec{E}$ and radiation resistance were first obtained for an infinitely thin element by Brillouin[17] and are summarized by Stratton[18]. The magnetic and electric fields are given by

$$H_\phi = \frac{j\, I(0)}{4\pi\rho \sin(kh)}\left[\exp(-jkr_o) - \cos(kh)\exp(-jkr) - \frac{-jz}{r}\sin(kh)\exp(-jkr)\right] \tag{3.2-4}$$

$$\begin{aligned} E_\rho &= \frac{j\, I(0)\,\eta}{4\pi\rho\sin(kh)}\left\{\frac{(z-h)\exp(-jkr_o)}{r_o} - \frac{z}{r}\cos(kh)\exp(-jkr)\right. \\ &\quad \left. + \sin(kh)\frac{\partial}{\partial z}\left[\frac{z}{kr}\exp(-jkr)\right]\right\} \\ &= \frac{j\, I(0)\,\eta}{4\pi\rho\sin(kh)}\left\{\frac{(z-h)\exp(-jkr_o)}{r_o} - \frac{z}{r}\cos(kh)\exp(-jkr)\right. \\ &\quad \left. + \sin(kh)\exp(-jkr)\left[\frac{1}{kr} - \frac{z^2}{kr^3} - \frac{jz^2}{r^2}\right]\right\} \end{aligned} \tag{3.2-5}$$

$$\begin{aligned} E_z &= \frac{-j\, I(0)\,\eta}{4\pi\sin(kh)}\left\{\frac{\exp(-jkr_o)}{r_o} - \cos(kh)\frac{\exp(-jkr)}{r}\right. \\ &\quad \left. + \sin(kh)\frac{\partial}{\partial z}\left[\frac{\exp(-jkr)}{r}\right]\right\} \\ &= \frac{-j\, I(0)\,\eta}{4\pi\sin(kh)}\left\{\frac{\exp(-jkr_o)}{r_o} - \cos(kh)\frac{\exp(-jkr)}{r}\right. \\ &\quad \left. - z\sin(kh)\exp(-jkr)\left[\frac{j}{r^2} + \frac{1}{kr^3}\right]\right\} \end{aligned} \tag{3.2-6}$$

where

$\eta = k/\omega\epsilon_o$ = wave impedance of free space = 376.73 ohms

$r_o = [\rho^2 + (z-h)^2]^{1/2}$

$r = (\rho^2 + z^2)^{1/2}$

Eqs. (3.2-4) - (3.2-6) are identical to the results given by Stratton [$\xi_2 = h$, $\xi_1 = 0$, $\ell = h$, $\alpha = kh$, $r_2 = r_o$, $r_1 = r$, $I_o = -I(0)/[\sin(kh)]$ after the substitution of $-j$ for j to account for the $\exp(-j\omega t)$ waveform of Stratton instead of the $\exp(j\omega t)$ waveform of Eq. (2.1-2). The fields given by Eqs. (3.2-4) - (3.2-6) are exact for an infinitely-thin element and are almost exact for an electrically-thin element with the same sinusoidal current distribution.

Far-fields

Consider a field point P at a sufficiently large radial distance r which satisfies both the far radiation zone and Fraunhofer diffraction conditions given by

$$h \ll r,\ kr \gg 1;\ \text{far radiation zone conditions} \qquad (3.2\text{-}7)$$

$$kh^2/2r \ll 2\pi;\ \text{Fraunhofer diffraction condition} \qquad (3.2\text{-}8)$$

For these conditions,

$$\exp(-jkr_o) \approx \exp[-kj(r - h\cos\theta)],\ h \ll r,\ (kh^2/2r) \ll 2\pi$$

$$1/r_o \approx 1/r,\ h \ll r$$

$$z - h \approx z = r\cos\theta,\ h \ll r \qquad (3.2\text{-}9)$$

$$(1/kr) - (z^2/kr^3) - (jz^2/r^2) \approx -j\cos^2\theta,\ kr \gg 1$$

$$(j/r^2) + (1/kr^3) \approx (j/r^2),\ kr \gg 1$$

For the approximations of Eq. (3.2-9), the "exact" fields given by Eqs. (3.2-4) - (3.2-6) reduce to the far-fields given by

$$H_\phi = \frac{j\, I(0)\, \exp(-jkr)}{4\pi r \sin\theta \sin(kh)} \left[\exp(jkh\cos\theta) - \cos(kh) - j\cos\theta \sin(kh)\right] \tag{3.2-10}$$

$$E_\rho = \frac{j\, I(0)\eta\cos\theta\, \exp(-jkr)}{4\pi r \sin\theta \sin(kh)} \left[1 - \cos(kh) - j\cos\theta \sin(kh)\right] \tag{3.2-11}$$

$$E_z = \frac{-j\, I(0)\, \eta\, \exp(-jkr)}{4\pi r \sin(kh)} \left[1 - \cos(kh) - j\cos\theta \sin(kh)\right] \tag{3.2-12}$$

The resultant electric field $\vec{E} = \hat{u}_\rho E_\rho + \hat{u}_z E_z$ reduces in the far field to

$$\vec{E} = \hat{u}_\theta E_\theta, \text{ far-field} \tag{3.2-13}$$

where

$$E_\theta = \frac{j\, I(0)\, \eta\, \exp(-jkr)}{4\pi r \sin\theta \sin(kh)} \left[1 - \cos(kh) - j\cos\theta \sin(kh)\right]$$

The time-averaged Poynting vector $\vec{S} = (1/2)\,(\vec{E} \times \vec{H}) = (1/2)\,(\hat{u}_\theta E_\theta \times \hat{u}_\phi H_\phi) = \hat{u}_r\, s(\theta)$ with a time-averaged radiated power density $s(\theta)$ given by

$$s(\theta) = |E_\theta|^2/(2\eta) = (\eta/2)|H_\phi|^2 = \frac{\eta\, |I(0)|^2\, f(\theta)}{32\pi^2 r^2 \sin^2(kh)} \tag{3.2-14}$$

where

$$f(\theta) \equiv \frac{[\cos(kh\cos\theta) - \cos(kh)]^2 + [\sin(kh\cos\theta) - \cos\theta \sin(kh)]^2}{\sin^2\theta}$$

The direction of maximum radiated power is $\theta = \pi/2$ rad.

Substituting Eq. (3.2-14) into Eqs. (2.2-6) and (2.2-7), the radiation resistance R, referred to the base-current, is given for an infinitely thin element by

$$R = \frac{\eta \int_0^{\pi} f(\theta) \sin\theta \, d\theta}{8\pi \sin^2(kh)} \quad \text{(ohms)}$$

$$= \frac{\eta}{4\pi \sin^2(kh)} [Cin(2kh) - \sin^2(kh)], \; b=0 \qquad (3.2\text{-}15)$$

where Cin(z) = modified cosine integral[19] $= \int_0^z \frac{dt}{t} (1-\cos t)$.

The result given for the definite integral of Eq. (3.2-15) is readily obtained by letting $t = \cos\theta$ and noting that

$$\frac{1}{1-t^2} = \frac{1}{2} \left[\frac{1}{x} + \frac{1}{y}\right]$$

where $x = 1+t$ and $y = 1-t$.

Substituting Eqs. (3.2-14) and (3.2-15) into Eq. (2.2-8), the numeric directive gain $d(\theta)$ is given by

$$d(\theta) = \frac{f(\theta)}{Cin(2kh) - \sin^2(kh)} \qquad (3.2\text{-}16)$$

where $f(\theta)$ is defined in Eq. (3.2-14).

For electrically-short monopole elements ($kh \ll 1$) and for $\eta = 376.73 \approx 120\pi$ ohms, Eqs. (3.2-14) - (3.2-16) reduce to

$$f(\theta) = \frac{1}{4} (kh)^4 \sin^2\theta, \quad kh \ll 1 \tag{3.2-17}$$

$$s(\theta) = \frac{15}{16} \frac{|I(0)|^2 (kh)^2 \sin^2\theta}{\pi r^2}, \quad kh \ll 1 \tag{3.2-18}$$

$$R = 5 (kh)^2 \text{ (ohms)}, \quad kh \ll 1, \; b = 0 \tag{3.2-19}$$

$$d(\theta) = \frac{3}{2} \sin^2\theta, \quad kh \ll 1 \tag{3.2-20}$$

The relative power radiation pattern $s(\theta)/s_{max} = s(\theta)/s(\pi/2)$, radiation resistance R, and the directive gain (directivity) $d(\theta)$ are tabulated in Appendix A1, Tables A1-1, A1-14, A1-26, A1-38 for $h/\lambda = 1/4$, 1/10, 1/40, and 1/100, respectively. The numeric directive gain pattern $d(\theta)$ for a quarterwave monopole element [see figure 8(a) in Section 3.9] is similar to that of a half-wave dipole except that its peak directivity is less (1.88 dbi vs. 1.76 dBi) and its 3 dB beamwidth is more (94 deg vs. 78 deg).

Input Impedance

The input impedance may be determined by the induced emf method introduced by Brillouin[17]. With reference to figure 4, the input impedance Z_{in} is given by[20]

$$Z_{in} = -(1/I_m) \int_0^h I_z(\rho = b, z = z') \, E_z(\rho = b, z = z') \, dz', \quad b > 0 \tag{3.2-21}$$

where

$$I_m = I(0)/\sin(kh).$$

The induced emf method is indeterminate for collinear current elements unless the elements are of radius $b > 0$. For sufficiently thin elements, the current I_z is given by Eq. (3.1-1) and the electric near field E_z is given almost exactly by Eq. (3.2-6). Substituting Eqs. (3.1-1) and (3.2-6) into Eq. (3.2-21),

$$Z_{in} = \frac{j\eta}{4\pi \sin(kh)} \int_0^h dz' \sin[k(h-z')] \left\{ \frac{\exp(-jkr_o)}{r_o} - \cos(kh) \frac{\exp(-jkr)}{r} + \sin(kh) \frac{\partial}{\partial z'} \left[\frac{\exp(-jkr)}{r} \right] \right\} \quad (3.2\text{-}22)$$

where

$$r_o = [b^2 + (z'-h)^2]^{1/2}$$
$$r = (b^2 + z'^2)^{1/2}$$

Each of the three terms of the integrand of Eq. (3.2-22) may be integrated by the methods summarized by Stratton[18]. However, the third term of the integrand should first be integrated by parts.
Accordingly,

$$Z_{in} = R_{in} + j X_{in} = Z_1 + Z_2 + Z_3 \quad (3.2\text{-}23)$$

where

$$Z_1 = \frac{j\eta}{4\pi \sin^2(kh)} \int_0^h dz' \sin[k(h-z)] \frac{\exp(-jkr_o)}{r_o} = R_1 + jX_1 \quad (3.2\text{-}24)$$

$$R_1 = \frac{\eta}{4\pi \sin^2(kh)} \left[\frac{1}{2} \mathrm{Cin}(x_1) + \frac{1}{2} \mathrm{Cin}(x_2) - \mathrm{Cin}(x_3) \right] \quad (3.2\text{-}25)$$

$$X_1 = \frac{\eta}{4\pi \sin^2(kh)} \left[\frac{1}{2} \mathrm{Si}(x_1) + \frac{1}{2} \mathrm{Si}(x_2) - \mathrm{Si}(x_3) \right] \quad (3.2\text{-}26)$$

$$Z_2 = \frac{j\eta}{4\pi \sin^2(kh)} \int_0^h -dz' \sin[k(h-z')] \cos(kh) \frac{\exp(-jkr)}{r} = R_2 + jX_2 \tag{3.2-27}$$

$$R_2 = \frac{\eta}{4\pi \sin^2(kh)} \left\{ \frac{-\sin(2kh)}{4} [Si(x_1) - Si(x_2)] + \cos^2(kh) \left[-Cin(x_3) + \frac{1}{2} Cin(x_2) + \frac{1}{2} Cin(x_1)\right] \right\} \tag{3.2-28}$$

$$X_2 = \frac{\eta}{4\pi \sin^2(kh)} \left\{ \frac{-\sin(2kh)}{4} [Cin(x_2) - Cin(x_1) + \ell n(x_1/x_2)] + \frac{\cos^2(kh)}{2} [Si(x_1) + Si(x_2) - 2\,Si(x_3)] \right\} \tag{3.2-29}$$

$$Z_3 = \frac{j\eta}{4\pi \sin^2(kh)} \int_0^h dz' \sin[k(h-z')] \sin(kh) \frac{\partial}{\partial z'} \left[\frac{\exp(-jkr)}{r}\right] = R_3 + jX_3 \tag{3.2-30}$$

$$R_3 = \frac{\eta}{4\pi \sin^2(kh)} \left\{ \frac{\sin^2(kh)}{2} \left[Cin(x_1) + Cin(x_2) - 2\,Cin(x_3) + \frac{2(x_1 + x_2)(\sin x_1 + \sin x_2)}{x_1^2 + x_2^2 + 2(kb)^2} - \frac{4\,x_3 \sin x_3}{x_3^2 + (kb)^2}\right] - \frac{\sin(2kh)}{4} \left[Si(x_2) - Si(x_1) - \frac{2(x_1 + x_2)(\cos x_1 - \cos x_2)}{x_1^2 + x_2^2 + 2(kb)^2}\right] \right\} \tag{3.2-31}$$

$$X_3 = \frac{\eta}{4\pi \sin^2(kh)} \left\{ \frac{\sin^2(kh)}{2} \left[Si(x_1) + Si(x_2) - 2Si(x_3) + \frac{2(x_1 + x_2)(\cos x_1 + \cos x_2)}{x_1^2 + x_2^2 + 2(kb)^2} - \frac{4\,x_3 \cos x_3}{x_3^2 + (kb)}\right] + \frac{\sin(2kh)}{4} \left[-Cin(x_1) + Cin(x_2) + \ell n(x_1/x_2) - \frac{2(x_1 + x_2)(\sin x_1 - \sin x_2)}{x_1^2 + x_2^2 + 2(kb)^2}\right] \right\} \tag{3.2-32}$$

where

$$x_1 = k[(b^2 + h^2)^{1/2} + h]$$
$$x_2 = k[(b^2 + h^2)^{1/2} - h]$$
$$x_3 = kb$$

$$\text{Cin}(x) = \text{modified cosine integral}^{(19)} = \int_0^x \frac{dt}{t}\,(1-\cos t)$$

$$\text{Si}(x) = \text{sine integral}^{(19)} = \int_0^x \frac{\sin t}{t}\,dt$$

Summing Eqs. (3.2-23) - (3.2-32),

$$R_{in} = \frac{\eta}{4\pi\sin^2(kh)}\left\{\text{Cin}(x_1) + \text{Cin}(x_2) - 2\,\text{Cin}(x_3)\right.$$
$$+ \frac{\sin(2kh)}{2}\left[\frac{(x_1 + x_2)(\cos x_1 - \cos x_2)}{x_1^2 + x_2^2 + 2x_3^2}\right]$$
$$\left. + \sin^2(kh)\left[\frac{(x_1 + x_2)(\sin x_1 + \sin x_2)}{x_1^2 + x_2^2 + 2x_3^2} - \frac{\sin x_3}{x_3}\right]\right\} \quad (3.2\text{-}33)$$

$$X_{in} = \frac{\eta}{4\pi\sin^2(kh)}\left\{\text{Si}(x_1) + \text{Si}(x_2) - 2\,\text{Si}(x_3)\right.$$
$$- \frac{\sin(2kh)}{2}\left[\frac{(x_1 + x_2)(\sin x_1 - \sin x_2)}{x_1^2 + x_2^2 + 2x_3^2}\right]$$
$$\left. + \sin^2(kh)\left[\frac{(x_1 + x_2)(\cos x_1 + \cos x_2)}{x_1^2 + x_2^2 + 2x_3^2} - \frac{\cos x_3}{x_3}\right]\right\} \quad (3.2\text{-}34)$$

where $x_1 = k[(b^2 + h^2)^{1/2} + h]$, $x_2 = k[(b^2 + h^2)^{1/2} - h]$, $x_3 = kb$.

For b=0, Eqs. (3.2-33) and (3.2-34) reduce to

$$R_{in} = \frac{\eta}{4\pi \sin^2(kh)} \left[Cin(2kh) - \sin^2(kh) \right] \quad , b=0 \qquad (3.2\text{-}35)$$

$$X_{in} = \frac{\eta}{4\pi \sin^2(kh)} \left[Si(2kh) - \frac{\sin^2(kh)}{kb} \right], \quad b \to 0 \qquad (3.2\text{-}36)$$

Eq. (3.2-35) agrees with the result for radiation resistance given by Eq. (3.2-15). A comparison of Eq. (3.2-33) with Eq. (3.2-35) reveals that the input resistance is relatively insensitive to the monopole element radius b for kb << 1. The input resistance given by Eq. (3.2-35) is plotted in figure 5. For kh = $\pi/2$ radians, R_{in} = 19.4 ohms.

The input reactance is sensitive to the element radius b as seen in Eq. (3.2-36). For b = 0, the input reactance is given by

$$X_{in} = \begin{cases} -\infty \text{ ohms}, & kh \neq n\pi \ , \ n = 1, 2, 3 \ldots \\ \infty \text{ ohms}, & kh = n\pi, \ n = 1, 2, 3 \ldots \end{cases} , \ b = 0 \qquad (3.2\text{-}37)$$

From Eq. (3.2-36), resonance (X_{in} = 0) occurs for

$$(kh)_{resonance} \approx n\pi \pm [kb \ Si(2n\pi)]^{1/2}, \ n = 1, 2, 3 \ldots \qquad (3.2\text{-}38)$$

The input resistance at resonance, for kh given by Eq. (3.2-38), is found from Eq. (3.2-35) to be

$$(R_{in})_{resonance} \approx \frac{\eta}{4\pi} \left[\frac{Cin(2n\pi)}{kb \ Si(2n\pi)} - 1 \right] \qquad (3.2\text{-}39)$$

Minima of input resistance occur for kh given by

$$(kh)_{minima} \approx \left(N + \frac{1}{2}\right)\pi \ , \ N = 1, 2, 3, \ldots \qquad (3.2\text{-}40)$$

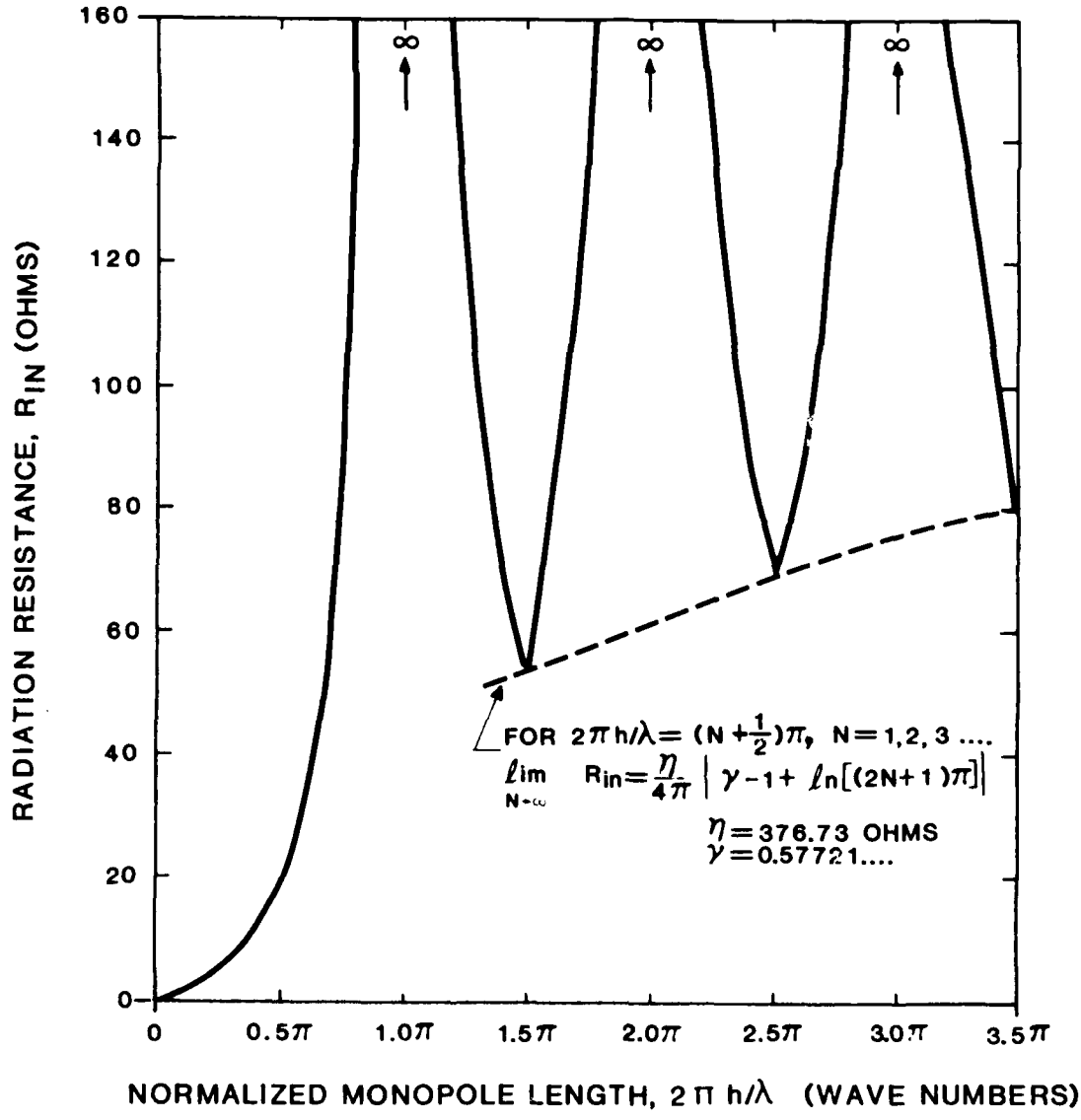

Figure 5. Radiation Resistance of Electrically-Thin ($kb \ll 1$) Monopole Elements

The input resistance at these minima element lengths is found from Eq. (3.2-35) to be

$$(R_{in})_{minima} \approx \frac{\eta}{4\pi} \left[\gamma - 1 + \ell n[(2N + 1)\pi] \right] \qquad (3.2\text{-}41)$$

where

γ = Euler's constant = 0.57721

The accuracy of Eq. (3.2-40) increases as $N \longrightarrow \infty$.

Summary of Results

The input impedance and directive gain properties of quarterwave and electrically-short monopole elements with groundplanes of zero, large, and infinite extent are compared in Table 4 of Section 3.9. The peak directivity is approximately 3 dB less with groundplanes of zero extent than with groundplanes of large extent. However, the directive gain on the horizon is approximately 3 dB more with groundplanes of zero extent than with groundplanes of large but finite extent. The radiation resistance with groundplanes of zero extent is approximately one-half that with groundplanes of large extent.

Unlike dipole elements in free space whose first resonance occurs for dipole half-lengths approximately equal to a quarterwave, monopole elements with groundplanes of zero extent have a first resonance for an element length approximately equal to a half-wave.

3.3 Integral Equation, $0 \leq ka \leq 2.75$

In Section 3.2 the fields generated by the monopole element were determined. These fields impinge on the groundplane and induce a groundplane current. For sufficiently small groundplanes, the fields generated by the groundplane current may be determined by Bardeen's integral equation method[1].

In this method a cylindrically symmetrical electromagnetic wave (generated by the element) is incident on the groundplane disc. The fields generated by the induced groundplane current are required. The solution depends upon solving an integral equation of the first kind. For groundplane radii of arbitrary radius, the integral equation is not readily solvable because it contains two integrals. However, for sufficiently small groundplane radii, Bardeen neglects one of the integrals so that the integral equation may be solved explicitly.

Although Bardeen gives a general formulation of the solution for the resulting single integrand integral equation, his only explicit results are for the case when the incident wave is generated by an infinitely thin dipole element whose base is at a non-zero height above the center of the groundplane. Bardeen restricted his solution to elements at a non-zero height above the groundplane in order to avoid having a source point (the base of the element) at a near-field point of interest which, for the integral equation method, includes the center of the groundplane. The total field is then given by the vector sum of the incident field and the induced field [see Eq. 3.1-12].

The present case of interest is a monopole element whose base is in the plane of the groundplane, i.e., at a vertical height v=0 above the center of the groundplane (see figure 6). For this case, the total magnetic field may be determined by first evaluating the field with the element at an arbitrary height $v > 0$ and then by evaluating the resulting expression in the lim $v \to 0$. By such a procedure, an indeterminate expression is avoided for the field generated by the induced groundplane current.

Accordingly, the total magnetic field intensity $H_\phi^{(total)}$ [see Eq. (3.1-1.2)] in the limit $v \to 0$ is given by

$$\lim_{v \to 0} H_\phi^{(total)} = \lim_{v \to 0} H_\phi^{(e)} + \lim_{v \to 0} H_\phi^{(g)} \qquad (3.3\text{-}1)$$

where $H_\phi^{(e)}$ and $H_\phi^{(g)}$ are the magnetic field intensities generated by the element and groundplane currents, respectively. In the following evaluation of the two terms of Eq. (3.3-1), the fields are assumed to have an $e^{j\omega t}$ time dependence [see Eq. 2.1-2] unlike the $e^{-j\omega t}$ time dependence assumed by Bardeen.

The first term of Eq. (3.3-1) is given exactly, for an infinitely thin element, by [see Eq. 3.2-4]

$$\lim_{v \to 0} H_\phi^{(e)} = \frac{j\, I(0)}{4\pi\rho \sin(kh)} \left[\exp(-jkr_o) - \cos(kh) \exp(-jkr) - \frac{j\, z}{r} \sin(kh) \exp(-jkr) \right] \qquad (3.3\text{-}2)$$

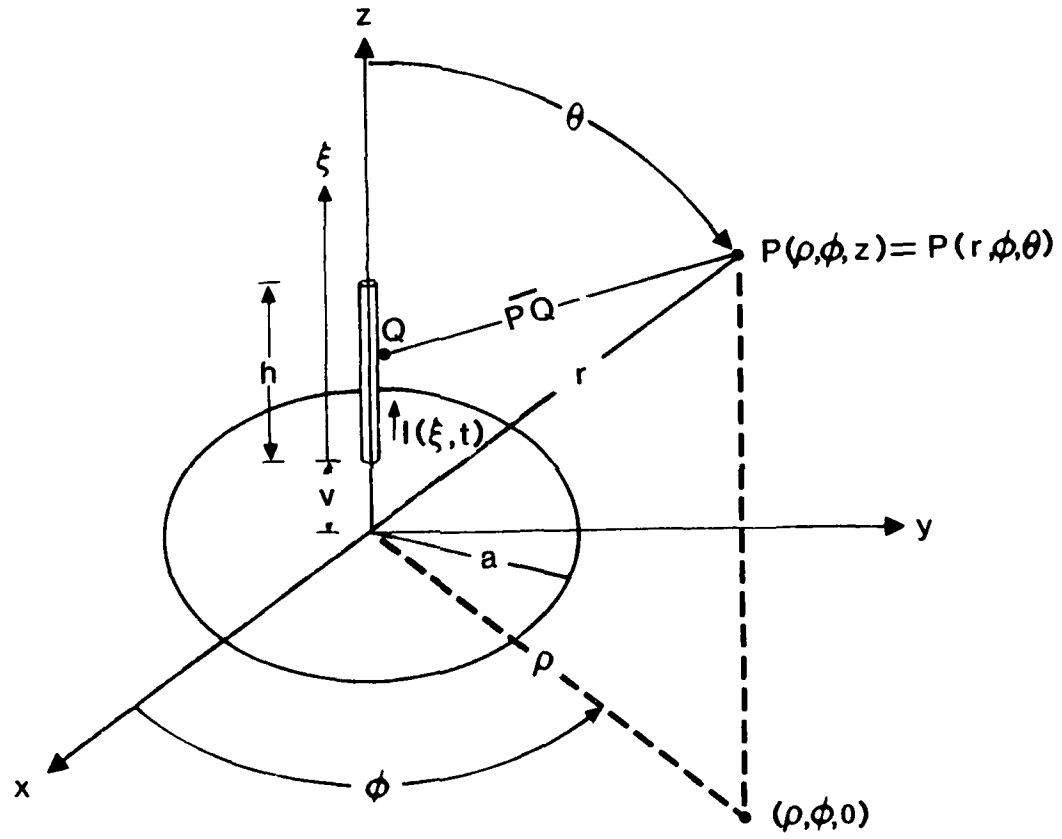

Figure 6. Thin Monopole Element Whose Base Is Above the Center of a Circular Groundplane

In the far-field, Eq. (3.3-2) reduces to [see Eq. (3.2-10)]

$$\lim_{v\to 0} H_\phi^{(e)} = A_o \left[j \exp(jkh\cos\theta) + j\cos(kh) + \cos\theta \sin(kh) \right]_{\text{far-field}}, \qquad (3.3\text{-}3)$$

where

$$A_o = \frac{-I(0)\, e^{-jkr}}{4\pi r \sin\theta \sin(kh)} .$$

The second term of Eq. (3.3-1) may be evaluated by utilizing Bardeen's Eq. (31) for $H_\phi^{(g)}$ which he obtained as a solution to his single integrand integral equation. For an infinitely thin element and for sufficiently small groundplanes ($ka \lesssim 1$), $H_\phi^{(g)}$ is given by Bardeen's Eq. (31) as

$$H_\phi^{(g)} = \operatorname{sgn}(z)\, \frac{-j\omega\epsilon_o}{k\rho} \int_0^a F(s)\, K(s)\, ds, \qquad ka \lesssim 1 \qquad (3.3\text{-}4)$$

where

$$K(s) = \frac{e^{-jkA_1} \sinh(kB_1) \sinh(ks) - e^{-jkA_2} \sinh(kB_2) \sinh(ka)}{\sinh(ka)}$$

$$\operatorname{sgn}(z) = \begin{cases} +1, & z \geq 0 \\ -1, & z < 0 \end{cases}$$

ϵ_o = permittivity of free space (farad/m)

$$A_1 - jB_1 = \left\{\rho^2 + [-ja + z\,\operatorname{sgn}(z)]^2\right\}^{1/2} = \left[r^2 - \operatorname{sgn}(z)\, 2jra\cos\theta - a^2\right]^{1/2}$$

$$A_2 - jB_2 = \left\{\rho^2 + [-js + z\,\operatorname{sgn}(z)]^2\right\}^{1/2} = \left[r^2 - \operatorname{sgn}(z)\, 2jrs\cos\theta - s^2\right]^{1/2}$$

s = dummy variable with the dimension of length

F(s) = excitation function related to the radial electric near-field intensity $E_r^{(e)}|_{z=0}$ which is incident on the groundplane.

The second term of Eq. (3.3-1) is therefore given by

$$\lim_{v\to 0} H_\phi^{(g)} = \mathrm{sgn}(z)\ \frac{-j\omega\epsilon_o}{k\rho}\ \lim_{v\to 0}\int_0^a F(s)K(s)\,ds, \qquad ka \lesssim 1$$

$$= \mathrm{sgn}(z)\ \frac{-j\omega\epsilon_o}{k\rho}\int_0^a \left[\lim_{v\to 0} F(s)\right] K(s)\,ds, \quad ka \lesssim 1 \tag{3.3-5}$$

The excitation function F(s) is given by Bardeen's Eq. (35) as

$$F(s) = -\frac{2}{\pi}\int_0^\infty p\ h(p)\ \frac{\sin[s\ (p^2 - k^2)^{1/2}]}{\left(p^2 - k^2\right)^{1/2}}\,dp \tag{3.3-6}$$

where

p = dummy variable with the dimensions of $(\text{length})^{-1}$

h(p) = function of the radial electric near-field intensity $E_\rho^{(e)}|_{z=0}$ which is incident on the groundplane.

The function h(p) is given by Bardeen's Eq. (33) as

$$-E_\rho^{(e)}|_{z=0} = \int_0^\infty h(p)\ J_1(\rho p)\ \ dp \tag{3.3-7}$$

where $J_1(x)$ = Bessel function of the first kind.

The electric field intensity $E_\rho^{(e)}|_{z=0}$ incident on the groundplane is given by

$$E_\rho^{(e)}|_{z=0} = \hat{u}_\rho \bullet \left.\frac{[\nabla x\ (\nabla x\ \vec{A}^{(e)})]}{j\omega\ \mu_o\epsilon_o}\right|_{z=0} \tag{3.3-8}$$

where

$\vec{A}^{(e)}$ = magnetic vector potential generated by the monopole source points

μ_o = permeability of free space (henry/m)

$\hat{u}_\rho$ = unit vector in the cylindrical radial direction

The magnetic vector potential $\vec{A}^{(e)}$ for the element base at an arbitrary height v is given by[16]

$$\vec{A}^{(e)} = \hat{u}_z \, (\mu_o/4\pi) \int_0^h I(\xi) \, (1/\overline{PQ}) \, \exp(-jk\overline{PQ}) \, d\xi \qquad (3.3\text{-}9)$$

where

$\hat{u}_z$ = unit vector along the z axis

$\overline{PQ}$ = distance from source point Q to field point P

$\approx [\rho^2 + (z - \xi - v)^2]^{1/2}$, $Q(x', y', \xi) \approx Q(0, 0, \xi)$.

$I(\xi)$ = monopole current distribution = $[I(0)/\sin(kh)] \sin[k(h-\xi)]$.

In order to facilitate the evaluation of h(p) in Eq. (3.3-7), it is convenient to express the factor $(1/\overline{PQ}) \exp(-jk\overline{PQ})$ in terms of Bessel functions. Using Sommerfeld's formula[21] and the dummy variable p introduced in Eq. (3.3-6),

$$\frac{e^{-jk\overline{PQ}}}{\overline{PQ}} = \int_0^\infty \frac{J_o(p\rho) \exp\left[- | z - \xi - v| \sqrt{p^2 - k^2} \right] p \, dp}{\left(p^2 - k^2\right)^{1/2}};$$

$$- (\pi/2) < \arg \sqrt{p^2 - k^2} \leq (\pi/2), \quad - \pi < \arg k \leq 0 \qquad (3.3\text{-}10)$$

Substituting Eq. (3.3-10) into Eq. (3.3-9),

$$\vec{A}^{(e)} = \frac{\mu_o I(0)}{4\pi \sin(kh)} \hat{u}_z \int_0^h d\xi \sin[k(\xi - h)] \int_0^\infty \frac{J_o(p\rho) \exp\left[-|z - \xi - v| \sqrt{p^2 - k^2}\right]}{(p^2 - k^2)^{1/2}} p\, dp;$$

$$-(\pi/2) < \arg \sqrt{p^2 - k^2} \leq (\pi/2), \quad -\pi < \arg k \leq 0 \qquad (3.3\text{-}11)$$

Since we are interested in evaluating $E_\rho^{(e)}\Big|_{z=0}$, consider the case $z < \xi + v$. Substituting Eq. (3.3-11) for such a case into Eq. (3.3-8) and noting that

$$\vec{A}^{(e)} \hat{u}_z = A_z \quad \text{and} \quad \frac{\partial J_o(p\rho)}{\partial \rho} = -pJ_1(p\rho),$$

$$E_\rho^{(e)}\Big|_{z=0} = \frac{1}{-j\omega\mu_o\epsilon_o} \frac{\partial^2 A_z}{\partial z \partial \rho}\Bigg|_{z=0}$$

$$= \frac{I(0)}{-j4\pi\omega\epsilon_o \sin(kh)} \int_0^\infty p^2 J_1(p\rho) \exp\left[(z-v)\sqrt{p^2 - k^2}\right] B(p)\, dp \Bigg|_{z=0} \qquad (3.3\text{-}12)$$

where

$$B(p) = \int_0^h \sin[k(h - \xi)] \exp\left[-\xi\sqrt{p^2 - k^2}\right] d\xi$$

$$= \frac{k \exp\left[-h\sqrt{p^2 - k^2}\right] + \sqrt{p^2 - k^2} \sin(kh) - k\cos(kh)}{p^2} \qquad (3.3\text{-}13)$$

Substituting Eq. (3.3-13) into Eq. (3.3-12) and letting $z=0$,

$$E_\rho^{(e)}\Big|_{z=0} = \frac{I(0)}{-j4\pi\omega\epsilon_o \sin(kh)} \int_0^\infty dp\, J_1(p\rho)\, e^{-v\sqrt{p^2 - k^2}} \left[e^{-h\sqrt{p^2 - k^2}} + \sqrt{p^2 - k^2} \sin(kh) - k\cos(kh) \right] \qquad (3.3\text{-}14)$$

Comparison of Eq. (3.3-14) with Eq. (3.3-7) yields

$$h(p) = \frac{I(0)}{j4\pi\omega\epsilon_o \sin(kh)} \left[k\, e^{-(h+v)\sqrt{p^2-k^2}} + \sqrt{p^2-k^2}\sin(kh)\, e^{-v\sqrt{p^2-k^2}} - k\cos(kh)\, e^{-v\sqrt{p^2-k^2}} \right] \tag{3.3-15}$$

Substituting Eq. (3.3-15) into Eq. (3.3-6)

$$F(s) = \frac{-2Ck}{\pi} \left[I_1 + \frac{\sin(kh)}{k} I_2 - \cos(kh)\, I_3 \right] \tag{3.3-16}$$

where

$$C \equiv \frac{I(0)}{j\,4\pi\omega\epsilon_o \sin(kh)}$$

$$I_1 = \int_0^\infty \frac{p\, e^{-(h+v)\sqrt{p^2-k^2}} \sin(s\sqrt{p^2-k^2})}{(p^2-k^2)^{1/2}}\, dp$$

$$I_2 = \int_0^\infty p \sin(s\sqrt{p^2-k^2})\, e^{-v\sqrt{p^2-k^2}}\, dp$$

$$I_3 = \int_0^\infty \frac{p \sin(s\sqrt{p^2-k^2})\, e^{-v\sqrt{p^2-k^2}}}{(p^2-k^2)^{1/2}}\, dp$$

In integrals I_1, I_2, I_3, we introduce a change in variable p to y given by

$$y = (p^2 - k^2)^{1/2}, \quad -(\pi/2) < \arg y \leq (\pi/2) \tag{3.3-17}$$

where the condition on y follows from the conditions of Eq. (3.3-10).

From Integral 2.663.1 of Ref. [22], it follows that I_1 is given by

$$I_1 = \int_{jk}^{\infty} e^{-(h+v)y} \sin(sy)\, dy = \frac{e^{-(h+v)y}}{(h+v)^2 + s^2} [-(h+v)\sin(sy) - s\cos(sy)] \Bigg|_{jk}^{\infty} = \frac{-e^{-k(h+v)}}{(v+h)^2 + s^2} [-j(h+v)\sinh(ks) - s\cosh(ks)] \tag{3.3-18}$$

From Integral 2.667.5 of Ref. [22], it follows that I_2 is given by

$$I_2 = \int_{jk}^{\infty} y \sin(sy)\, e^{-vy}\, dy = \frac{e^{-vy}}{v^2 + s^2} \left[\left(-vy + \frac{s^2 - v^2}{v^2 + s^2} \right) \sin(sy) - \left(sy + \frac{2vs}{s^2 + v^2} \right) \cos(sy) \right] \Bigg|_{ik}^{\infty}$$

$$= \frac{-e^{-jkv}}{s^2 + v^2} \left[kv\sinh(ks) - jks\cosh(ks) - \frac{j(v^2 - s^2)\sinh(ks) - 2vs\cosh(ks)}{s^2 + v^2} \right] \tag{3.3-19}$$

From Integral 2.663.1 of Ref. [22] it follows that I_3 is given by

$$I_3 = \int_{jk}^{\infty} \sin(sy)\, e^{-vy}\, dy = e^{-vy} \left[\frac{-v\sin(sy) - s\cos(sy)}{s^2 + v^2} \right] \Bigg|_{jk}^{\infty} \tag{3.3-20}$$

$$= -e^{-jkv} \left[\frac{-jv\sinh(ks) - s\cosh(ks)}{s^2 + v^2} \right]$$

Consider now the limits of I_1, I_2, and I_3 as $v \to 0$.

$$\lim_{v \to 0} I_1 = \frac{e^{-ikh}}{h^2 + s^2} [-jh\sinh(ks) - s\cosh(ks)] \tag{3.3-21}$$

$$\lim_{v\to 0} I_2 = -\pi k \delta(s) \sinh(ks) + \frac{j\, k \cosh(ks)}{s}$$

$$+ j\pi^2 \delta^2(s) \sinh(ks) - \frac{j \sinh(ks)}{s^2} - \pi \delta'(s) \cosh(ks) \qquad (3.3\text{-}22)$$

$$\lim_{v\to 0} I_3 = j\pi\delta(s) \sinh(ks) + \frac{\cosh(ks)}{s} \qquad (3.3\text{-}23)$$

where[23]

$\delta(x)$ = Dirac delta function = $\lim_{v\to 0}\left[\frac{1}{\pi} \quad \frac{v}{v^2 + x^2}\right]$.

$$\int_a^b \delta(x-x_o)\, dx = \begin{cases} 1, & a < x_o < b \\ 1/2, & a = x_o < b \text{ or } a < x = b \\ 0, & x_o < a \text{ or } x_o > b \end{cases}$$

$$\delta'(x) = \frac{d}{dx}[\delta(x)] = \lim_{v\to 0} \frac{\partial}{\partial x}\left[\frac{1}{\pi} \quad \frac{v}{v^2 + x^2}\right] = \lim_{v\to 0}\left[-\frac{1}{\pi} \quad \frac{2\,vx}{\left(v^2 + x^2\right)^2}\right]$$

In Eqs. (3.3-22) and (3.3-23), those terms containing the product $\delta(s) \sinh(ks)$ may be set equal to zero since from Eq. (B. 2-12) of Ref. [23], $x\,\delta(x) = 0$.

The $\lim_{v\to 0} F(s)$ is found by substituting Eqs. (3.3-21)-(3.3-23) into Eq. (3.3-16).

Accordingly,

$$\lim_{v\to 0} F(s) = \frac{2Ck}{\pi} \quad \frac{e^{-jkh}}{h^2 + s^2} \quad [-j\, h \sinh(ks) - s \cosh(ks)]$$

$$+ \frac{2C \sin(kh)}{\pi}\left[\frac{-j\, k \cosh(ks)}{s} - \frac{j \sinh(ks)}{s^2} + \pi\delta'(s) \cosh(ks)\right]$$

$$+ \frac{2C\, k \cos(kh)}{\pi} \quad \frac{\cosh(ks)}{s} \qquad (3.3\text{-}24)$$

The magnetic field intensity generated by the groundplane current, for the case $v \to 0$, is found by substituting Eq. (3.3-24) into Eq. (3.3-5). The total magnetic field is explicitly determined by numerical evaluation of Eqs. (3.3-1) - (3.3-5).

In the far-field, the factor K(s) and the parameters A_1, A_2, B_1, B_2, in Eqs. (3.3-4) and (3.3-5) reduce to a simpler form.

In the far-field when $r \to \infty$, then $a \ll r$ and $s \ll r$. For these conditions,

$$A_1 - jB_1 \approx [r^2 - \text{sgn}(z)\, 2jra\cos\theta - a^2\cos^2\theta]^{1/2} = r - \text{sgn}(z)\, ja\cos\theta, \quad a \ll r \qquad (3.3\text{-}25)$$

$$A_2 - jB_2 \approx [r^2 - \text{sgn}(z)\, 2jra\cos\theta - s^2\cos^2\theta]^{1/2} = r - \text{sgn}(z)\, js\cos\theta, \quad s \ll r \qquad (3.3\text{-}26)$$

Equating real and imaginary parts in Eqs. (3.3-25) and (3.3-26)

$$A_1 = A_2 = r; \qquad a \ll r, \quad s \ll r \qquad (3.3\text{-}27)$$

$$B_1 = \text{sgn}(z)\, a\cos\theta, \qquad a \ll \rho \qquad (3.3\text{-}28)$$

$$B_2 = \text{sgn}(z)\, s\cos\theta, \qquad s \ll \rho \qquad (3.3\text{-}29)$$

Substituting Eqs. (3.3-27), (3.3-28), (3.3-29) into Eqs. (3.3-4) and (3.3-5), the far-field magnetic field intensity due to the groundplane current, for the case $v \to 0$, is given by

$$\lim_{v\to 0} H_\phi^{(g)} = \frac{-j\omega\epsilon_o \exp(-jkr)}{kr\sin\theta} \int_0^a \left[\lim_{v\to 0} F(s)\right] g(s)\, ds; \quad \text{far-field, } ka \lesssim 1 \qquad (3.3\text{-}30)$$

where

$$g(s) = \frac{\sinh(ka\cos\theta)\sinh(ks) - \sinh(ks\cos\theta)\sinh(ka)}{\sinh(ka)}$$

and $\lim_{v\to 0} F(s)$ is given by Eq. (3.3-24)

Eq. (3.3-30) can be reduced further by utilizing the properties of the Dirac delta function given by Eq. (B.2-7) of Ref. [23] and the relation

$$\int_0^a \delta'(x)\, f(x)\, dx = -\frac{1}{2} f'(0^+).$$

It follows that Eq. (3.3-30) reduces to

$$\lim_{v\to 0} H_\phi^{(g)} = \frac{2A_o}{\pi}\int_0^a ds\, g(s)\left\{\frac{e^{-jkh}}{h^2+s^2}\left[-j\,h\sinh(ks) - s\cosh(ks)\right]\right.$$

$$\left. + \sin(kh)\left[\frac{-j\cosh(ks)}{s} + \frac{j}{ks^2}\sinh(ks) + \frac{\cos(kh)\cosh(ks)}{s}\right]\right\}$$

$$- A_o\sin(kh)\left[\frac{\sinh(ka\cos\theta) - \cos\theta\sinh(ka)}{\sinh(ka)}\right];\ \text{far-field},\ ka \lesssim 1 \qquad (3.3\text{-}31)$$

where A_o and $g(s)$ are defined in Eq. (3.3-3) and Eq. (3.3-30), respectively.

The total far-field magnetic field intensity generated by the element and groundplane currents, for the case $v\to 0$, is found by substituting Eq. (3.3-3) and Eq. (3.3.-31) into Eq. (3.3-1). The resulting expression for $\lim_{v\to 0} H_\phi^{(total)}$ is in a form suitable for computer evaluation.

The radiated power density $s(\theta)$, directive gain $d(\theta)$, and radiation resistance R are found from Eqs. (2.2-4) and (2.2-7). These quantities are computed in program "BARDEEN" in Appendix B1. Computer printouts of the relative power radiation pattern $s(\theta)/s_{max}$, radiation resistance R, and the directive gain $d(\theta)$ are given in tables (A1-1 - A1-13), (A1-14 - A1-25), (A1-26 - A1-37), (A1-38 - A1-49) for normalized element lengths h/λ = 0.25, 0.1, 0.040, 0.01, respectively, and normalized groundplane radii = 0, 0.25, 0.50, ... 3.0 wavenumbers.

The radiation patterns have no appreciable change in shape for groundplane radii $0 \leq ka \lesssim 1.75$ and resemble that of a dipole in free space with peak gains approximately in the direction of the horizon and with directivities less than that of a dipole whose total element length is twice that of the monopole element length. For a quarterwave monopole element, the directive gain on the horizon deceases from 1.88 dBi for ka = 0 to 1.23 dBi for ka = 1.75.

In table 5 of Section 3.9, the radiation resistances obtained by the integral equation method are compared with those obtained by the method of moments for a quarterwave element and groundplane radii $0 \leq ka \leq 3.0$. The values, obtained by the integral equation method, differ from those obtained by the method of moments by less than 1% for $0 \leq ka \leq 1.75$ and by less than 10% for $0 \leq ka \leq 2.75$. These results suggest that the integral equation method is accurate for groundplane radii $0 \leq ka \leq 1.75$ and is useful for $0 \leq ka \leq 2.75$. It is suspected that the best available results are obtained by the integral equation method for $0 \leq ka \leq 1.0$.

3.4 Method of Moments, $0 < ka \leq 14$

In Section 3.3 it was shown that the integral equation method, for determining the fields generated by the groundplane current when the current distribution on the monopole element is initially specified, is accurate only for groundplane radii less than approximately 1.75 wavenumbers. In Section 3.5 it will be shown that the algorithms utilized in the oblate spheroidal wave function method are accurate only for groundplane radii no smaller than 3.0 wavenumbers. The question arises: What method is accurate over a range of groundplane radii which includes the region $1.75 < ka < 3.0$?

We have found that Richmond's method of moments[2] is the only method in the present literature to be accurate over a range of groundplane radii which includes the region $1.75 < ka < 3.0$. Although this method is primarily intended for use when the current distribution on the monopole element is initially unknown, this method is also applicable when the element is specified to have a sinusoidal current distribution.

This method is discussed in Section 4.2. In this method the element is subdivided into N equal segments and the groundplane is subdivided into M concentric annular zones of equal width. The unknown current distributions on the element and groundplane are expanded as a series of N + M overlapping sinusoidal dipole modes (sinusoidal-Galerkin method) each with an unknown current distribution. The N + M currents are determined by inversion of a $(N + M) \times (N + M)$ matrix. The numbers of subdivisions, N and M, are

limited by the cost of computation time and by the precision of the computer. The accuracy of the solution can be decreased appreciably if either N or M is too small or too large. The method of moments converges to a solution when an increase or decrease of unity in the value of N or M does not appreciably alter the solution for input impedance.

A particularly useful property of the sinusoidal - Galerkin method is the sinusoidal current distribution which is imposed on the element by setting N=1.

The input impedance and radiation pattern of thin quarterwave elements ($b/\lambda = 10^{-6}$, $h/\lambda = 0.25$), for groundplane radii $0 < ka \leq 14$ wave numbers, were determined by Richmond's method of moments by utilizing MITRE programs "RICHMD1" and "RICHMD2" which are discussed in Section 4.2 and listed in Appendix B5. With N=1, convergent solutions were obtained for values of M given by:

$M = 3$, $ka = 0.25$
$M = 7$, $ka = 0.50$
$M = 16$, $ka = 0.75, 1.0 \ldots\ldots 8.5$
$M = 3\ ka$, $ka = 8.75, 9.0, \ldots\ldots 14.0$.

Computer printouts of the input admittance, groundplane current distribution, radiation resistance, directive gain, and radiation patterns are given in Appendix A5.

The input resistance and reactance -- as determined by the method of moments or methods which give similar results -- are plotted for thin quarterwave elements on groundplanes of radii $0 \leq ka \leq 14$ in

figures 9 and 10 of Section 3.9. The directive gain on the horizon, peak directivity, and elevation angle of the peak directivity given by the computer printouts of Appendix A5 are plotted in figures 11 - 13 of Section 3.9.

The input impedance of thin elements with a sinusoidal current distribution were also determined for element lengths $h/\lambda = 0.1$ and 0.025 and groundplane radii $0 < ka \leq 8.0$ wavenumbers by utilizing program RICHMD1 with N=1. The radiation resistance of these elements is compared in figure 14 of Section 3.9 with those of a quarterwave element. In figure 14 the radiation resistance is normalized to the value of radiation resistance of each element for $ka = 0$.

Values of the radiation resistance for quarterwave elements are determined in Appendix A5 by matrix inversion (program RICHMD1) and also by the far-field radiation pattern (program RICHMD2). The values determined by both methods differ by less than 1% for small groundplane radii and differ by less than 3% for the larger groundplane radii.

The values of radiation resistance obtained from program RICHMD2 are compared in table 5 of Section 3.9 with the values obtained by the integral equation method and the oblate spheroidal wave function method. Richmond's method of moments gives useful results over the entire range $0 < ka \leq 14$ and gives good agreement with the integral equation method for $0 < ka \leq 1.75$ and with the oblate spheroidal wave function method for $3.0 \leq ka \leq 6.5$. Whereas the method of moments gives useful results in the regions $1.75 < ka < 3.0$ and $6.5 < ka \leq 14$, the other methods fail in these regions. For $ka > 14$, Richmond's method of moments is not as useful because of increased computation time and decreased accuracy. It is suspected that for thin monopole

elements the best available results are obtained by the method of moments for $1.25 \leq ka \leq 2.75$ and $6.75 \leq ka \leq 14$. For relatively thick monopole elements, Richmond's method of moments gives the best available results for groundplane radii $0 < ka \leq 14$ as discussed in Section 4.2.

3.5 Oblate Spheroidal Wave Functions, $3.0 \leq ka \leq 6.5$

Oblate spheroidal coordinates (see table 1 in Section 2.1) are particularly convenient for handling the boundary conditions of the magnetic field intensity on the groundplane. The requirement for constant tangential magnetic field intensity across the upper and lower hemispheres at the groundplane interface may be specified at all points of the groundplane disc by a boundary condition at only the oblate "radial" coordinate $\xi = 0$.

For groundplane radii of the same order of magnitude as the excitation wavelength, Leitner and Spence[3]-[5] utilized oblate spheroidal wave functions to determine the groundplane current induced by a thin quarterwave element with a sinusoidal current distribution. Leitner and Spence give numerical values of the groundplane current distribution, radiation resistance, and far-field power density (at constant element base current) for groundplane radii $ka = 3, 4, 5, \sqrt{42}$ wavenumbers. The complex current distributions on both the top and bottom faces of the groundplane are reported.

In this section, we report the results of a computer program "MONOPL," based on the theory of Leitner and Spence, which calculates the directivity pattern and radiation resistance for groundplane radii including the cases $ka = 3, 4, 5, \sqrt{42}$ wavenumbers. Our results are consistent with (but not identical to) the results reported by Leitner and Spence. The form of the solution, corrections, regions of calculation validity, accuracy, and numerical results of program MONOPL are discussed in the remainder of this section.

Form of Solution

For a quarterwave monopole ($h = \lambda/4$), the far-field power density $s'(\eta)$ and radiation resistance R, expressed in oblate spheroidal wave functions, are given with reference to figure 1 of Section 2.1, by[5]

$$s'(\eta) = [I^2(0)/8\pi^2 r^2]\ (\mu_o/\epsilon_o)^{1/2}\ \epsilon^4\ \left|\ \sum_{\ell=1}^{\infty} B_\ell\ u_{\ell 1}\ (\eta)\right|^2 \qquad (3.5\text{-}1)$$

$$R = (1/2\pi)\ (\mu_o/\epsilon_o)^{1/2}\ \epsilon^4 \sum_{\ell=1}^{\infty} N_{\ell 1}\ \ |B_\ell|^2 \ \text{ ohms} \qquad (3.5\text{-}2)$$

where

$(\mu_o/\epsilon_o)^{1/2}$ = wave impedance in free-space (ohms)

$\epsilon \equiv ka = 2\pi a/\lambda$ = groundplane radius (wavenumbers)

$u_{\ell 1}(\eta)$ = angular oblate spheroidal wave function of order one and degree ℓ

$$N_{\ell 1} = \int_{-1}^{1} u^2_{\ell 1}(\eta)d\eta = \text{norm of } u_{\ell 1}(\eta)$$

$$_2w_{\ell 1}(\xi) = (1 + \xi^2)^{1/2}\ \ _2v_{\ell 1}(\xi)$$

$$B_\ell = (-1)^{\ell-1}\ _2w_{\ell 1}(\pi/2\epsilon)\Big/\alpha_{\ell 1} N_{\ell 1} q_{\ell 1}\ \ ^{(3)}v_{\ell 1}'(0)$$

The reader is referred to reference [3] for a definition of the oblate spheroidal wave functions $\alpha_{\ell 1}$, $q_{\ell 1}$, $^{(3)}v_{\ell 1}'(\xi)$, and $_2v_{\ell 1}(\xi)$.

Substitution of Eqs. (3.5-1) and (3.5-2) into Eq. (2.2-4) yields the directivity $d'(\eta)$ given by

$$d'(\eta) = 2 \left| \sum_{\ell=1}^{\infty} B_\ell \, u_{\ell 1}(\eta) \right|^2 / \sum_{\ell=1}^{\infty} N_{\ell 1} \, |B_\ell|^2 \qquad (3.5\text{-}3)$$

Corrections

Problems were encountered in generating the eigenvalues of the oblate spheroidal wave functions. These problems were narrowed down to the continued fractions that generate the eigenvalues. These continued fractions were derived from the recurrence relations which in turn come from the differential equation. A discrepancy was discovered between our derived continued fractions and the published continued fractions [3] . The corrected continued fractions appear below.

$\ell - m$ even

$$\gamma_{\ell m} = \cfrac{-(\ell+m)(\ell-m)\,\epsilon^2}{2(2\ell-1)+\gamma_{\ell m} + \cfrac{(\ell+m-2)(\ell-m-2)\,\epsilon^2}{4(2\ell-3)+\gamma_{\ell m} + \cfrac{(\ell+m-4)(\ell-m-4)\,\epsilon^2}{6(2\ell-5)+\gamma_{\ell m} + \ddots}}}$$

$$+ \cfrac{(\ell+m+2)(\ell-m+2)\,\epsilon^2}{2(2\ell+3)-\gamma_{\ell m} + \cfrac{(\ell+m+4)(\ell-m-4)\,\epsilon^2}{4(2\ell+5)-\gamma_{\ell m} + \cfrac{(\ell+m+6)(\ell-m+6)\,\epsilon^2}{6(2\ell+7)-\gamma_{\ell m} + \ddots}}} \qquad (3.5\text{-}4)$$

ℓ - m odd

$$\gamma_{\ell m} = \cfrac{-(\ell+m-1)(\ell-m-1)\,\epsilon^2}{2(2\ell-1)+\gamma_{\ell m} + \cfrac{(\ell+m-3)(\ell-m-3)\,\epsilon^2}{4(2\ell-3)+\gamma_{\ell m} + \cfrac{(\ell+m-5)(\ell-m-5)\,\epsilon^2}{6(2\ell-5)+\gamma_{\ell m} + \ddots}}}$$

$$+ \cfrac{(\ell+m+1)(\ell-m+1)\,\epsilon^2}{2(2\ell+3)-\gamma_{\ell m} + \cfrac{(\ell+m+3)(\ell-m+3)\,\epsilon^2}{4(2\ell+5)-\gamma_{\ell m} + \cfrac{(\ell+m+5)(\ell-m+5)\,\epsilon^2}{6(2\ell+7)-\gamma_{\ell m} + \ddots}}} \qquad (3.5\text{-}5)$$

The eigenvalues can also be expressed in terms of a series expansion, which has the form

$$\gamma_{\ell m} = \sum_{k=1}^{\infty} f_{2k}^{\ell m} \epsilon^{2k} \qquad (3.5\text{-}6)$$

The first two terms in this expansion were checked against the continued fractions and were found to agree. This is important, since the continued fraction method by which values of the eigenvalues are obtained depends upon the accuracy of the roots $\gamma_{\ell m}$ in equation (3.5-6).

Regions of Calculation Validity

A lower bound on the value of $\epsilon = 2\pi a/\lambda$ for which the calculations are valid depends upon the following equations [see Eqs. (34) and (48) of Ref. 3]:

$$^{(1)}v_{\ell 1}(\xi) = (1+\xi^2)^{1/2} \sum_{n=0,1}{}' a_n^{\ell 1} \xi^n \quad \text{for } \xi = \pi/2\epsilon \qquad (3.5\text{-}7)$$

and

$$g_{\ell 1}(\xi) = (1+\xi^2)^{-1/2} \sum_{n=0,1}{}' b_n^{\ell 1} \xi^n \quad \text{for } \xi = \pi/2\epsilon \qquad (3.5\text{-}8)$$

where the prime indicates summation over alternate n, starting with n=0 if $(\ell - 1)$ is even, with n=1 if $(\ell - 1)$ is odd.

Eq. (3.5-7) is the expression for the first order radial spheroidal wave function of the first kind. Eq. (3.5-8) is used in another expression to obtain the first order radial spheroidal wave function of the second kind. As ϵ becomes small, ξ becomes large, so more terms are needed in Eqs. (3.5-7) and (3.5-8). In theory, Eq. (3.5-7) and (3.5-8) converge for all real values of $\xi = \pi/2\epsilon$. Computationally, however, because of the finite accuracy of the computer, Eqs. (3.5-7) and (3.5-8) will not converge for all real values of $\xi = \pi/2\epsilon$. To be on the safe side, we can restrict ξ so that ξ is less than unity. With this assumption, we get the computational constraint $\xi = \pi/2\epsilon < 1$ which implies a lower bound on ϵ given by $\epsilon > \pi/2 \approx 1.57$.

An even tighter lower bound on ϵ is obtained by observing what happens in the algorithm that is used to obtain the eigenvalues. This algorithm is not well behaved for values of ϵ less than $\epsilon = 2.5$. Therefore ϵ is lower bounded by $\epsilon \geq 2.5$. For accurate values of radiation resistance, ϵ is lower bounded by $\epsilon \geq 3.0$ (see table B of Section 3.9).

An upper bound on ϵ is obtained by observing what happens in the continued fraction algorithm that is used to obtain the eigenvalues. For values of ϵ greater than 6.5, the series expansion for the eigenvalues, given by Eq. (3.5-6), does not give an accurate enough answer using only the first four terms. The resulting values for the eigenvalue are far enough from the correct eigenvalues to cause the continued fraction algorithm of Eqs. (3.5-4) and (3.5-5) to converge to a root which is not the eigenvalue. As a consequence, erroneous values of radiation resistance can be obtained for $\epsilon > 6.5$ (see table 5 of Section 3.9).

Consequently, the range of ϵ for which Leitner and Spence's method of oblate spheroidal wave functions is useful is $2.5 \leq \epsilon \leq 6.5$. It is suspected that the best available results are obtained by the method of oblate spheroidal wave functions for $3.0 \leq \epsilon \leq 6.5$.

Accuracy

There are many equations involved in the calculation of directivity and radiation resistance. Some of these equations involve series expansions. When we varied the number of terms in these series, the radiation resistance was found to vary only in the fifth or sixth significant figure.

Another problem that was mentioned previously was the accuracy by which Eq. (3.5-6) computes the eigenvalues. Because of computational reasons, only the first four terms in Eq. (3.5-6) were used. Because of this, a raw eigenvalue is computed using Eq. (3.5-6), which is then used as an initial guess in the continued fractions. The continued fractions have many roots in $\gamma_{\ell m}$. The number of roots is dependent upon the number of fraction terms used in the continued fraction. Only one of these roots however can be the eigenvalue. If the raw eigenvalue is far enough from the correct eigenvalue then the continued fraction will converge to a root which is not an eigenvalue. This will produce wrong results.

The eigenvalues that were computed were checked against published values[24]. The computed values were found to be within the percentage error of the published values.

The computed values of directivity on the horizon and radiation resistance, for different values of groundplane extent, were found to agree with the relationship given by Eq. (2.3-3) to at least five places after the decimal point for the free space wave impedance η = 376.73037 ohms.

Numerical Results

The far-field power density $s'(\eta)$, radiation resistance R, and directive gain $d'(\eta)$ of quarterwave elements given by Eqs. (3.5-1), (3.5-2) and (3.5-3), respectively, were numerically evaluated by program MONOPL written in FORTRAN 77 language for use on a DEC PDP-11/70 computer. The program listing is given in Appendix B3. Numerical values were obtained for the cases $2.5 \leq ka \leq \sqrt{42}$.

The computed eigenvalues are given in table 2. Computer printouts of the directivity patterns are given in Appendix A3 for ka = 3, 4, 5, $\sqrt{42}$. The patterns are plotted in figure 8 of Section 3.9 as polar graphs on the same linear scale. In these plots the total radiated power is held constant.

The directional gain on the horizon, radiation resistance and peak directivity are summarized in table 3.

Table 2. Eigenvalues $\gamma_{\ell 1}$ For $2\pi a/\lambda = 3,4,5,\sqrt{42}$

ℓ	$\gamma_{\ell 1}$			
	$2\pi a/\lambda = \epsilon = 3$	$\epsilon = 4$	$\epsilon = 5$	$\epsilon = \sqrt{42}$
1	6.7305791912	11.0907992567	15.056611686	21.687439619
2	4.8215414322	8.1301387077	11.872162474	17.738230003
3	5.0070741733	9.4059031099	15.750367134	28.127723151
4	4.7772522576	8.6287184908	13.694959245	23.237303490
5	4.6896340053	8.4462229270	13.439315734	23.585994650
6	4.6368101196	8.3210439564	13.161309568	22.624607030
7	4.6032991570	8.2427831207	12.999910517	22.234563635
8	4.5807102835	8.1899480807	12.890952874	21.960565094
9	4.5647761329	8.1526212369	12.814155253	21.770549914
10	4.5531234272	8.1252813999	12.757940027	21.632114595

Table 3

Directive Gain on Horizon and Radiation Resistance of Quarterwave Element, $2.5 \leq 2\pi a/\lambda \leq \sqrt{42}$.

Groundplane radius, $\epsilon = 2\pi a/\lambda$ (Wavenumbers)	Directive Gain on Horizon		Radiation Resistance, R (ohms)		Peak Directivity	
	$d(\pi/2)$ (numeric)	$D(\pi/2) = 10 \log_{10} d(\pi/2)$ (dBi)	Program MONOPL	Leitner*	D_{peak} (dBi)	θ_{peak} (degrees)
2.5	1.09745	0.40383	27.31731			
3.0	0.79995	-0.96938	37.47646	39.32	2.52250	46
3.4	0.66233	-1.78923	45.26299			
3.5	0.65086	-1.86515	46.06128			
3.6	0.64812	-1.88346	46.25589			
3.7	0.65316	-1.84980	45.89866			
4.0	0.70254	-1.53326	42.67237	42.10	3.89943	40
4.5	0.82743	-0.82271	36.23191			
5.0	0.92059	-0.35934	32.56526	31.87	3.37175	36
5.25	0.93879	-0.27430	31.93379			
5.5	0.93294	-0.30146	32.13410			
6.0	0.85088	-0.70134	35.23337			
$\sqrt{42}$	0.74637	-1.27045	40.16661	39.88	2.55213	56

* Research Report No. EM-19, New York University, Washington Square College, April 1950.

3.6 Scalar Diffraction Theory, Geometric Theory of Diffraction, $6.5 \lesssim ka < \infty$

For an element on a groundplane of sufficiently large radius, Tang[6] utilized a scalar theory of diffraction to calculate the far-field elevation pattern. For elevation angles near the horizon ($\theta \approx \pi/2$) the far-field magnetic field intensity is determined by linear extrapolation to the result for the element itself given by Eq. (3.2-10) with $\theta = \pi/2$ rad. Tang's method for the radiation pattern is more accurate than that obtained by the variational method of Section 3.7 because it includes an additional term in the expansion for the total magnetic field intensity. Since the variational method is useful for groundplane radii as small as ka=30 wavenumbers, Tang's method should be useful for even smaller groundplane radii provided $ka \gg 1$.

The geometric theory of diffraction (GTD) is another method which is applicable for sufficiently large groundplane radii. In GTD, the fields are determined by ray optics (an incident ray plus a reflected ray) and diffraction by the edge. However, the effect of edge diffraction is only approximated because in GTD the edge is treated point by point as though it were a straight knife edge of infinite extent. For this reason, GTD may be applied to an element at the center of a circular groundplane only when the groundplane is of sufficiently large radius. The method of GTD is reviewed by Balanis[27] who also gives a computer program for calculating the diffraction coefficient.

In Section 4.3, the method of moments combined with GTD yields results for input impedance which are useful for groundplanes of radii $ka \gtrsim 6$ wavenumbers and are accurate for $ka > 8$. Therefore, when the element current distribution is constrained to be sinusoidal, the method of GTD is expected to give useful results for groundplane radii $ka \gtrsim 6.5$ wavenumbers over which range the method of oblate spheroidal wave functions does not give useful results.

3.7 Variational Method, $30 \lesssim ka < \infty$

For an element on a groundplane of very large radius ($ka \gtrsim 30$ wavenumbers), differences in the input impedance and radiation pattern from that for a groundplane of infinite extent may be determined by utilizing a variational method of Storer[7],[8].

With reference to figure 1 of Section 2.1 and for a sinusoidal current distribution on the element given by Eq. (3.1-1), the input impedance difference is given by Eq. (20) of [7] as

$$Z_{in} - Z_{\infty} = \frac{-j\eta \exp(j2ka)}{4\pi ka} \left[\frac{1 - \cos(kh)}{\sin(kh)}\right]^2 \left\{1 + \frac{\exp[j(2ka + 3\pi/4)]}{(4\pi ka)^{1/2}}\right\}^{-1} \qquad ka \gtrsim 30 \qquad (3.7\text{-}1)$$

where

Z_{in} = input impedance for an element on a groundplane of radius ka wavenumbers (ohms)

Z_{∞} = input impedance for the same element on a groundplane of radius ka $= \infty$ wavenumbers (ohms)

η = wave impedance in free space = 376.73037 ohms

Since $(4\pi ka)^{1/2} \gg 1$ for $ka \gtrsim 30$, the input resistance difference $R_{in} - R_{\infty}$ and input reactance difference $X_{in} - X_{\infty}$ are given approximately by

$$R_{in} - R_{\infty} \approx \left[\frac{1 - \cos(kh)}{\sin(kh)}\right]^2 \frac{\sin(2ka)}{4\pi ka}, \quad ka \gtrsim 30 \qquad (3.7\text{-}2)$$

$$X_{in} - X_{\infty} \approx \left[\frac{1 - \cos(kh)}{\sin(kh)}\right]^2 \frac{\cos(2ka)}{4\pi ka}, \quad ka \gtrsim 30 \qquad (3.7\text{-}3)$$

The maxima, nulls, and minima of $R_{in} - R$ occur for values of ka given approximately by

$$ka = \begin{cases} (2N + \frac{1}{2})(\pi/2) & \text{(maxima)} \\ N(\pi/2) & \text{(nulls)} \\ (2N + \frac{3}{2})(\pi/2) & \text{(minima)} \end{cases}, \quad N = 0,1,2,..... \tag{3.7-4}$$

The input impedance $Z_{in} - Z_{\infty}$ given by Eq. (3.7-1) is calculated in computer program "MONOSTOR" whose listing is given in Appendix B-4.

For very thin quarterwave elements, $R_{\infty} = 36.54$ ohms and $X_{\infty} = 21.26$ ohms (see Section 3.8). The numeric directivity on the horizon, $d(\pi/2)$, is related to the radiation resistance $R = R_{in}$ by Eq. (2.3-2). Computer printouts of the maxima and minima of $R_{in} - R_{\infty}$, $X_{in} - X_{\infty}$ are given in Appendix A4. For very thin quarterwave elements, Appendix A5 also gives computer printouts of R_{in}, X_{in}, $d(\pi/2)$, and $D(\pi/2) = 10 \log_{10} d(\pi/2)$.

Differences in the far-field radiation pattern from that for a groundplane of infinite extent are given in [8]. For the waveform of Eq. (2.1-2) and an element sinusoidal current distribution I(z) (see figure 1 of Section 2.1), the difference in the far-field magnetic field intensity is given by Eq. (6) of [8] as

$$H_\phi - H_\phi|_{ka=\infty} = \text{sgn}\ \theta \left[\frac{j\ I(0)\ \exp(-jkr)\ [1-\cos(kh)]}{\sin(kh)\ 2\pi r \cdot 2\pi\sqrt{2}} \right] \left[\int_0^{2\pi} \frac{\exp[-jka(1-\sin\theta\ \cos\phi)]\ \cos\phi}{(1-\sin\theta\ \cos\phi)^{1/2}}\ d\phi \right], \quad ka \gtrsim 30 \tag{3.7-5}$$

where

H_ϕ = far-field magnetic field intensity for an element on a groundplane of radius ka wavenumbers (amp/m)

$H_\phi|_{ka=\infty}$ = far-field magnetic field intensity for an element on a groundplane of infinite extent (amp/m)

$$\text{sgn}\ \theta = \begin{cases} +1, & 0 \leq \theta < \pi/2 \\ 0 & \\ -1, & \pi/2 < \theta \leq \pi \end{cases}$$

The magnetic field intensity $H_\phi|_{ka=\infty}$ is given by (see Section 3.8)

$$H_\phi|_{ka=\infty} = \begin{cases} \dfrac{j\ I(0)\ \exp(-jkr)}{\sin(kh)\ \ 2\pi r} \left[\dfrac{\cos(kh\ \cos\theta) - \cos(kh)}{\sin\theta} \right], & 0 \leq \theta \leq \pi/2 \\ 0, & \pi/2 < \theta \leq \pi \end{cases} \tag{3.7-6}$$

The far-field electric field intensity $E_\theta = \eta H_\phi$ where H_ϕ is given by Eq (3.7-5) and η is the free-space wave impedance.

One of the distinguishing features of the far-field radiation pattern for groundplane of large radii is the occurrence of a fine-structured lobing pattern, $H_\phi - H_\phi|_{ka=\infty}$, superimposed on the pattern for a groundplane of infinite extent. The lobing pattern, given by Eq. (3.7-5), is symmetrical about the horizon (expect for a phase shift of π rad) with the most prominent lobes near the zenith and nadir directions. The n^{th} maximum of the lobing pattern in each quardrant decreases with increasing values of n where n=1 corresponds to the lobe nearest the zenith or nadir direction.

The lobing structure is characterized in [8] by the elevation angle θ_n of the n^{th} maxima, the angular separation $\Delta\theta$ between lobes, the angle θ_{max} within which all prominent maxima occur, and the number N of prominent lobes. The elevation angle θ_n in radians is given approximately by

$$\theta_n \approx \begin{cases} 0.59\ (\pi/ka), \ n=1 \\ \\ (n + 0.75)(\pi/ka), \ n = 2, 3, \ldots .N \end{cases} , \ ka \gtrsim 30 \qquad (3.7\text{-}7)$$

The angular separation $\Delta\theta$ in radians is given approximately by

$$\Delta\theta \approx \begin{cases} 1.16\ (\pi/ka), \ n=1 \\ \\ \pi/ka, \ n = 2, 3, \ldots .N \end{cases} , \ ka \gtrsim 30 \qquad (3.7\text{-}8)$$

Prominent lobes are defined in [8] as lobes whose maxima are less than one-fourth the amplitude for that of a groundplane of infinite extent. The angle θ_{max} in radians is given approximately by

$$\theta_{max} \approx 1.87\ (\pi/ka)^{1/3} \left[\frac{1 - \cos(kh)}{kh \sin(kh)}\right]^{2/3} , \quad ka \gtrsim 30 \qquad (3.7\text{-}9)$$

The number N of prominent lobes is determined by

$$\theta_{max} = \theta_1 + (\Delta\theta)_{n=1} + (N-2)(\Delta\theta)_{n\neq 1} , \quad ka \gtrsim 30 \qquad (3.7\text{-}10)$$

where $\theta_1, \Delta\theta$, and θ_{max} are given by Eqs. (3.7-7) - (3.7-9), respectively.

Solving for N,

$$N = [\theta_{max}/(\pi/ka)] - 0.25 = 1.87(\pi/ka)^{-2/3} - 0.25, \ ka \gtrsim 30 \qquad (3.7\text{-}11)$$

3.8 Method of Images, ka = ∞

For the idealized case of a monopole element mounted on a groundplane of infinite extent and of infinite conductivity, the monopole antenna may be modelled by the method of images as a dipole with one-half the input impedance and double the peak numeric directivity of the dipole.[25] The infinite groundplane prevents monopole radiation into the hemisphere below the groundplane but allows a radiation pattern identical to that of the dipole in the upper hemisphere.

In this section, it is assumed that the current has a waveform given by Eq. (2.1-2) and a current distribution I(z) on the element and its image (see figure 7) given by

$$I(z) = \begin{cases} [I(0)/\sin(kh)]\ \sin[k(h-z)], & 0 \le z \le h \text{ (element)} \\ [I(0)/\sin(kh)]\ \sin[k(h+z)], & -h \le z \le 0 \text{ (image)} \end{cases} \qquad (3.8\text{-}1)$$

The near-fields, far-fields, and input impedance of an electrically-thin element on a groundplane of infinite-extent are summarized in the remainder of this section.

Near-fields

The exact magnetic field intensity $\vec{H} = \hat{u}_\phi H_\phi$ and electric field intensity $\vec{E} = \hat{u}_\rho E_\rho + \hat{u}_z E_z$ for an infinitely thin element are given with reference to Eqs. (7-15) and (7-17) of [25], as

$$H_\phi = \begin{cases} \dfrac{j\ I(0)}{4\pi\rho\ \sin(kh)} \left[\exp(-jkR_1) + \exp(-jkR_2) - 2\cos(kh)\ \exp(-jkr)\right], & z \ge 0 \\ 0, & z < 0 \end{cases} \qquad (3.8\text{-}2)$$

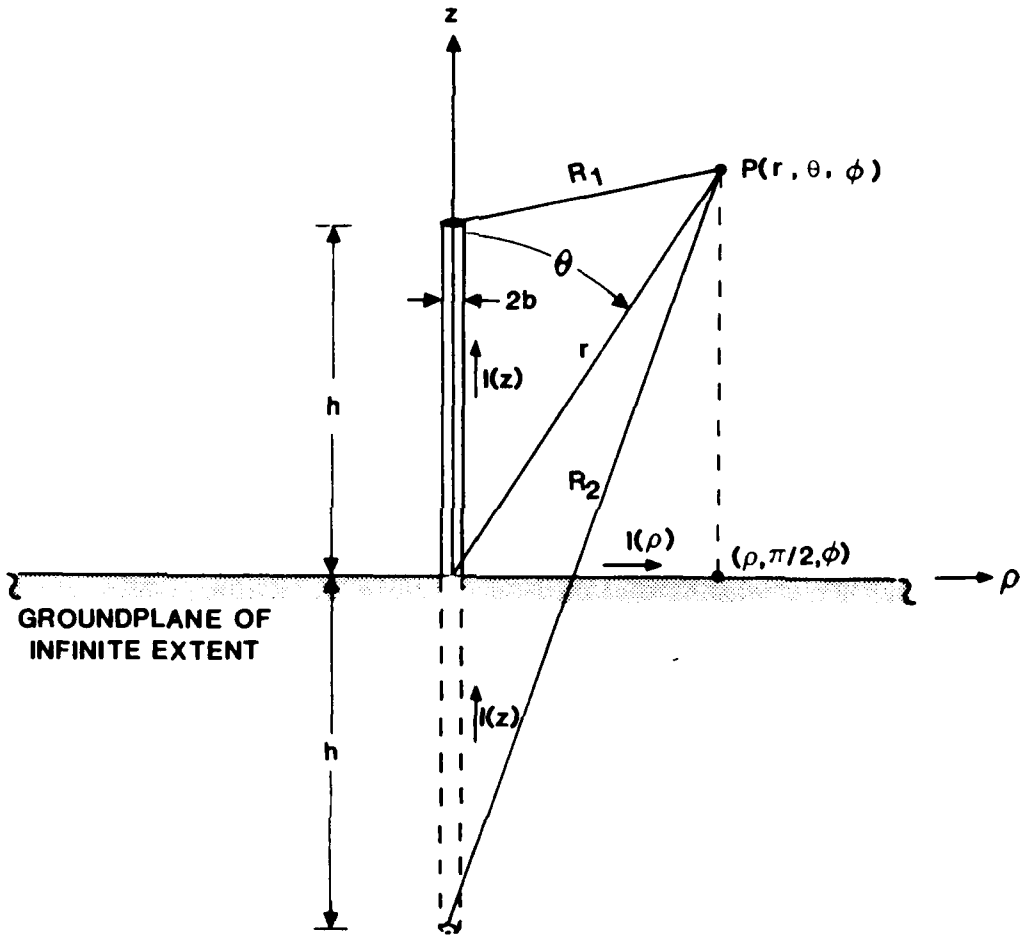

Figure 7. Method of Images for a Monopole Element at the Center of a Circular Groundplane of Infinite Extent

$$E_\rho = \begin{cases} \dfrac{j\eta I(0)}{4\pi\rho \sin(kh)}\left[\dfrac{(z-h)\exp(-jkR_1)}{R_1} + \dfrac{(z+h)\exp(-jkR_2)}{R_2} - 2z\cos(kh)\dfrac{\exp(-jkr)}{r}\right], & z \geq 0 \\ 0, & z < 0 \end{cases} \quad (3.8\text{-}3)$$

$$E_z = \begin{cases} \dfrac{-j\eta I(0)}{4\pi \sin(kh)}\left[\dfrac{\exp(-jkR_1)}{R_1} + \dfrac{\exp(-jkR_2)}{R_2} - 2\cos(kh)\dfrac{\exp(-jkr)}{r}\right], & z \geq 0 \\ 0, & z < 0 \end{cases} \quad (3.8\text{-}4)$$

where

$$R_1 = [\rho^2 + (z-h)^2]^{1/2}$$
$$R_2 = [\rho^2 + (z+h)^2]^{1/2}$$

The magnetic field intensity at the top and bottom surfaces of the groundplane are given by Eq. (3.8-2) as

$$H_\phi|_{z=0_+} = \frac{j\, I(0)}{2\pi\rho \sin(kh)}\left[\exp(-jkR_3) - \cos(kh)\exp(-jk\rho)\right], \quad \text{top of groundplane} \quad (3.8\text{-}5)$$

$$H_\phi|_{z=0_-} = 0, \text{ bottom of groundplane} \quad (3.8\text{-}6)$$

where

$$R_3 = (\rho^2 + h^2)^{1/2}$$

The incremental groundplane current $\Delta I(\rho)$ contained within a differential azimuthal angle $d\phi$ may be determined from Eqs. (3.8-5), (3.8-6), and Ampere's circuital law applied to a closed path along the top and bottom surfaces of the groundplane along arc lengths within $d\phi$. Since the groundplane current $I(\rho)$ is defined to be positive in the positive ρ direction (see figure 1 of Section 2.1), the path is taken in the clockwise direction.

Accordingly,

$$\Delta I(\rho) = (-\hat{u}_\phi \cdot \vec{H}_{top} + \hat{u}_\phi \cdot \vec{H}_{bottom})\ \rho\ d\phi = [-H_\phi|_{z=0+} + H_\phi|_{z=0-}]\ \rho\ d\phi \tag{3.8-7}$$

The total groundplane current $I(\rho)$ is given by

$$I(\rho) = \int_0^{2\pi} \Delta I(\rho)\ d\phi = 2\pi\rho\,[-H_\phi|_{z=0+} + H_\phi|_{z=0-}]$$

$$= \frac{j\ I(0)}{\sin(kh)}\ [\cos(kh)\ \exp(-jk\rho) - \exp(-jkR_3)] \tag{3.8-8}$$

Eq. (3.8-8) agrees with that given by Eq. (33) of [2].

Far-fields

For the far-field conditions given by Eqs. (3.2-7) and (3.2-8), Eqs. (3.8-2) - (3.8-4) reduce to the far-fields $\vec{H}=\hat{u}_\phi H_\phi$ and $\vec{E}=\hat{u}_\theta E_\theta=\hat{u}_\theta \eta H_\theta$ where, with reference to Eq. (4-62) in [25], H_ϕ is given by

$$H_\phi = \begin{cases} \dfrac{j\ I(0)\ \exp(-jkr)}{\sin(kh)\ 2\pi r}\ \left[\dfrac{\cos(kh\ \cos\theta) - \cos(kh)}{\sin\theta}\right], & 0 \le \theta \le \pi/2 \\ 0, & \pi/2 < \theta \le \pi \end{cases} \tag{3.8-9}$$

The time-averaged radiated power density $s(\theta) = (\eta/2)|H_\phi|^2$ is given by

$$s(\theta) = \begin{cases} \dfrac{\eta |I(0)|^2\ f(\theta)}{8\pi^2 r^2\ \sin^2(kh)}, & 0 \le \theta \le \pi/2 \\ 0, & \pi/2 < \theta \le \pi \end{cases} \tag{3.8-10}$$

where

$$f(\theta) = \left[\frac{\cos(kh\ \cos\theta) - \cos(kh)}{\sin\theta}\right]^2$$

The direction of maximum radiated power is $\theta = \pi/2$ rad.

The input impedance of a monopole element of length h on a groundplane of infinite extent is one-half that of a dipole of total length 2h in free space. Accordingly, the radiation resistance R of an infinitely thin element on a groundplane of infinite extent is given by [compare with Eqs. (4-70) and (4-79) in [25]]

$$R = \frac{\eta}{4\pi \sin^2(kh)} \left\{ \mathrm{Cin}(2kh) + \frac{1}{2} \sin(2kh)[\mathrm{Si}(4kh) - 2\,\mathrm{Si}(2kh)] + \frac{1}{2} \cos(2kh)[2\,\mathrm{Cin}(2kh) - \mathrm{Cin}(4kh)] \right\}, \quad h=0 \tag{3.8-11}$$

where Si(x) and Cin(x) are the sine integral and modified cosine integrals, respectively, which are defined following Eq. (3.2-32). Eq. (3.8-9) is also approximately valid for thin elements ($kb \ll 1$). [For example, compare Eqs. (3.2-33) and (3.2-35) for a thin monopole element in the absence of a groundplane.]

Substituting Eqs. (3.8-10) and (3.8-11) into Eq. (2.2-8), the numeric directive gain $d(\theta)$ is given by

$$d(\theta) = \frac{4\, f(\theta)}{B} \tag{3.8-12}$$

where

$$B \equiv \mathrm{Cin}(2kh) + \frac{1}{2} \sin(2kh)[\mathrm{Si}(4kh) - 2\,\mathrm{Si}(2kh)] + \frac{1}{2} \cos(2kh)[2\,\mathrm{Cin}(2kh) - \mathrm{Cin}(4kh)]$$

For a quarterwave monopole element ($kh=\pi/2$), Eqs. (3.8-11) and (3.8-12) reduce to

$$R = \frac{\eta}{4\pi} \quad \frac{Cin(2\pi)}{2} = 36.5395 \text{ ohms; } kh=\pi/2, \; b=0 \tag{3.8-13}$$

$$f(\theta) = \frac{\cos^2[(\pi/2)\cos\theta]}{\sin^2\theta} \quad , \; kh=\pi/2 \tag{3.8-14}$$

$$d(\theta) = \frac{4\cos^2[(\pi/2)\cos\theta]}{\sin^2\theta} \cdot \frac{2}{Cin(2\pi)} \quad , \; kh=\pi/2 \tag{3.8-15}$$

The peak numeric directivity $d(\pi/2) = 3.2818$ corresponding to $D(\pi/2) = 10 \log_{10} d(\pi/2) = 5.1612$ dBi. The directional gain is plotted in figure 8(f) of Section 3.9.

For an electrically short monopole element ($kh << 1$) and $\eta \approx 120\pi$ ohms, Eqs. (3.8-11) and (3.8-12) reduce to

$$R = 10\,(kh)^2, \qquad (kh) << 1 \tag{3.8-16}$$

$$f(\theta) = \frac{(kh)^4}{4} \sin^2\theta, \qquad (kh) << 1 \tag{3.8-17}$$

$$d(\theta) = 3 \sin\theta, \qquad (kh) << 1 \tag{3.8-18}$$

The peak numeric directivity $d(\pi/2) = 3.0$ corresponding to $D(\pi/2) = 10 \log_{10} d(\pi/2) = 4.7712$ dBi.

Input Impedance

The input resistance R_{in} is given by Eq. (3.8-11) which is exact for an infinitely thin element and approximately correct for thin elements provided that the element current distribution is sinusoidal.

The input reactance X_{in} for thin elements ($kb << 1$) is given by [compare with Eqs. (7-33) and (7-30) in [25]

$$X_{in} = \frac{\eta}{4\pi\sin^2(kh)}\Big\{Si(2kh) + \cos(2kh)[Si(2kh) - \tfrac{1}{2}\,Si(4kh)]$$

$$- \sin(2kh)[\ln(h/b) - Cin(2kh) + \tfrac{1}{2}\,Cin(4kh) + \tfrac{1}{2}\,Cin(kb^2/h)]\Big\} \qquad (3.8\text{-}19)$$

For a quarterwave element, in the limit $b \to 0$, Eq. (3.8-19) gives an input reactance $X_{in} = 21.2576$ ohms. In Eq. (3.8-19), $X_{in}=0$ for element lengths slightly less than $kh = (2n-1)(\pi/2)$, $n=1, 2, 3, \ldots$, which are approximately one-half the resonant lengths for a monopole element with no groundplane [see Eq. (3.2-38)].

3.9 Summary of Results

In Section 3 a sinusoidal current distribution is assumed on the monopole element. Although such a current distribution is never exactly realized even for an infinitely thin element (see Section 3.1), it is a useful approximation for sufficiently thin elements. For example, for a quarterwave element of radius $b=10^{-6}\lambda$, the input impedances computed by determining the actual element current distribution and that computed by assuming a sinusoidal current distribution differ by no more than 5% for groundplane radii $ka = 6 - 14$ (compare table 7 of Section 4.5 with tables A2-24 - A2-42 of Appendix A). The assumption of a sinusoidal element current distribution allows for models which are computationally simpler in determining input impedance and radiation patterns than the models which follow in Section 4. The results of these simpler models are summarized in this section.

The electrical properties of electrically-short and quarterwave monopole elements on groundplanes of zero, large, and infinite extent are compared in table 4 with the corresponding properties of

ANTENNA STRUCTURE	GROUNDPLANE RADIUS (WAVENUMBERS) $2\pi a/\lambda$	ELEMENT LENGTH (WAVELENGTHS) h/λ	PEAK DIRECTIVITY *		DIRECTIVITY ON HORIZON		INPUT IMPEDANCE		REFERENCE EQUATIONS
			$d(\theta_p)$ (NUMBERIC)	$D(\theta_p)$ (dBi)	$d(\theta=\pi/2)$ (NUMERIC)	$D(\theta=\pi/2)$ (dBi)	RADIATION RESISTANCE (OHMS)	REACTANCE*** (OHMS)	
MONOPOLE	0	<< 1	1.500	1.761	1.500	1.761	$20\pi^2(h/\lambda)^2$	$-\infty$	3.2-19, 3.2-20
	0	0.25	1.543	1.882	1.543	1.882	19.43	$-\infty$	3.2-15, 3.2-16
	>>> 1, FINITE	<< 1	3.000	4.771	0.750	-1.249	$40\pi^2(h/\lambda)^2$	$-\infty$	3.7-1, 3.8-18, 2.3-2
	>>> 1, FINITE	0.25	3.282	5.161	0.820	-0.859	36.54	21.26	3.7-1. 3.8-15. 2.3-2
	∞	<< 1	3.000	4.771	3.000	4.771	$40\pi^2(h/\lambda)^2$	$-\infty$	3.8-16, 3.8-18, 3.8-19
	∞	0.25	3.282	5.161	3.282	5.161	36.54	21.26	3.8-13, 3.8-15, 3.8-19
DIPOLE**	0	<< 1	1.500	1.761	1.500	1.761	$80\pi^2(h/\lambda)^2$	$-\infty$	C. A. Balanis [15],
	0	0.25	1.641	2.151	1.641	2.151	73.08	42.52	pp. 108, 112, 131, 132
IDEALIZED ISOTROPIC RADIATOR			1.000	0	1.000	0	----	----	----

* DIRECTION OF PEAK DIRECTIVITY IS $\theta_p = \pi/2$ RAD EXCEPT FOR MONOPOLE ELEMENTS ON GROUNDPLANES OF FINITE BUT NON-ZERO EXTENT IN WHICH CASE $\theta_p < \pi/2$ RAD.

** VERY THIN DIPOLE OF HALF-LENGTH h.

*** REACTANCE IS IN THE LIMIT OF AN INFINITELY THIN ELEMENT.

Table 4. Electrical Properties of Very Thin Monopole Elements on Groundplanes of Zero, Large, and Infinite Extent

electrically-short and half-wave dipoles. The peak directivity of a quarterwave monopole is 1.88 dBi and 5.16 dBi for groundplanes of zero and infinite extent, respectively. The directivity on the horizon of a quarterwave monopole is 1.88 dBi and -0.86 dBi for groundplanes of zero and very large but finite extent, respectively. Slightly smaller directivities are obtained for electrically-short elements than for quarterwave elements.

The radiation resistances obtained by different methods are compared in table 5 for a thin quarterwave element on a groundplane of radius $0 \leq ka \leq 8.5$ wavenumbers. The suspected best available results are obtained by the integral equation method for $0 \leq ka \leq 1.0$, by the method of moments (N=1) for $1 < ka < 3.0$, by the oblate spheroidal wave function method for $3.00 \leq ka \leq 6.5$, and by the method of moments (N=1) for $6.5 < ka \leq 14$. The results obtained by the method of moments is in good agreement with the suspected best available results obtained by other methods.

The numeric directive gain patterns of a quarterwave element on groundplanes of radii ka = 0, 3, 4, 5, $\sqrt{42}$, and ∞ wavenumbers are plotted in figure 8. These polar graphs of directive gain should not be confused with the polar graphs of radiated power density plotted in Ref. [5] for constant base current. It should be noted that the peak directivity and direction of peak directivity are not monotonic functions of the groundplane radius.

The input impedance of a thin quarterwave element is plotted in figures 9 and 10 for groundplane radii $0 \leq ka \leq 14$ wavenumbers. The input resistance varies between 19.4 and 46.1 ohms and asymptotically approaches 36.5 ohms for increasingly large groundplane radii. The input reactance varies between $-\infty$ and +32.5 ohms and asymptotically approaches + 21.3 ohms for increasingly large groundplane radii.

Normalized Groundplane Radius, $2\pi a/\lambda$	Radiation Resistance (ohms)		
	Integral Equation Method	Oblate Spheroidal Wave Function Method	Moment Method
0	*19.43		
0.25	*19.48		19.49
0.50	*19.62		19.62
0.75	*19.86		19.86
1.00	*20.23		20.21
1.25	20.76		*20.71
1.50	21.51		*21.25
1.75	22.59		*22.44
2.00	24.15		*23.89
2.25	26.46		*25.99
2.50	29.95	27.32	*29.02
2.75	35.44	31.92	*33.24
3.00	44.60	*37.48	38.62
3.25		*43.01	44.12
3.50		*46.06	47.57
3.75		*45.55	47.35
4.00		*42.67	44.43
4.25		*39.23	40.58
4.50		*36.23	37.13
4.75		*34.00	34.46
5.00		*32.57	32.68
5.25		*31.93	31.70
5.50		*32.13	31.53
5.75		*33.23	32.26
6.00		*35.23	34.04
6.25		*37.85	36.94
6.50		*40.33	40.56
6.75		30.12	*43.53
7.00		30.09	*44.20
7.25			*42.30
7.50			*39.10
7.75			*35.96
8.00			*33.50
8.25			*31.88
8.50			*31.16

***SUSPECTED BEST AVAILABLE RESULT**

Table 5. Radiation Resistance of a Thin Quarterwave Element at the Center of a Circular Groundplane of Radius $0 \leq ka \leq 8.5$ Wavenumbers. (Sinusoidal current distribution assumed on element.)

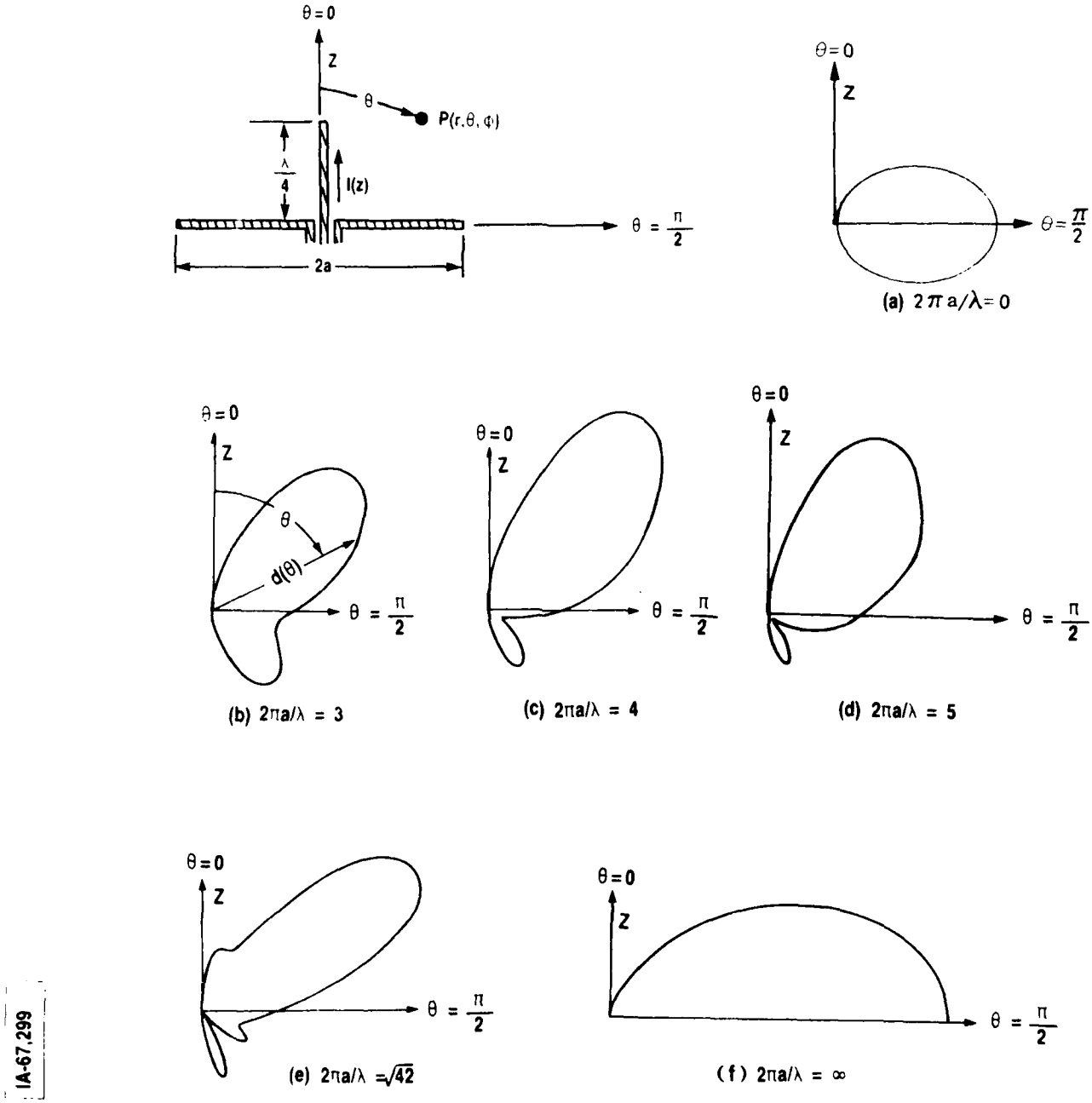

Figure 8 Elevation Directive Gain Patterns, for Any Azimuthal Direction, of a Quarterwave Element Mounted on a Groundplane of Radius a. (The patterns are polar graphs on the same linear scale.)

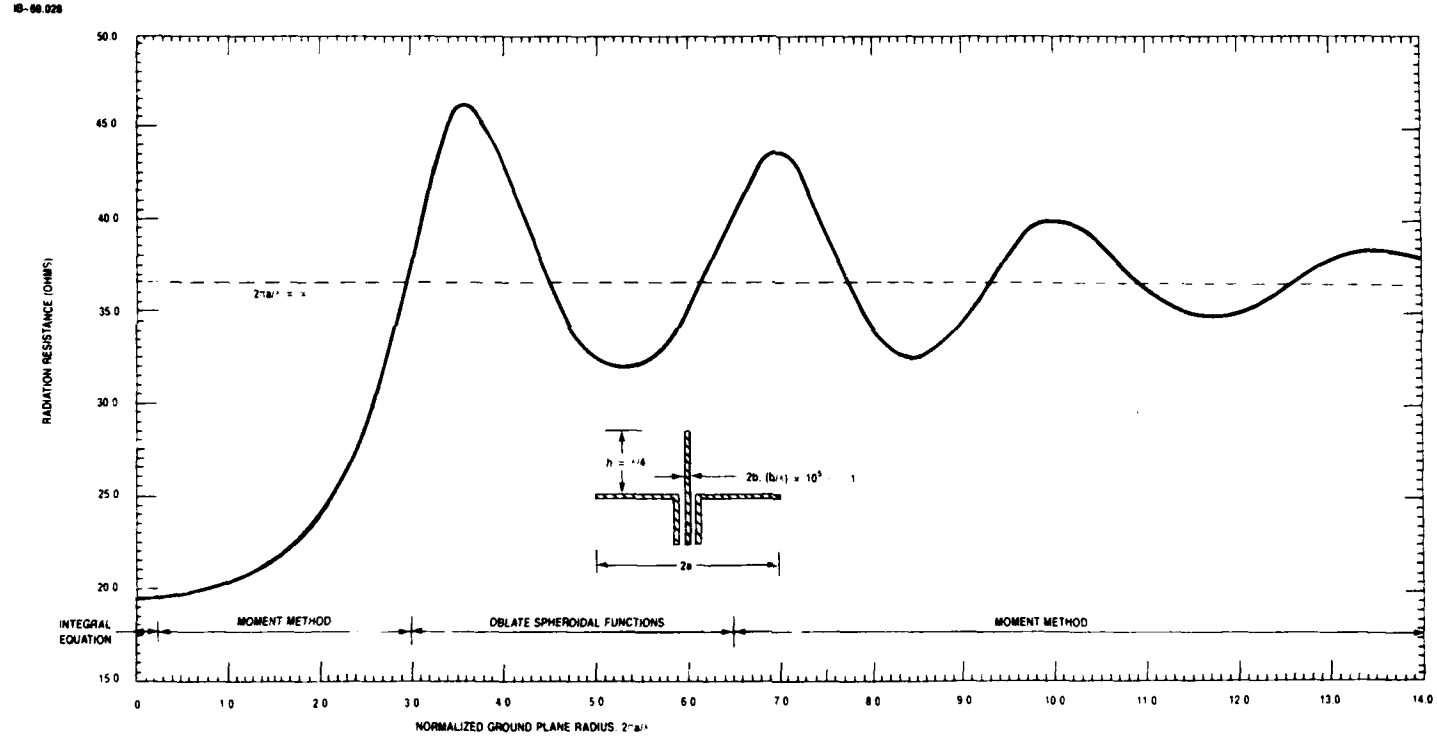

Figure 9. Radiation Resistance of a Thin Quarterwave Element at the Center of a Circular Groundplane of Radius $0 \leq ka \leq 14$ Wavenumbers

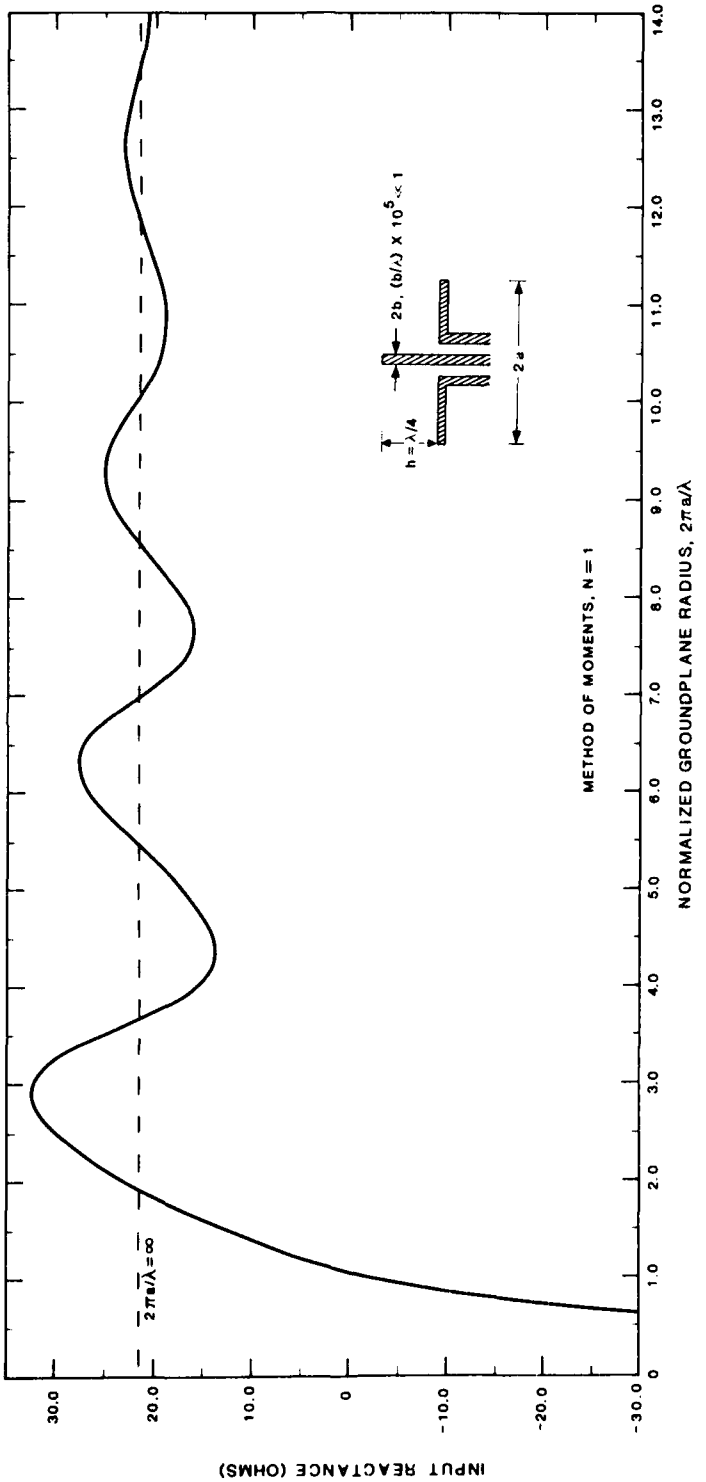

Figure 10. Input Reactance of a Thin Quarterwave Element at the Center of a Circular Groundplane of Radius $0 \leq ka \leq 14$ Wavenumbers

The directive gain on the horizon, peak directivity, and elevation angle of the peak directivity of a quarterwave element are plotted in figures 11 - 13 for groundplane radii $0 \leq ka \leq 14$ wavenumbers. The directive gain on the horizon varies between +1.9 and -1.9 dBi and asymptotically approaches -0.86 dBi for increasingly large but finite groundplane radii. The peak directivity varies between +1.0 and +5.3 dBi and asymptotically approaches +5.2 dBi for increasingly large groundplane radii. The elevation angle of the peak directivity varies between 33 and 90 degrees and asymptotically approaches 90 degrees for increasingly large groundplane radii.

The radiation resistances of thin elements of length $h/\lambda = 0.25$, 0.1 and 0.025 for groundplane radii $0 \leq ka \leq 8$ wavenumbers are compared in figure 14. The radiation resistance of each element is normalized to its radiation resistance for a groundplane of zero extent. The normalized radiation resistance, as a function of groundplane radius, is approximately independent of the element length. For an electrically-short, thin element ($h/\lambda \lesssim 0.1$) whose length is small or comparable to the groundplane radius, the input reactance (not shown) is approximately independent of groundplane radius.

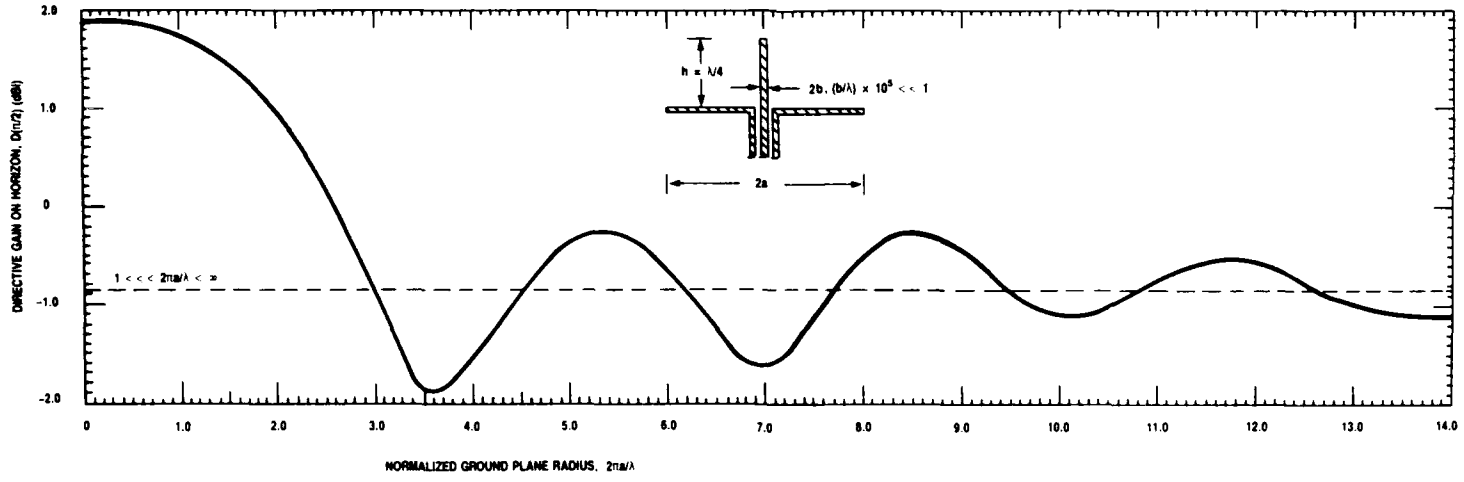

Figure 11. Directive Gain on Horizon of Thin Quarterwave Element at the Center of a Circular Groundplane of Radius $0 \leq ka \leq 14$ Wavenumbers

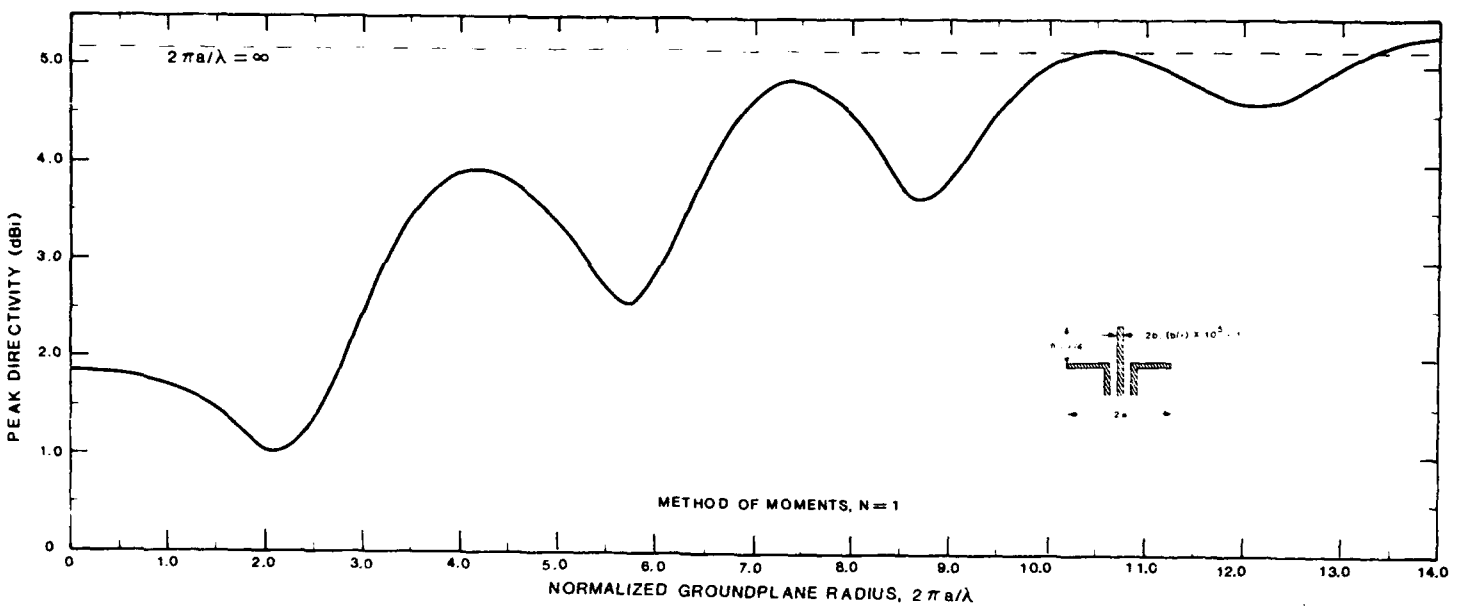

Figure 12. Peak Directivity of a Thin Quarterwave Element at the Center of a Circular Groundplane of Radius $0 \leq ka \leq 14$ Wavenumbers

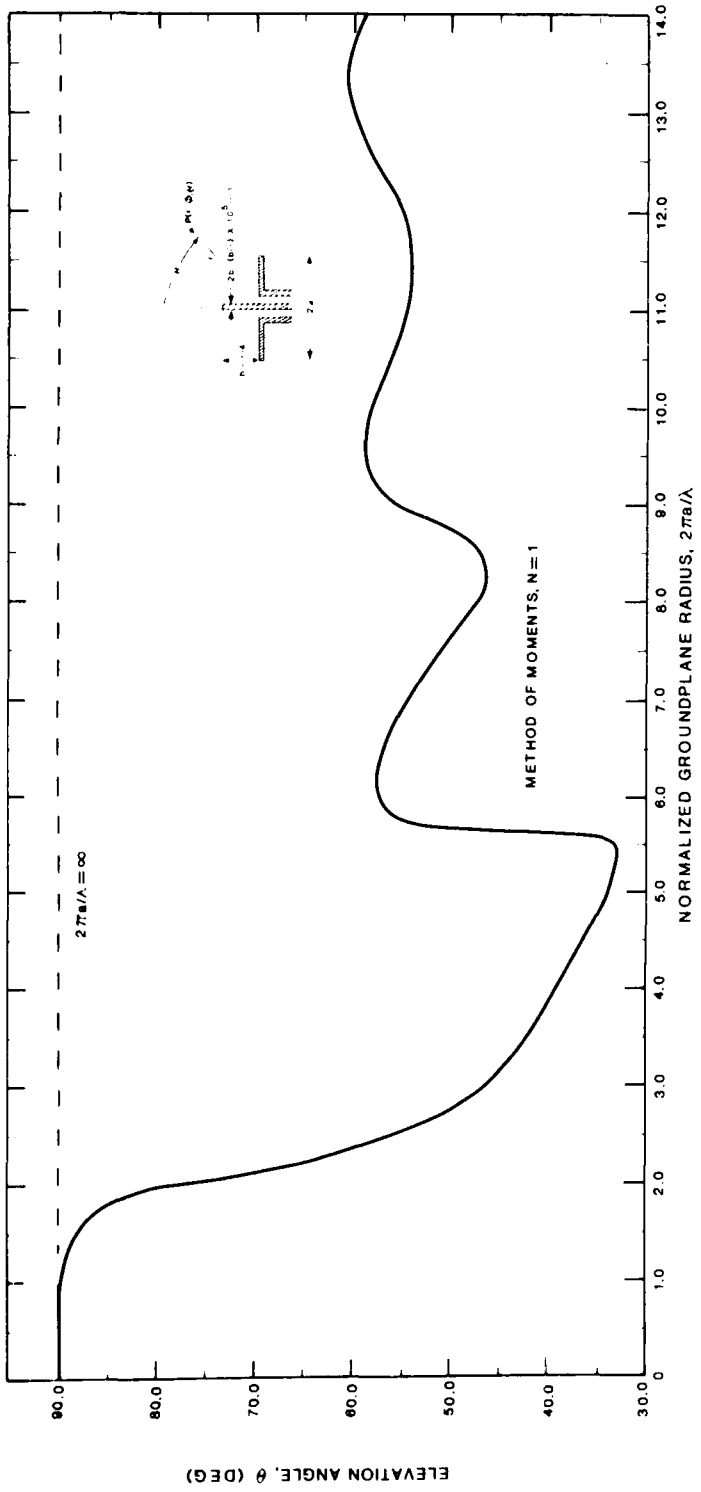

Figure 13. Elevation Angle of Peak Directivity for a Thin Quarterwave Element at the Center of a Circular Groundplane of Radius $0 \leq ka \leq 14$ Wavenumbers

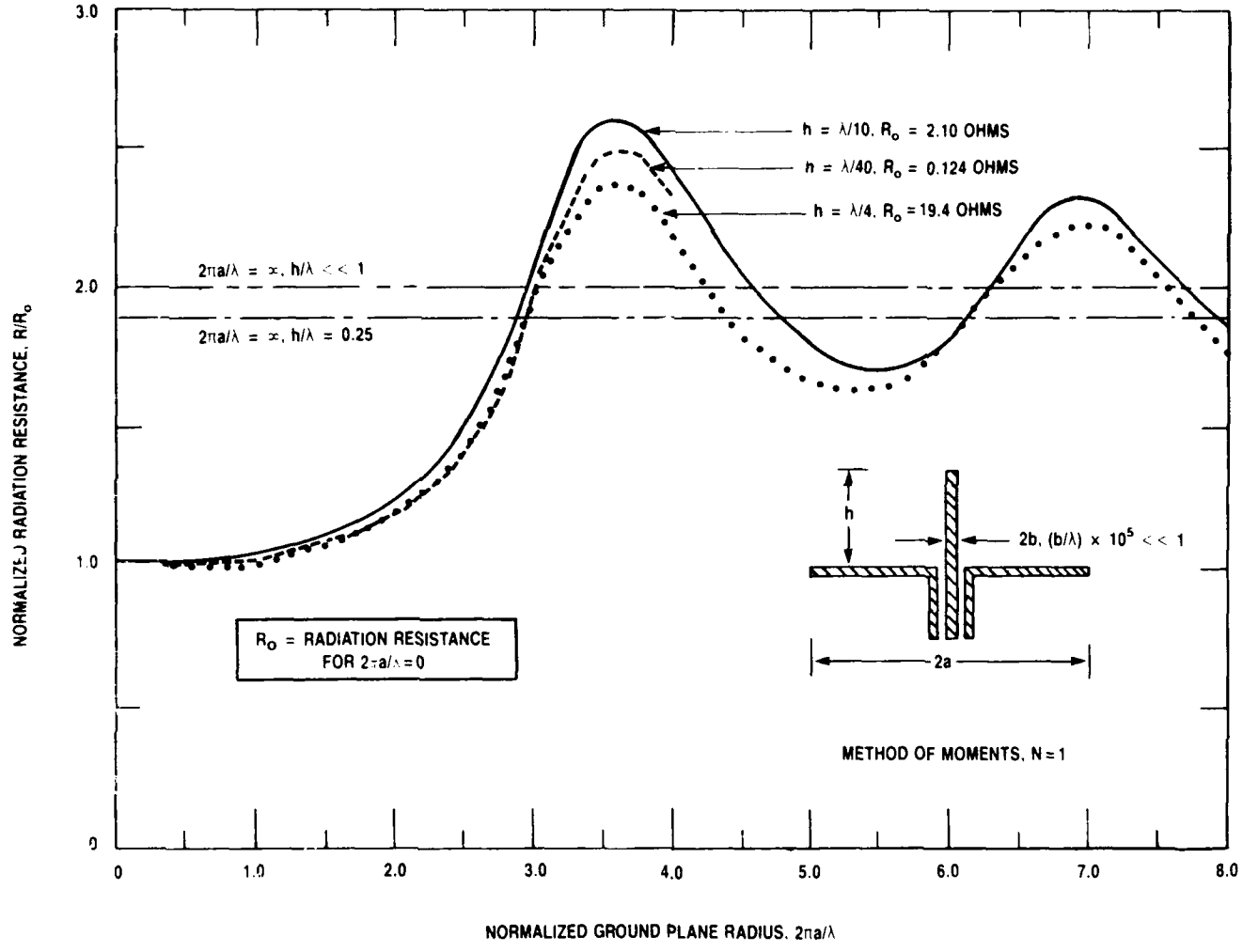

Figure 14 Radiation Resistance of Various Length Thin Elements at the Center of a Circular Groundplane in Free Space

SECTION 4

MODELS IN WHICH THE CURRENT DISTRIBUTIONS ON THE MONOPOLE ELEMENT AND GROUNDPLANE ARE BOTH INITIALLY UNKNOWN

4.1 Boundary Conditions

In Section 3 the total field at an arbitrary field point could be expressed simply as the vector sum of an incident field and an induced field [see Eq. (3.1-12)] because the incident field was specified from the initially known current distribution on the monopole element. In this section, such a procedure is not possible because the current distributions on the element and groundplane are both initially unknown. Instead, in this section, the total field is determined by representing the unknown current distribution on either the element, groundplane, or both by a finite series of overlapping modes with unknown current amplitudes. The current amplitudes are determined by matrix inversion subject to boundary conditions comprising current constraints and the excitation voltage across the coaxial line feed.

The antenna geometry is shown in figure 1 of Section 2.1. The current waveform is given by Eq. (2.1-2). The models which follow in this section are based on the current characterization and circuit idealization in figure 2(c) of Section 2.4.

The coaxial line feed and excitation voltage, which is not explicitly shown in figure 1, is characterized in figure 2(c) by a surface magnetic current density (magnetic frill) M_ϕ which sits on top of a thick groundplane of radius b_1 where b_1 is the radius of the outer conductor of the coaxial line feed. The magnetic frill M_ϕ is defined over the groundplane by Eq. (2.4-8).

Constraints on the various circuit currents of figure 2(c) are given by Eqs. (2.4-3) - (2.4-7). These constraints, together with the magnetic frill, constitute the boundary conditions on the current amplitudes.

4.2 Method of Moments, $0 < ka \leq 14$

When the element and groundplane current distribution are initially unknown, the current distributions may be determined by a sinusoidal-Galerkin moment method employed by Richmond[2]. The antenna geometry is shown in figure 1 of Section 2.

In the moment method, the element is divided into N equal segments (see figure 15) of length d' given by

$$d' = h/N, \quad N \text{ is a positive integer} \tag{4.2-1}$$

where h is the element length. The groundplane is divided into M concentric annular zones (see figure 16) of width d given by

$$d = (a-b)/M > b_1 - b, \quad M \text{ is a positive integer} \tag{4.2-2}$$

where a is the groundplane radius, b is the element radius, and b_1 is the radius of the outer conductor of the coaxial line feed. The groundplane extends from the coaxial line inner conductor because of the equivalent circuit representation in figure 2(b) of the coaxial line excitation. The element current distribution I(z) and groundplane current distribution $I(\rho)$ are the sum of the current distributions on each element segment and groundplane annular zone, respectively, and are given by

$$I(z) = \sum_{n=1}^{N} I_n(z) \tag{4.2-3}$$

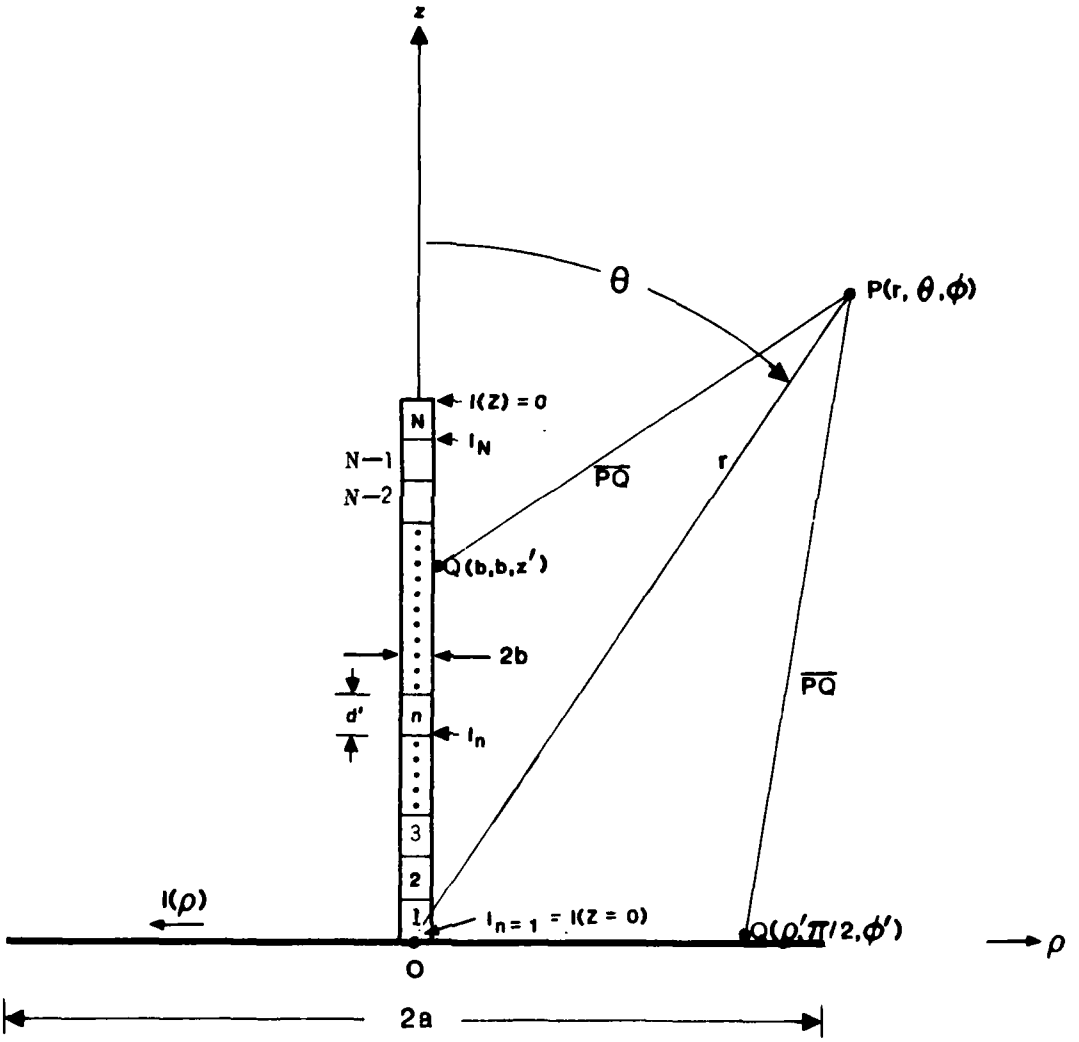

Figure 15. Element with N Equal Segments of Length d'

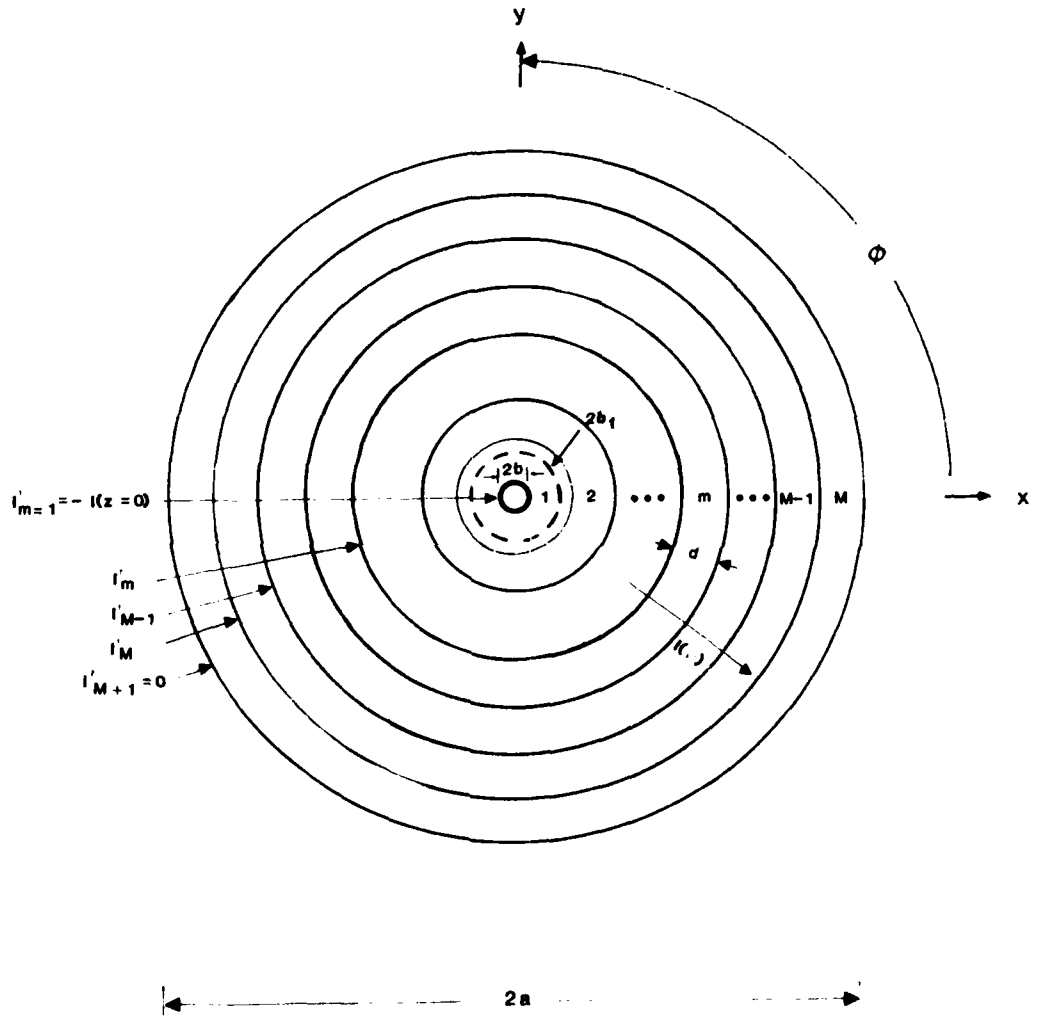

Figure 16. Groundplane with M Annular Zones of Width d

$$I(\rho) = \sum_{m=1}^{M} I'_m(\rho) \qquad (4.2\text{-}4)$$

where $I_n(z)$ and $I'_m(\rho)$ are the current distributions on the n^{th} segment and m^{th} annular zone, respectively.

In the sinusoidal Galerkin method, the current distribution $I_n(z)$ on the n^{th} element segment is approximated by

$$I_n(z) \approx \frac{I_n \sin[k(nd'-z)] + I_{n+1} \sin\{k[z-(n-1)]d'\}}{\sin(kd')} ;$$
$$(n-1)d' \leq z \leq nd'; \; n=1,2,3, \ldots .N \qquad (4.2\text{-}5)$$

where $I_{n=1} = I(z=0)$ and $I_{N+1} = 0$.

The current distribution $I'_m(\rho)$ on the m^{th} annular zone is approximated by

$$I'_m(\rho) \approx \frac{I'_m \sin\{k[md+b-\rho]\} + I'_{m-1} \sin\{k[\rho-(m-1)]d-b\}}{\sin(kd)} ;$$
$$b + (m-1)d \leq \rho \leq b+md; \; m=1, 2, 3, \ldots M \qquad (4.2\text{-}6)$$

where $I'_{m=1} = -I_{n=1} = -I(z=0)$ and $I'_{M+1} = 0$.

The current distribution on each segment and annular zone is therefore the sum of two overlapping dipole modes except for the segment and annular zone adjacent to the base of the element. The "base" mode may be thought of as a dipole mode comprising an element monopole mode (n=1) and a groundplane monopole mode (m=1) with terminals along the circumference of the base of the element. The element and groundplane dipole modes are functionally tied to each other by means of the base mode amplitude constraint $I_{n=1} = -I'_{m=1} = I(z=0)$.

The element and groundplane total current distributions are represented in Eqs. (4.2-3) - (4.2-6), as a series of N+M overlapping sinusoidal dipole modes with N+M unknown complex current amplitudes. The N+M amplitudes are determined in Richmond's moment method by inversion of a (N+M) x (N+M) matrix subject to the boundary conditions discussed in Section 4.1. The constraint $I_{n=1} = -I'_{m=1}$ reduces the matrix size to (N+M-1) x (N+M-1).

The numbers of subdivisions, N and M, are limited by the cost of computation time and by the precision of the computer. The accuracy of the solution can be decreased appreciably if either N or M is too small or too large. The method of moments converges to a solution when an increase or decrease of unity in the value of N or M does not appreciably alter the solution for input impedance.

A method of moments computer program for a monopole element at the center of a circular groundplane in free space was obtained from Prof. Richmond of Ohio State University. The program computes the input impedance and the N+M complex current amplitudes on the element and groundplane for a voltage input V(0) = 1 volt. The program, written in FORTRAN IV language and in single precision, was edited and converted by The MITRE Corporation to double precision for use on a DEC VAX 11/780 computer. A listing of the MITRE version, designated "RICHMD1", is given in Appendix B2.

Our experience with this program suggests the following constraints on the use of the program. At least double precision is required to give convergent results. Meaningful results were obtained for element radii $b/\lambda \geq 10^{-10}$ and groundplane radii ka > 0.25. As a rule of thumb, N=2-3 kh and M=2-3 ka give reasonably accurate and convergent results. The amount of central processing unit (CPU) time on the VAX 11/780 computer is approximately 2 minutes for N+M = 20, 6

minutes for N+M=30, 34 minutes for N+M=60, and 50 minutes for N+M=75. It is most likely that the CPU time could be considerably reduced if a more efficient method than the Crout method were employed for matrix inversion.

The versatility of a sinusoidal - Galerkin method of moments is illustrated by the case N=1. A sinusoidal current distribution is imposed on the element by setting N=1 [see Eq. (4.2-5)].

The element and groundplane current distributions obtained from program RICHMD1 can be utilized to obtain the far-field radiation pattern in the following manner.

The magnetic field intensity $\vec{H}(P)$ at a far-field point $P(r, \theta, \phi)$ and for an $e^{j\omega t}$ waveform is related to the magnetic vector potential $\vec{A}(P)$ by[26]

$$\vec{H}(P) = -j(1/\eta)\,\omega\,\hat{u}_r \times \vec{A}(P) \tag{4.2-7}$$

where $\hat{u}_r$ is a unit vector in the radial direction and η is the free-space wave impedance. The magnetic vector potential $\vec{A}(P)$ at the far-field point P resulting from a current source point $Q(x', y', z') = Q(b, b, z')$ on the element or a source point $Q(\rho', \pi/2, \phi')$ on the groundplane (see figure 4) is given by[26]

$$\vec{A}(P) = (\mu_o/4\pi) \int_v J(Q)\, \exp(-jk\bar{PQ})\, (1/\bar{PQ})\, dv$$

$$\approx [\mu_o \exp(-jkr)/4\pi r] \int_v J(Q)\, \exp(jk\hat{u}_r \cdot \vec{OQ})\, dv \tag{4.2-8}$$

where

$$\overline{PQ} = [r^2 - 2r\,\hat{u}_r \cdot \overrightarrow{OQ} + x'^2 + y'^2 + z'^2]^{1/2} \approx \overrightarrow{r} - \hat{u}_r \cdot \overrightarrow{OQ},\quad r >> (x'^2 + y'^2 + z'^2)^{1/2}$$

$$\hat{u}_r \cdot \overrightarrow{OQ} = x' \sin\theta \cos\phi + y' \sin\theta \sin\phi + z' \cos\theta$$

μ_o = permeability of free space = $4\pi \times 10^{-7}$ henry/m.

J(Q) = source surface current density at an arbitrary source point Q on either the element or groundplane (amp/m)

r = $\overline{OP}$ = radial distance between the origin O(0,0,0) and the far-field point P(r, θ, ϕ)

dv = differential surface area containing the current source points Q (m^2)

Substituting Eq. (4.2-3) into Eq. (4.2-8), the far-field magnetic field intensity $H_\phi^{(e)}$ resulting from the monopole current distribution is given by

$$H_\phi^{(e)} = \frac{j \exp(-jkr) \sin\theta}{4\pi r} \int_0^h \sum_{n=1}^{N} I_n(z') \exp(jkz'\cos\theta)\, dz'$$

$$= \frac{j \exp(-jkr)}{4\pi r \sin\theta \sin(kd')} \left\{ \left[\sum_{n=1}^{N} I_n \exp(jnkd'\cos\theta) \right] \right.$$

$$\left[1 - \cos(kd') \cos(kd'\cos\theta) - \cos\theta \sin(kd') \sin(kd'\cos\theta) \right.$$

$$\left. + j \cos(kd') \sin(kd'\cos\theta) - j \cos\theta \sin(kd') \cos(kd'\cos\theta) \right]$$

$$- \left[\sum_{n=2}^{N} I_n \exp[j(n-2)\, kd'\cos\theta] \right] \left[\cos(kd') \cos(kd'\cos\theta) \right.$$

$$\left. \left. + \cos\theta \sin(kd') \sin(kd'\cos\theta) - 1 + j \cos(kd') \sin(kd'\cos\theta) - j \cos\theta \sin(kd') \cos(kd'\cos\theta) \right] \right\} \qquad (4.2\text{-}9)$$

Substituting Eq. (4.2-4) into Eq. (4.2-8), the far field magnetic field intensity $H_{\phi}^{(g)}$ resulting from the groundplane current distribution is given by

$$H_{\phi}^{(g)} = \frac{-j \exp(-jkr)}{4\pi r} \int_0^a \int_0^{2\pi} \frac{1}{2\pi} \sum_{m=1}^{M} I_m'(\rho') \exp[jk\rho' \cos(\phi-\phi)] \cos\theta \cos(\phi'-\phi)\, d\phi'\, d\rho' \tag{4.2-10}$$

Eq. (4.2-10) is not readily evaluated when Eq. (4.2-6) is substituted into it. An approximate simplified solution can be found when each annular zone of the groundplane is subdivided into X smaller annular zones of width $\Delta\rho = d/X$ so that the current distribution in each subdivided zone is almost constant and approximately equal to its average current. The total number J of subdivided annular zones on the entire groundplane is given by

$$J = XM \tag{4.2-11}$$

The average current I_u in the uth subdivided zone is given by

$$I_u = \frac{1}{\Delta\rho} \int_{(u-1)\Delta\rho + b}^{u\Delta\rho + b} \frac{I_m' \sin[k(md+b-\rho)] + I_{m+1}' \sin\{k[\rho - (m-1)d - b]\}}{\sin(kd)} d\rho, \tag{4.2-12}$$

$$[b+(m-1)d] < \rho < (b+md)$$

The current distribution $I(\rho)$ on the groundplane is therefore given approximately by

$$I(\rho) \approx \sum_{u=1}^{J} I_u \tag{4.2-13}$$

Substituting $I_u(\rho')$ for $I_m(\rho')$ in Eq. (4.2-10),

$$H_\phi^{(g)} \approx \frac{-j\ \exp(-jkr)}{4\pi r} \int_0^a \int_0^{2\pi} \frac{1}{2\pi} \left\{ \sum_{u=1}^{J} I_u(\rho') \exp[\, jk\rho' \cos(\phi' - \phi)\,] \right\} \cos\theta\ \cos(\phi' - \phi)\, d\phi'\, d\rho'$$

$$= \frac{\exp(-jkr)\cos\ \theta}{4\pi r\ \sin\theta} \sum_{u=1}^{J} I_u(\rho') \left[J_o\{k\ \sin\theta[(u-1)\Delta\rho + b]\} - J_o\{k \sin\theta[u\ \Delta\rho + b]\} \right] \quad (4.2\text{-}14)$$

where J_o is the Bessel function of the first kind, of order zero.

The total far-field magnetic field intensity $H_\phi^{(total)}$ is given by

$$H_\phi^{(total)} = H_\phi^{(e)} + H_\phi^{(g)} \quad (4.2\text{-}15)$$

where $H_\phi^{(e)}$ and $H_\phi^{(g)}$ are given by Eqs. (4.2-9) and (4.2-14), respectively.

The time-averaged radiated power density $s(\theta)$, directive gain $d(\theta)$, and radiation resistance R are found from Eqs. (2.2-4), and (2.2-7) where $H_\phi^{(total)}$ is given by Eq. (4.2-15) and $I(z=0) = I_{n=1}$. Numerical evaluation of $s(\theta)$, $d(\theta)$, and R are implemented by means of MITRE computer program "RICHMD2" written in FORTRAN language for use on a DEC VAX 11/780 computer. A listing of program RICHMD2 is given in Appendix B2.

A discussion of the results obtained by the method of moments, for a sinusoidal current distribution on the element (N=1), is given in Section 3.4.

Computer printouts of the directive gain and far-field radiation pattern of the experimental monopole antennas discussed in Section 5 were obtained by the method of moments and are given in Appendix A2.

The input impedance determined by the method of moments (N=4, M=3ka) for a quarterwave element of radius $b=10^{-6}\lambda$ and groundplane radii $6 \leq ka \leq 30$ wavenumbers is compared in table 7 of Section 4.5 with that obtained by the method of moments combined with the geometric theory of diffraction (GTD). For $ka > 14$, Richmond's method of moments is inaccurate. In addition to the large CPU time required (greater than 30 minutes for $ka > 14$), convergent results are difficult to obtain for $ka > 14$. It is most likely that the usefulness of Richmond's method of moments could be extended to significantly larger groundplane radii if a more efficient method of matrix inversion, different from the Crout method employed by Richmond, were utilized. When the element current distribution is not assumed, Richmond's method of moments presently gives the best available results for groundplane radii $ka \leq 14$ wavenumbers.

The lower limit of ka, for accurate results utilizing Richmond's method of moments, has not been firmly established. For an element segment number $N > 1$, we have obtained useful results for ka as small as 0.25 wavenumbers but *not for* groundplanes of zero extent. For N=1, accurate results were obtained (subject to the constraint of a sinusoidal element current distribution) for groundplanes of zero extent.

The radiation resistance of various diameter resonant (zero input reactance) elements is compared in figure 17 of Section 4.5 with the radiation resistance of an infinitely thin quarterwave element for groundplane radii $0 \leq ka \leq 8.5$ wavenumbers. For $ka \longrightarrow 0$, the radiation resistance of the resonant elements is appreciably different from that of the infinitely thin quarterwave element because an infinitely thin element on a groundplane of zero extent is resonant for an element length equal to 0.5λ and not 0.25λ [see Eq. (32-38)].

The lengths and radiation resistances of various diameter resonant elements, for groundplanes of radii $0.25 \leq ka \leq 7$ wavenumbers, are plotted in figures 18 and 19 of Section 4.5.

4.3 Method of Moments Combined with Geometric Theory of Diffraction, $8.5 \lesssim ka < \infty$

The method of moments, when used to determine the current distributions on both the element and the groundplane, can require considerable computation time for large groundplane radii. For example, Richmond's method of moments requires approximately one-half hour of CPU time on the VAX 11/780 computer for a groundplane radius ka=20 with N=4 element segments and M=60 groundplane annular zones (see Section 4.2). Although it may be possible to reduce the computation time by use of a more efficient program than the one employed by Richmond, it is of interest to find an alternative method for large groundplanes.

Awadalla and Maclean[9],[10] have reduced the computation time for large groundplanes by combining the method of moments with the geometric theory of diffraction (GTD). The element current distribution is determined by the method of moments and the effect on input impedance by groundplane edge diffraction is determined by GTD.

The antenna geometry is shown in figure 1 of Section 2.1. The method of Awadalla and Maclean is described in [9] for determining the input impedance and in [10] for determining the radiation pattern.

A fictitious magnetic edge current is defined and expressed in terms of a GTD diffraction coefficient to account for diffraction by the edge of the groundplane. The method of GTD is valid only for sufficiently large groundplane radii. Unfortunately, this method, as applied by Awadalla and Maclean, does not determine the groundplane current distribution.

The groundplane current distribution is idealized by Awadalla and Maclean in determining the radiation pattern. The current distribution on the top of the groundplane is assumed to be that for an infinite groundplane but defined only over the finite extent of the groundplane. The net current at the edge of the groundplane is set equal to zero. This constraint satisfies the boundary condition given by Eq. (2.4-4) and requires, at the edge of the groundplane, that the current on the bottom of the groundplane be equal but in the opposite direction to that on the top of the groundplane. The current distribution on the bottom of the groundplane is then assumed to decrease linearly from the edge of the groundplane to zero at the base of the element.

The method of moments employed by Awadalla and Maclean is not a sinusoidal-Galerkin method. Consequently, one cannot impose a sinusoidal current distribution on the element by setting the number of element segments N=1 as a test case for purposes of comparison with other models.

A program listing was obtained from Prof. Awadalla and edited at The MITRE Corporation. A listing of the edited program "AWADALLA" is given in Appendix A5. Program AWADALLA is written in FORTRAN language for use on a DEC VAX 11/780 computer. The CPU time for N=30 element segments is less than 10 seconds.

Program AWADALLA was utilized to obtain the input impedance, directive gain, and far-field elevation pattern of a quarterwave element of radius $b=10^{-6}\lambda$ on groundplane of radii $8 \leq ka \leq 50$ wavenumbers. The results for input impedance are given in table 6. These results are compared in table 7 of Section 4.5 with those obtained by the method of moments (N=4). Concerning input impedance, the method of moments combined with GTD gives useful results for $ka \gtrsim 6$, accurate results for $ka > 8$, and the suspected best available results for $14 < ka < \infty$.

TABLE 6. INPUT IMPEDANCE OF A QUARTERWAVE ELEMENT OF RADIUS $b=10^{-6}\lambda$ AT THE CENTER OF A CIRCULAR GROUNDPLANE OF RADIUS $8 \leq ka \leq 50$ WAVENUMBERS
(Method of moments combined with geometric theory of diffraction)

ka	INPUT RESISTANCE (OHMS)	INPUT REACTANCE (OHMS)
8	35.96	18.28
9	36.55	24.45
10	41.45	21.82
11	37.54	18.67
12	36.30	23.08
13	40.49	22.51
14	38.44	19.17
15	36.36	22.18
16	39.72	22.82
17	38.99	19.70
18	36.58	21.51
19	39.09	22.89
20	36.87	21.05
22	38.58	22.84
23	39.45	20.63
24	37.20	20.73
25	38.17	22.67
26	39.48	21.06
27	37.55	20.56
28	37.87	22.46
29	39.41	21.40
30	37.88	20.47
31	37.67	22.19
32	39.27	21.68
33	38.19	20.49
34	37.55	21.93
35	39.08	21.90
36	38.45	20.56
37	37.51	21.65
38	38.87	22.06
39	38.66	20.68
40	37.54	21.42
41	38.64	22.13
42	38.82	20.86
43	37.62	21.21
44	38.43	22.14
45	38.92	21.05
46	37.75	21.04
47	38.23	22.10
48	38.96	21.26
49	37.91	20.93
50	38.06	21.99

A sample computer printout of directive gain and the far-field elevation pattern obtained by program AWADALLA for ka=20 is given in Appendix A5. Unfortunately, the idealizations, made by Awadalla and Maclean in characterizing the groundplane current distribution, yield unrealistic peak directivities and elevation patterns. For example, for ka=49, a peak directivity of 7.5 dBi was obtained. This result for a thin quarterwave element seems unlikely because a thin quarterwave element with a sinusoidal current distribution and mounted on a groundplane of infinite extent has a peak directivity of only 5.2 dBi.

The method of moments combined with GTD via the definition of a fictitious magnetic edge current has also been reported by Thiele and Newhouse[11] for computing input impedance and by Stutzman and Thiele[28] for computing the far-field radiation pattern. In the method of Stutzman and Thiele[28], the far-field pattern is determined without idealizing the groundplane current distribution.

4.4 Method of Images, ka= ∞

For the idealized case of a monopole element mounted on a groundplane of infinite extent and of infinite conductivity, a monopole antenna of length h may be modelled by the method of images as a dipole of total length 2h but with one-half the input impedance and double the peak numeric directivity of the dipole (see Section 3.8). The infinite groundplane prevents radiation into the hemisphere below the groundplane but generates fields in the upper hemisphere identical to those of a dipole.

A detailed treatment of the fields and input impedance of a dipole is given in [13]. An excellent summary of the present state of the art of dipole theory, including plots of input impedance as a function of dipole length and dipole radius, is given in [14].

4.5 Summary of Results

In Section 4, the current distribution on the element is determined by the method of moments rather than being assumed as was the case in Section 3. The determination of the element current distribution is particularly important for element radii $b > 10^{-4}\lambda$.

The essential difference, in the two models utilized in Section 4, is the treatment of the groundplane current distribution. In Richmond's model, the groundplane current distribution is determined by the method of moments. Useful results are obtained for $0 < ka \leq 14$ wavenumbers. In the model of Awadalla and Maclean for large but finite groundplanes, the input impedance is accurately computed by the introduction of a fictitious magnetic edge current determined by the Geometric Theory of Diffraction (GTD). However, in that model the groundplane current distribution is not determined but instead is idealized -- causing unrealistic peak directivities and far-field radiation patterns.

The input impedances, determined by the method of moments and the method of moments combined with GTD, are compared in table 7 for a quarterwave element of radius $b=10^{-6}\lambda$ and groundplane radii $6 \leq ka \leq 30$ wavenumbers. The suspected best available results for input impedance are obtained by the method of moments for $0 < ka \lesssim 8.5$ and by the method of moments combined with GTD for $8.5 \lesssim ka < \infty$. The method of moments combined with GTD is inaccurate for $ka \leq 8$ (approximately 6% error in input reactance for ka=8 and 7% error in input resistance for ka=6). Richmond's method of moments is inaccurate for $ka > 14$ (approximately 11% error in input reactance and 5% error in input resistance for ka=15). Richmond's method of moments would be useful for $ka > 14$ wavenumbers if a more efficient method than the Crout method were employed for matrix inversion.

TABLE 7. INPUT IMPEDANCE OF A QUARTERWAVE ELEMENT AT THE CENTER OF A CIRCULAR GROUNDPLANE OF RADIUS $6 \leq ka \leq 30$ WAVENUMBERS. ($h/\lambda = 0.25$, $b/\lambda = 10^{-6}$)

NORMALIZED GROUNDPLANE RADIUS, ka	INPUT RESISTANCE (OHMS)			INPUT REACTANCE (OHMS)		
	(1) Moment Method	(2) Moment Method with GTD	$\frac{\lvert(1)-(2)\rvert}{(1)} \times 100$	(1) Moment Method	(2) Moment Method with GTD	$\frac{\lvert(1)-(2)\rvert}{(1)} \times 100$
6	*35.2988	37.7258	6.88	*26.7927	26.6729	0.45
7	*45.7499	42.6747	6.72	*20.5664	20.2537	1.52
8	*35.7335	35.9640	0.65	*17.1839	18.2823	6.39
9	36.2886	*36.5496	0.72	24.7424	*24.4496	1.16
10	42.0987	*41.4538	1.53	21.5758	*21.8225	1.14
11	38.1401	*37.5375	1.58	18.8073	*18.6728	0.72
12	36.7590	*36.2962	1.26	22.0824	*23.0841	4.54
13	39.7689	*40.4928	1.82	22.6158	*22.5061	0.49
14	39.6986	*38.4400	2.60	20.3449	*19.1676	5.79
15	38.3512	*36.3630	5.18	20.0026	*22.1845	10.91
20	38.4250	*39.3019	2.28	22.2706	*20.1706	9.43
25	39.0594	*38.1746	2.26	21.5934	*22.6704	4.99
30	38.8703	*37.8798	2.55	21.0052	*20.4663	2.57

(1) RICHMOND, METHOD OF MOMENTS (N=4, M=3 ka)
(2) AWADALLA AND MACLEAN, METHOD OF MOMENTS COMBINED WITH GEOMETRIC THEORY OF DIFFRACTION (N=30).

*SUSPECTED BEST AVAILABLE RESULT

The radiation resistance of various diameter resonant (zero input reactance) elements is compared in figure 17 with the radiation resistance of an infinitely thin quarterwave element for groundplane radii $0 \leq ka \leq 8.5$ wavenumbers. The radiation resistance of the resonant elements is not too appreciably different from the quarterwave element for $ka > 1$ wavenumber. However as $ka \longrightarrow 0$, the radiation resistances of the resonant elements become increasingly different from that of the infinitely thin element because an infinitely thin element on a groundplane of zero extent is resonant for an element length equal to 0.5λ and not 0.25λ [see Eq. (3.2-38)].

The lengths and radiation resistance of various diameter resonant elements for groundplane of radii $0.25 \leq ka \leq 7$ wavenumbers are plotted in figures 18 and 19. For these groundplane radii, the element resonant length h_{res}/λ varies from approximately 0.22 to 0.34 wavelengths for element radii $10^{-7} \leq b/\lambda < 10^{-2}$ wavelengths. The resonant radiation resistance, for these groundplane and element radii, varies from approximately 21 to 65 ohms.

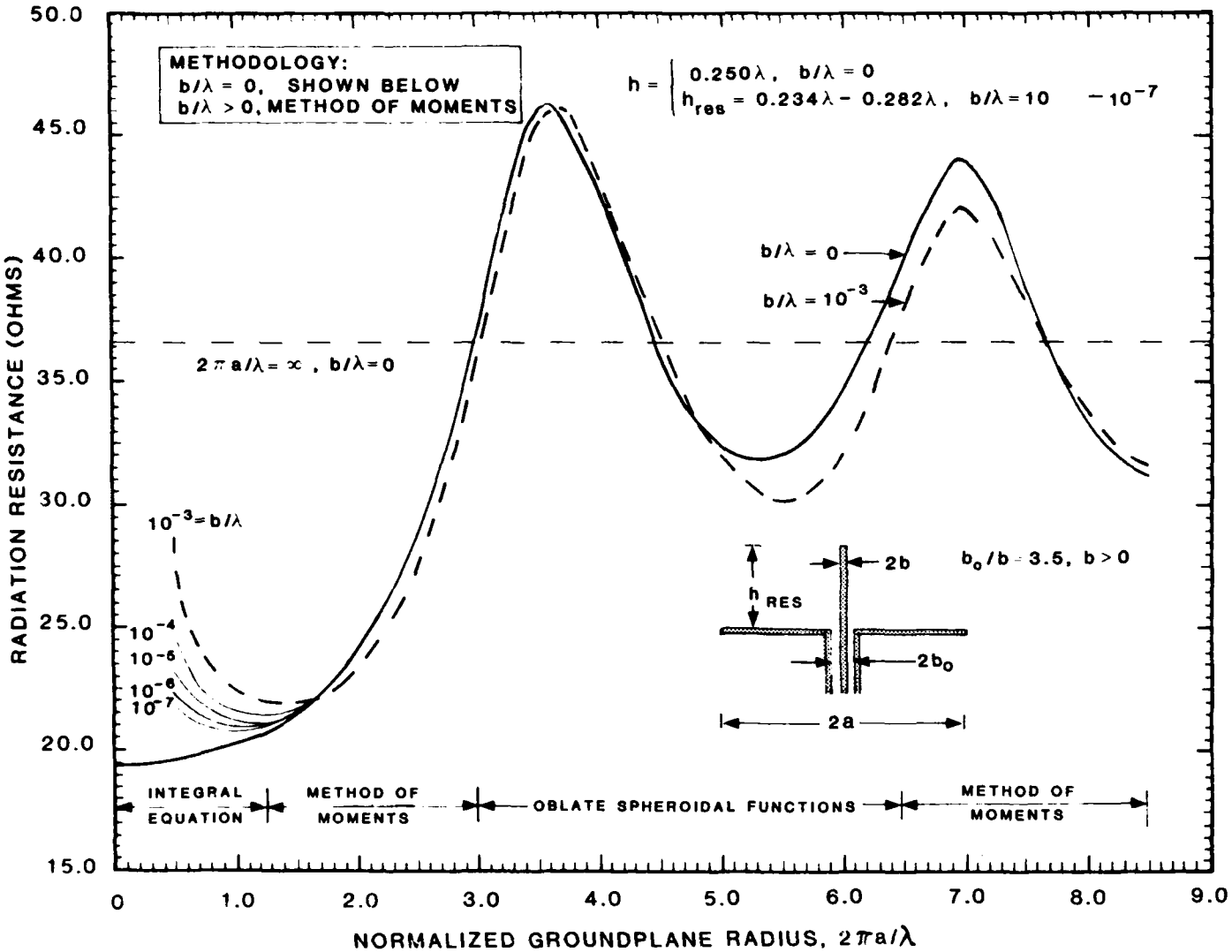

Figure 17. Radiation Resistances of Various Diameter Resonant Elements and an Infinitely-Thin Quarterwave Element at the Center of a Circular Groundplane of Radius $0 \leq ka \leq 8.5$ Wavenumbers

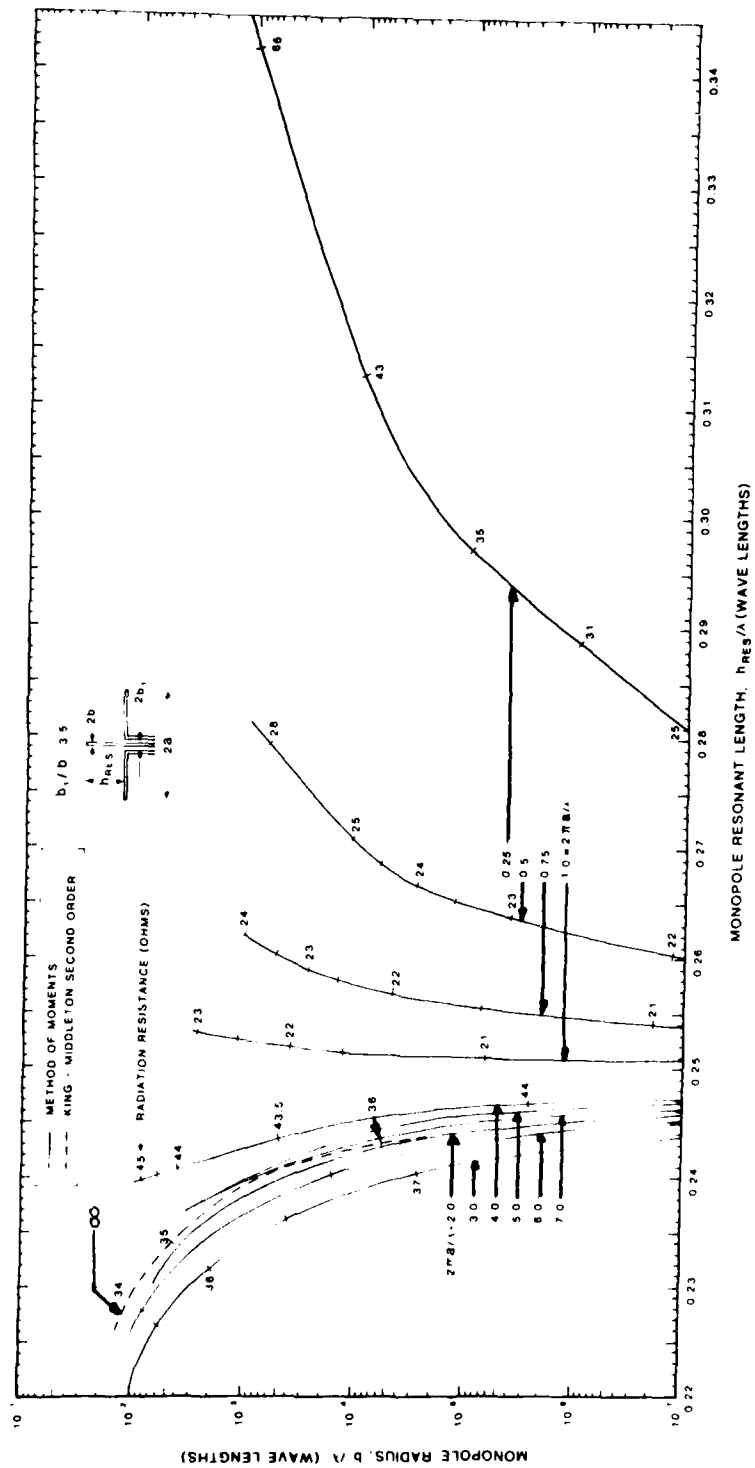

Figure 18. Resonant Length of Various Diameter Elements at the Center of a Circular Groundplane of Radius $0.25 \leq ka \leq 7$ Wavenumbers

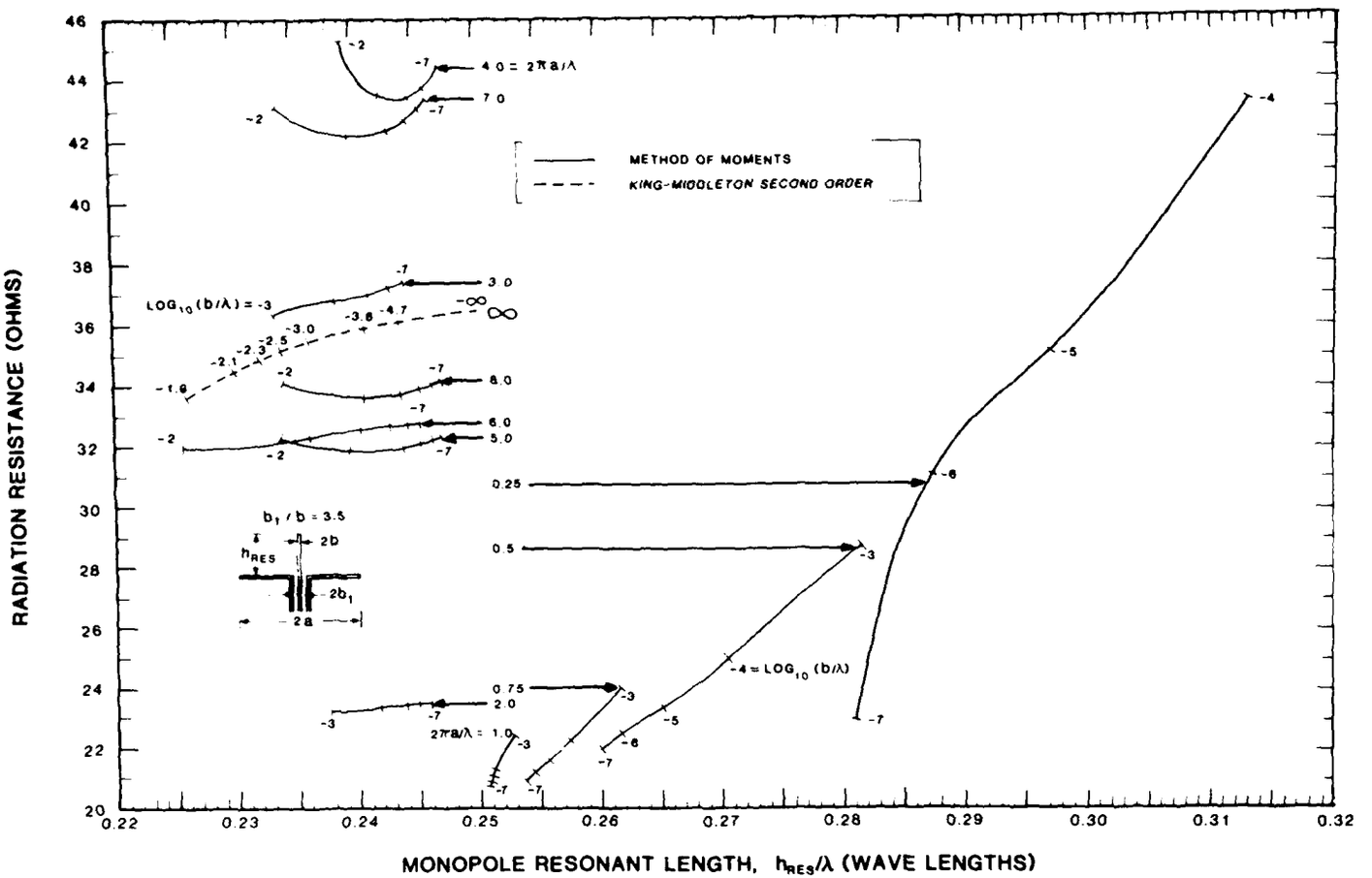

Figure 19. Radiation Resistances and Lengths of Various Diameter Resonant Elements at the Center of a Circular Groundplane of Radius $0.25 \leq ka \leq 7$ Wavenumbers

SECTION 5

COMPARISON WITH EXPERIMENTAL RESULTS

The input impedance and elevation patterns of several monopole antennas were measured, each at a different frequency within the frequency band 30-254 MHz, on the MITRE Corporation VHF antenna range. Each antenna consisted of a tubular element of radius b=0.25 in. mounted at the center of a groundplane of radius a=4 ft. and fed by a 50 ohm RG-214 coaxial cable with a type N panel connector and a 50 ohm tapered adapter to the element. The length h of each element was approximately a quarterwave. The exact length of each element length was chosen to be resonant (input reactance = zero ohms) for a groundplane of infinite extent. On a groundplane of finite extent, the input reactance is expected to asymptotically approach zero as $ka \longrightarrow \infty$.

The VHF antenna range is located on the roof of MITRE E-Building. The transmitting and receiving antennas are at a height 27 ft. above the roof and are separated by approximately 40 ft. A conducting fence 16 ft. high and 48 ft. wide is located on the roof midway between the transmitting and receiving antennas to minimize multipath reflections from the roof. Lossy ferrite toroids (Ferronics, Type B material, 0.540 in. I. D. x 0.870 in O. D. x 0.25 in.) are spaced along the receiving and transmitting cables to minimize currents on the outside of the cables. Outside rf interference is reduced to at least 40 dB below the desired signal by the use of narrowband rf filters.

The monopole test antenna was operated in the receiving mode to obtain elevation patterns and on the same platform for input impedance measurements. The monopole groundplane was supported by a 10 ft. wooden vertical mast mounted on an antenna pedestal.

The input impedance was measured with a Hewlett-Packard HP-8754A Network Analyzer with a computerized printout. The measurement test set-up is shown in figure 20. The predicted input impedance of each experimental monopole antenna was determined by Richmond's method of moments utilizing program RICHMD1. The predicted and measured input impedances are compared in Table 8. The measured input resistance differs from predicted values by approximately 1-10% over a range of normalized groundplane radii = 0.77 - 6.5 wavenumbers. The measured input reactance differs by approximately 2-12 ohms from the predicted values. Since some of the predicted values are near resonance, a percentage comparison is not made for input reactance.

Measured elevation patterns of most of the test monopole antennas specified in Table 8 are compared in figures 21 - 29 with theoretical patterns predicted by the method of moments (see Appendix A2 for the computer printouts). Allowing for some multipath distortion by the VHF test range, the received patterns are in good agreement with the predicted pattern. It should be noted the measured pattern for ka = 0.766 is not appreciably different from that predicted for the monopole element itself. The effect of the groundplane on the shape of the pattern is not readily apparent until ka $\gtrsim$ 2.0.

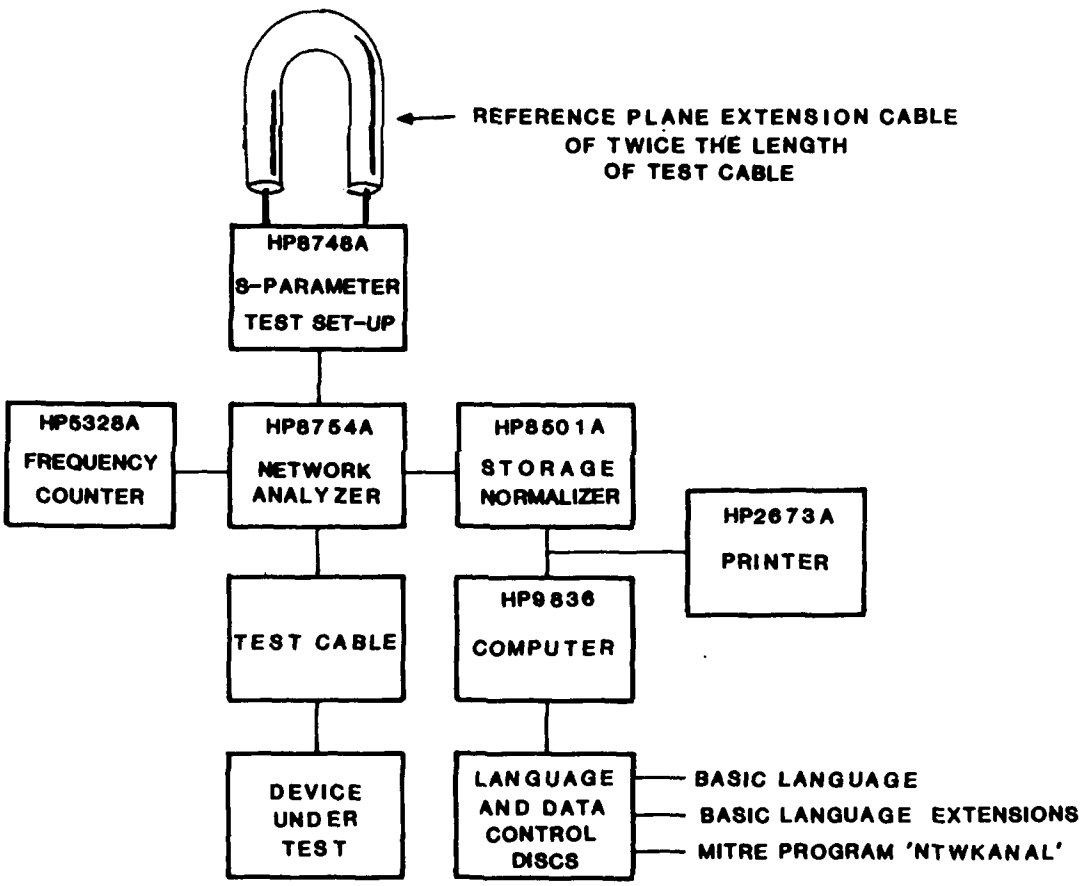

Figure 20. Input Impedance Test Set-up

Frequency (MHz) [Wavelength, λ (in.)]	Element Length*, h (in.)	Normalized Groundplane Radius, ka	Normalized Element Radius, $(b/\lambda) \times 10^{-4}$	Normalized Element Length, h/λ	Input Resistance, R_{in} (ohms)			Input Reactance*, X_{in} (ohms)		
					Predicted By Moment Method (1)	Measured By MITRE** (2)	Percentage Difference $\frac{(1)-(2)}{(1)} \times 100$	Predicted By Moment Method (3)	Measured By MITRE** (4)	Difference* (3) - (4) (ohms)
30.0 [393.43]	94.26	0.766	6.35	0.2396	17.76	17.62	0.8	-35.97	-30.92	-5.1
36.0 [327.86]	78.55	0.919	7.63	0.2396	18.35	18.57	-1.2	-25.48	-13.59	-11.9
43.0 [274.48]	65.46	1.097	9.11	0.2385	18.77	19.05	-1.5	-19.33	-16.38	-3.0
54.0 [218.57]	52.07	1.379	11.43	0.2382	19.93	20.15	-1.1	-12.11	-5.92	-6.2
62.4 [189.15]	45.00	1.593	13.21	0.2379	20.80	22.82	-9.7	-4.73	-0.48	-4.3
75.0 [157.37]	37.36	1.915	15.89	0.2374	22.95	23.23	-1.2	-0.43	1.60	-2.3
86.0 [137.24]	32.48	2.197	18.22	0.2366	25.35	27.63	-9.0	3.34	7.39	-4.1
89.7 [131.58]	31.13	2.300	19.00	0.2366	26.59	28.16	-5.9	4.99	-1.05	6.0
97.5 [121.05]	28.60	2.500	20.65	0.2363	29.41	31.22	-6.2	7.29	11.05	-3.8
117.0 [100.88]	23.76	3.000	24.78	0.2355	39.27	40.50	-3.1	8.27	15.21	-6.9
136.5 [86.47]	20.34	3.500	28.91	0.2352	45.76	46.23	-1.0	0.84	7.18	-6.3
156.0 [75.66]	17.75	4.000	33.04	0.2346	40.39	38.59	4.7	-8.16	-1.09	-7.1
175.5 [67.25]	15.77	4.500	37.17	0.2344	34.00	30.94	9.0	-7.45	-1.91	-5.5
195.0 [60.53]	14.14	5.000	41.30	0.2335	30.54	28.58	6.4	-4.36	0.51	-4.9
214.5 [55.02]	12.82	5.500	45.44	0.2330	30.33	28.28	6.8	-0.18	4.87	-5.1
234.0 [50.44]	11.74	6.000	49.56	0.2328	33.69	31.44	6.7	3.64	5.56	-1.9
253.5 [46.56]	10.87	6.500	53.69	0.2335	40.25	41.13	2.2	3.91	6.57	-2.7

* The element lengths were selected to be resonant when mounted on a groundplane of infinite extent [see R.W.P. King, Theory of Linear Antennas (Harvard University Press, 1956) fig. 30.7a]. On groundplanes of finite extent, the input reactance is expected to asymptotically approach zero as $ka \longrightarrow \infty$.

** MITRE measurements were made on 1-7-85 and 1-10-85 utilizing computerized printout of network analyzer.

Table 8. Input Impedance of 0.50 Diameter Monopole Elements on an 8 ft. Diameter Groundplane. (Comparison of moment method predictions with MITRE measurements.)

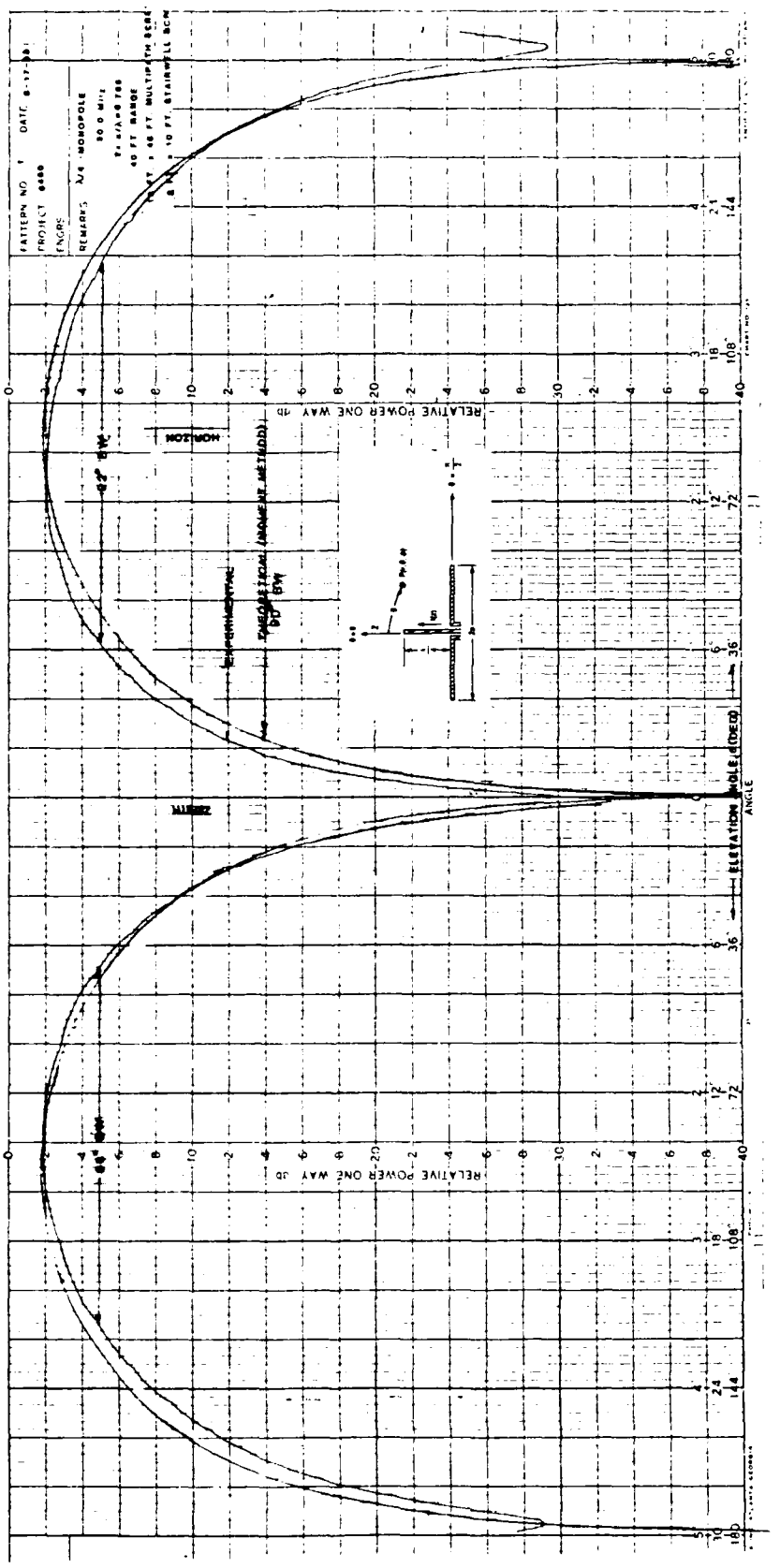

Figure 21. Measured and Theoretical Elevation Patterns, 30 MHz (h/λ =0.2396, b/λ =6.35 x 10^{-4}, ka = 0.766

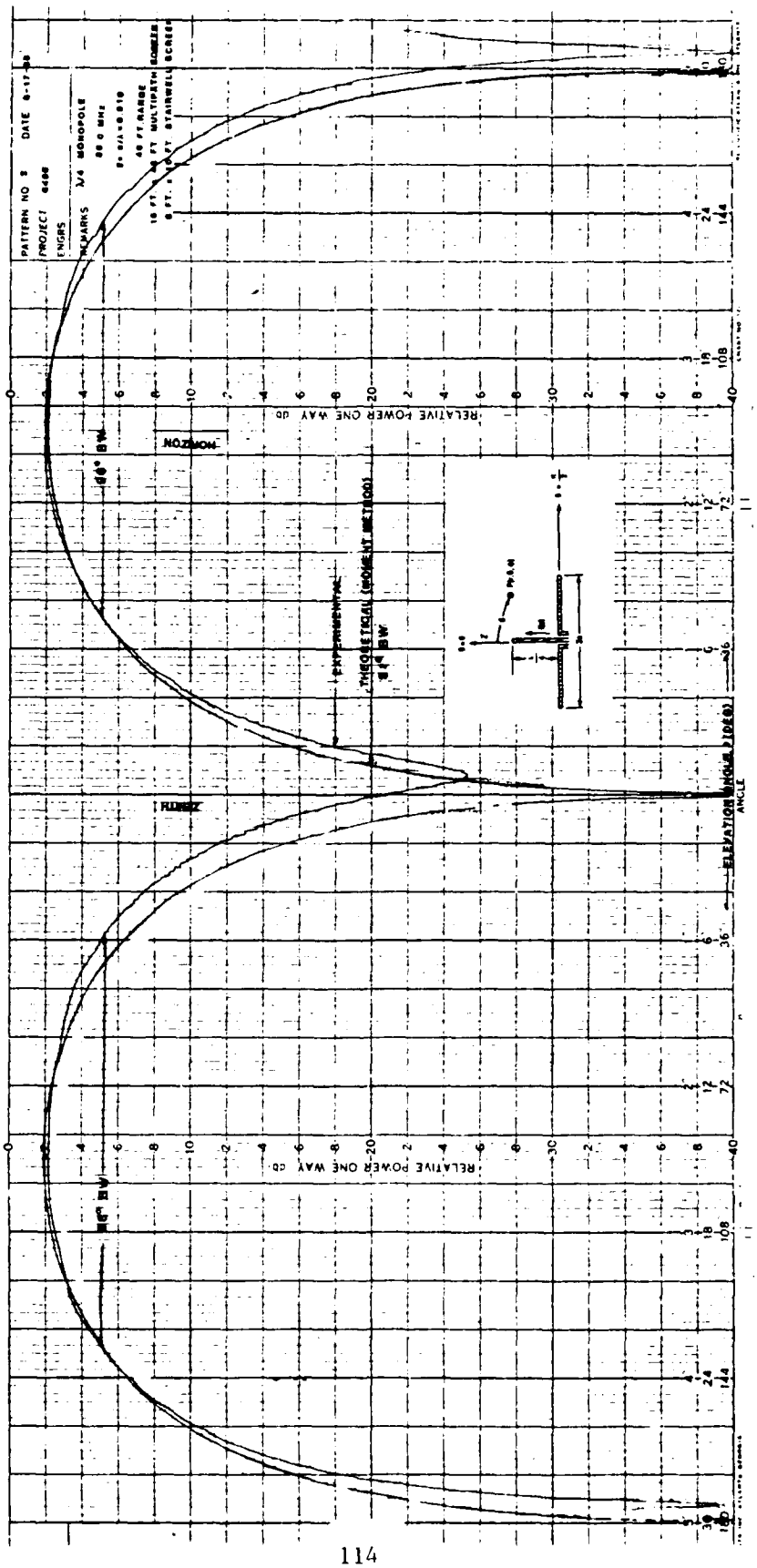

Figure 22. Measured and Theoretical Elevation Patterns, 36 MHz ($h/\lambda = 0.2396$, $b/\lambda = 7.63 \times 10^{-4}$, $ka = 0.919$)

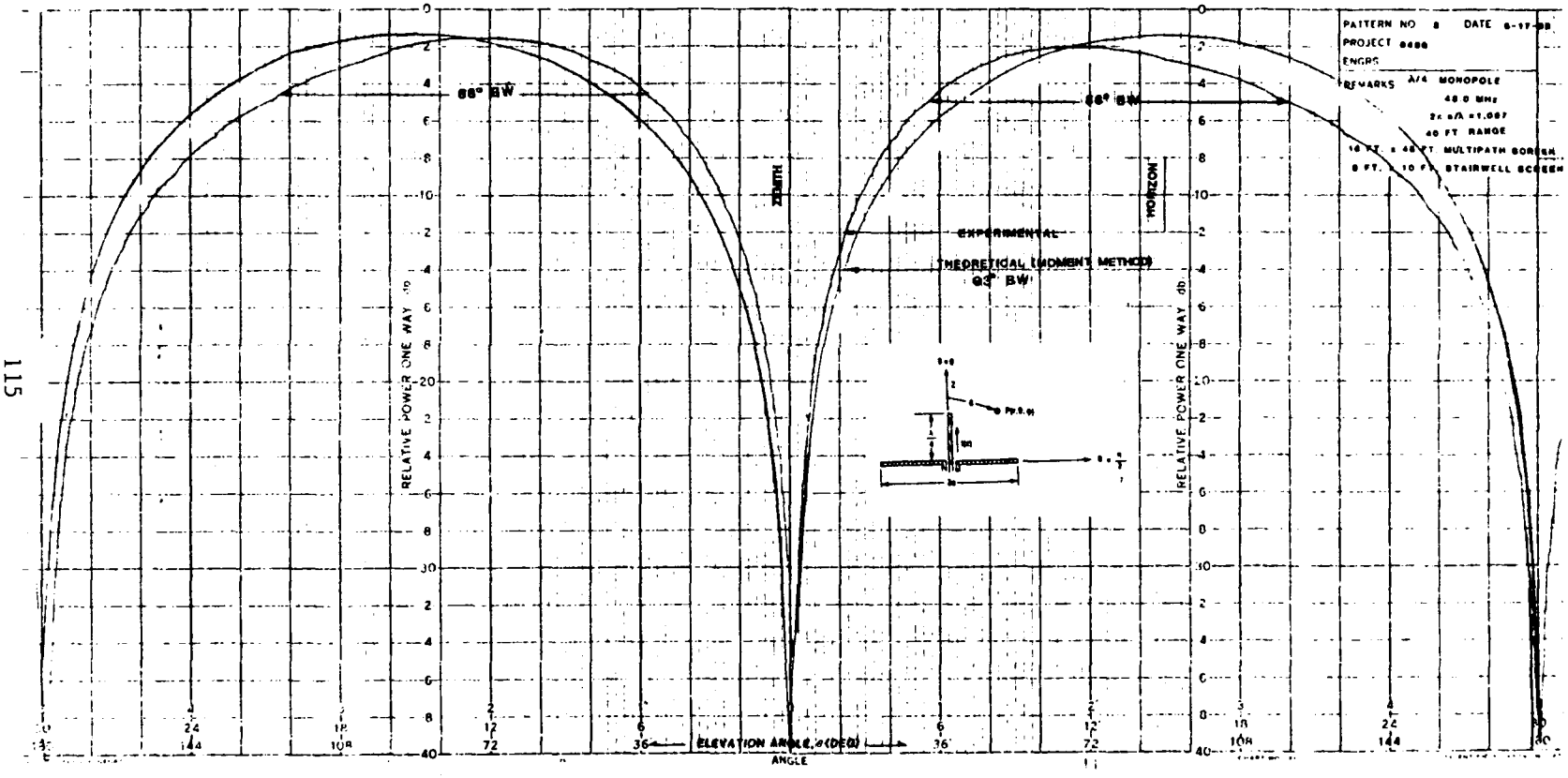

Figure 23. Measured and Theoretical Elevation Patterns, 43 MHz ($h/\lambda = 0.2385$, $b/\lambda = 9.11 \times 10^{-4}$, $ka = 1.097$)

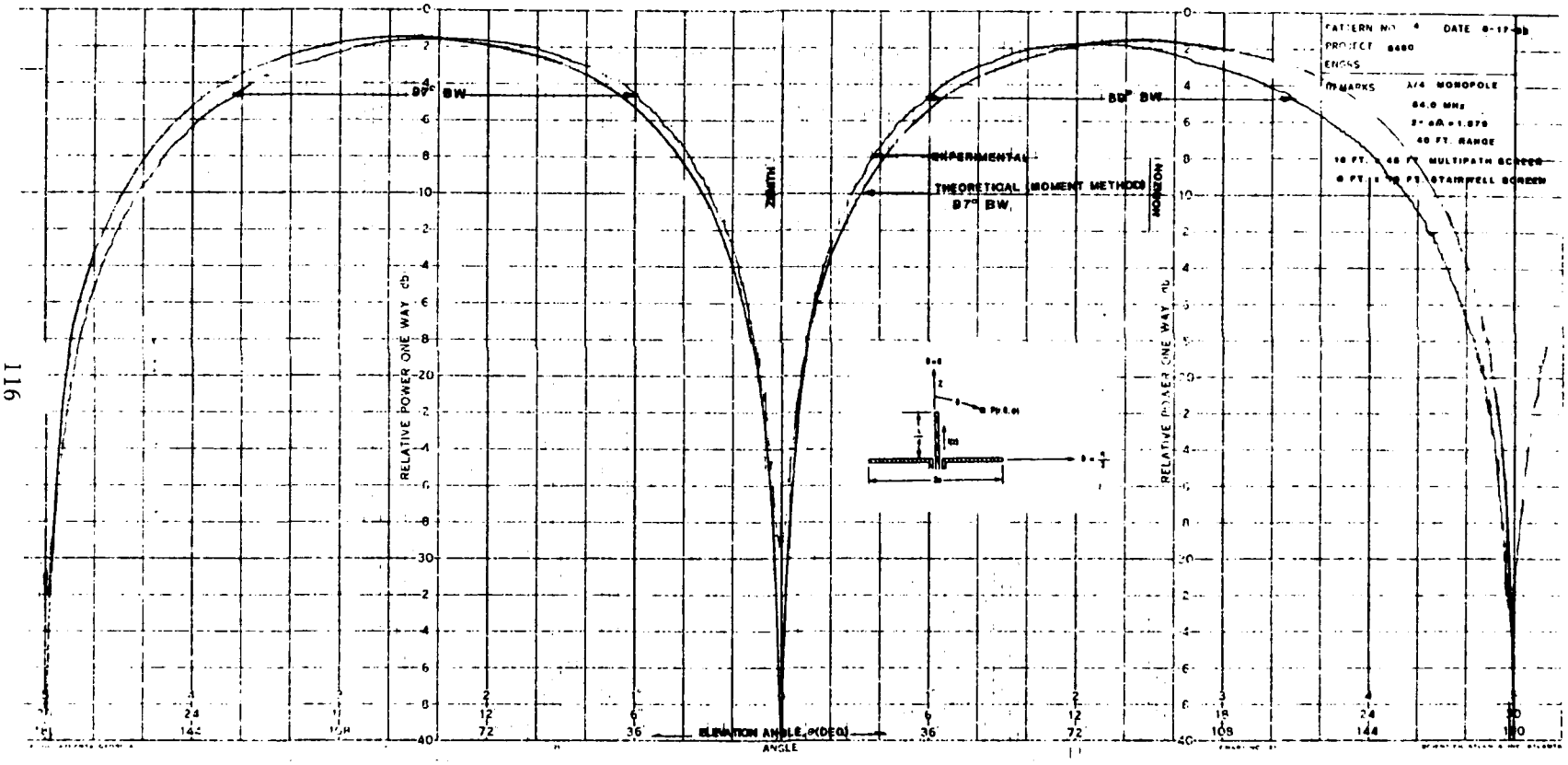

Figure 24. Measured and Theoretical Elevation Patterns, 54 MHz
(h/λ =0.2382, b/λ =11.43 x 10^{-4}, ka = 1.379)

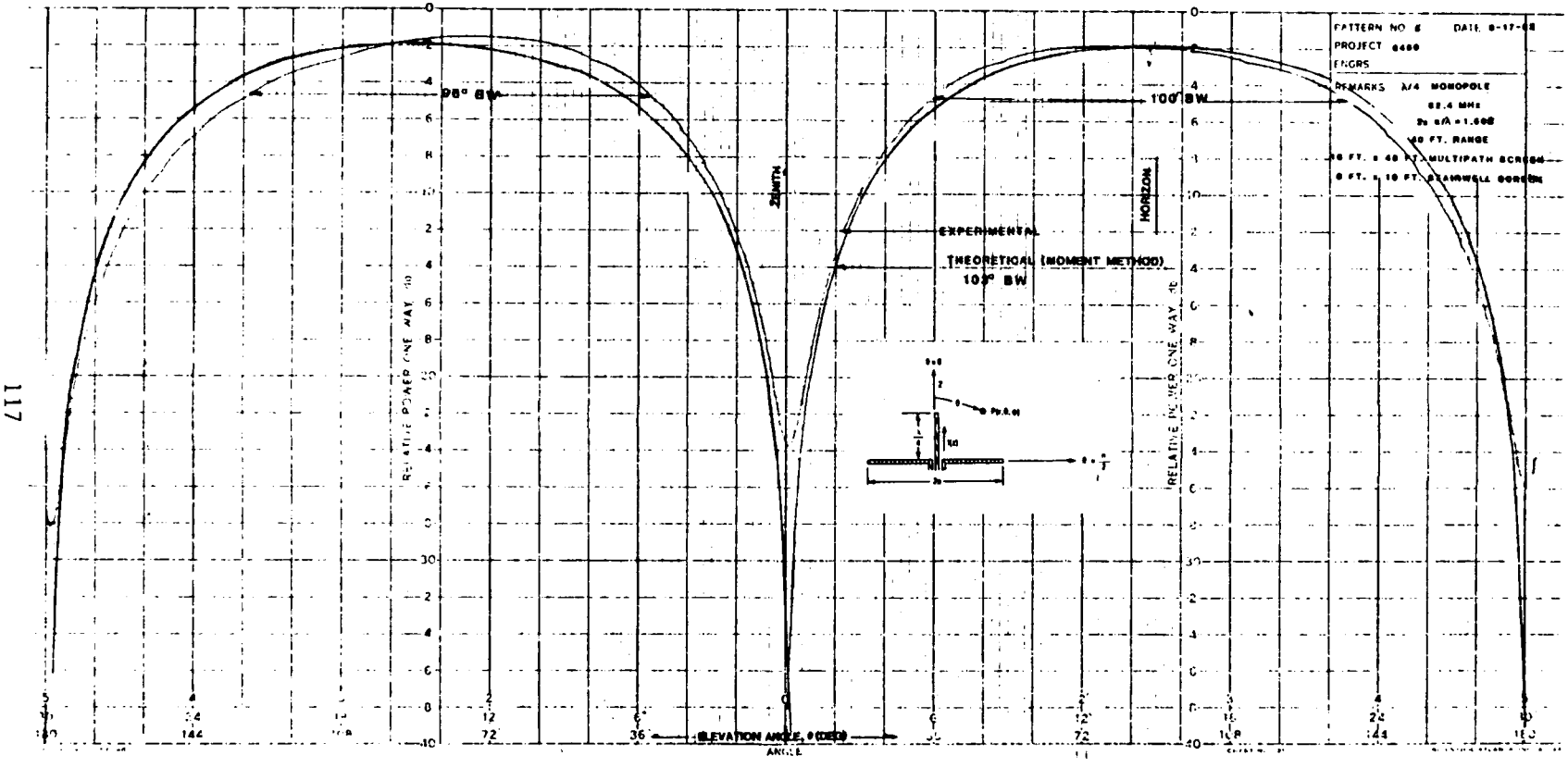

Figure 25. Measured and Theoretical Elevation Patterns, 62.4 MHz (h/λ =0.2379, b/λ =13.21 x 10^{-4}, ka = 1.593)

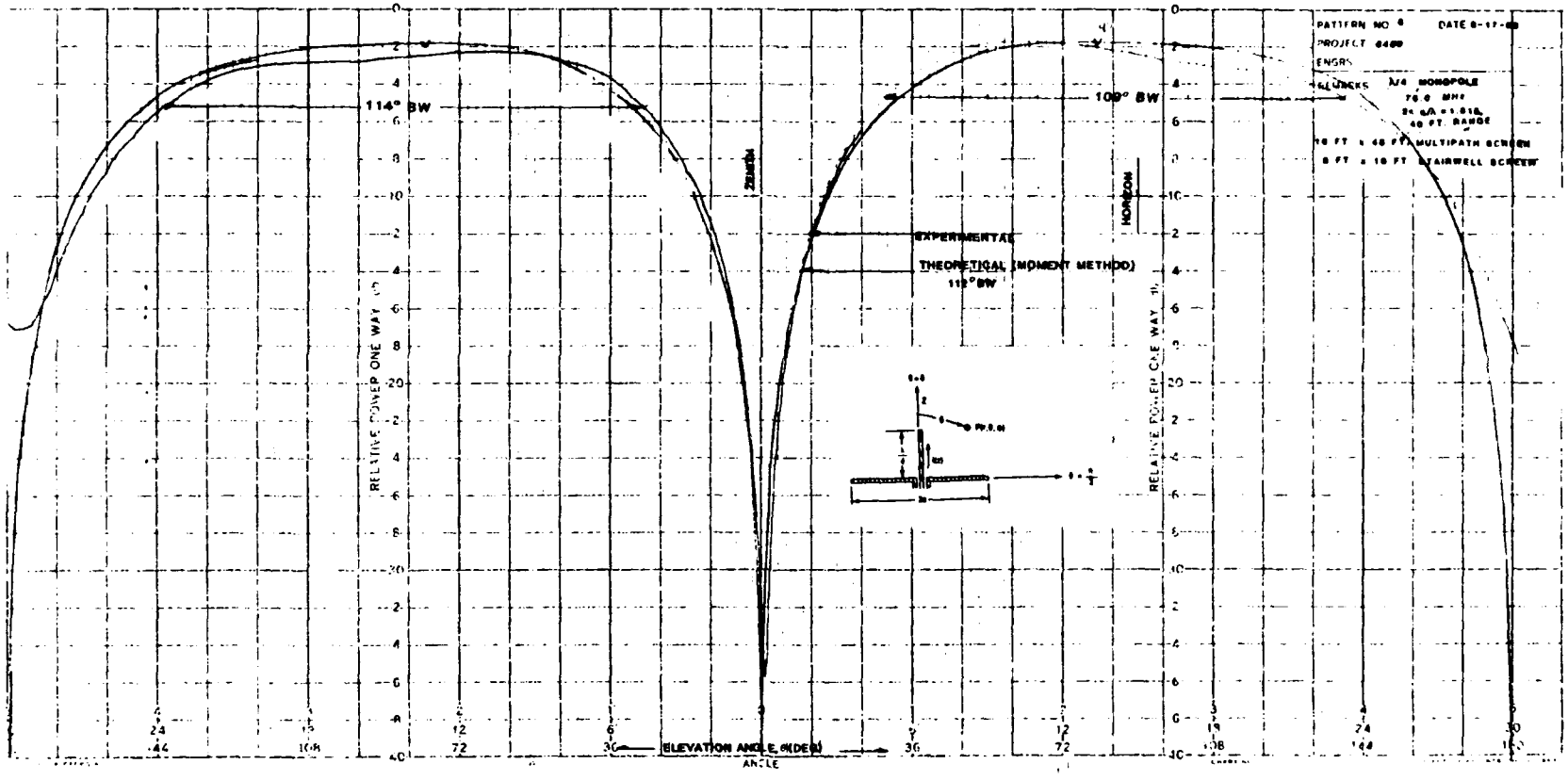

Figure 26. Measured and Theoretical Elevation Patterns, 75 MHz (h/λ =0.2374, b/λ = 15.89 x 10^{-4}, ka = 1.915)

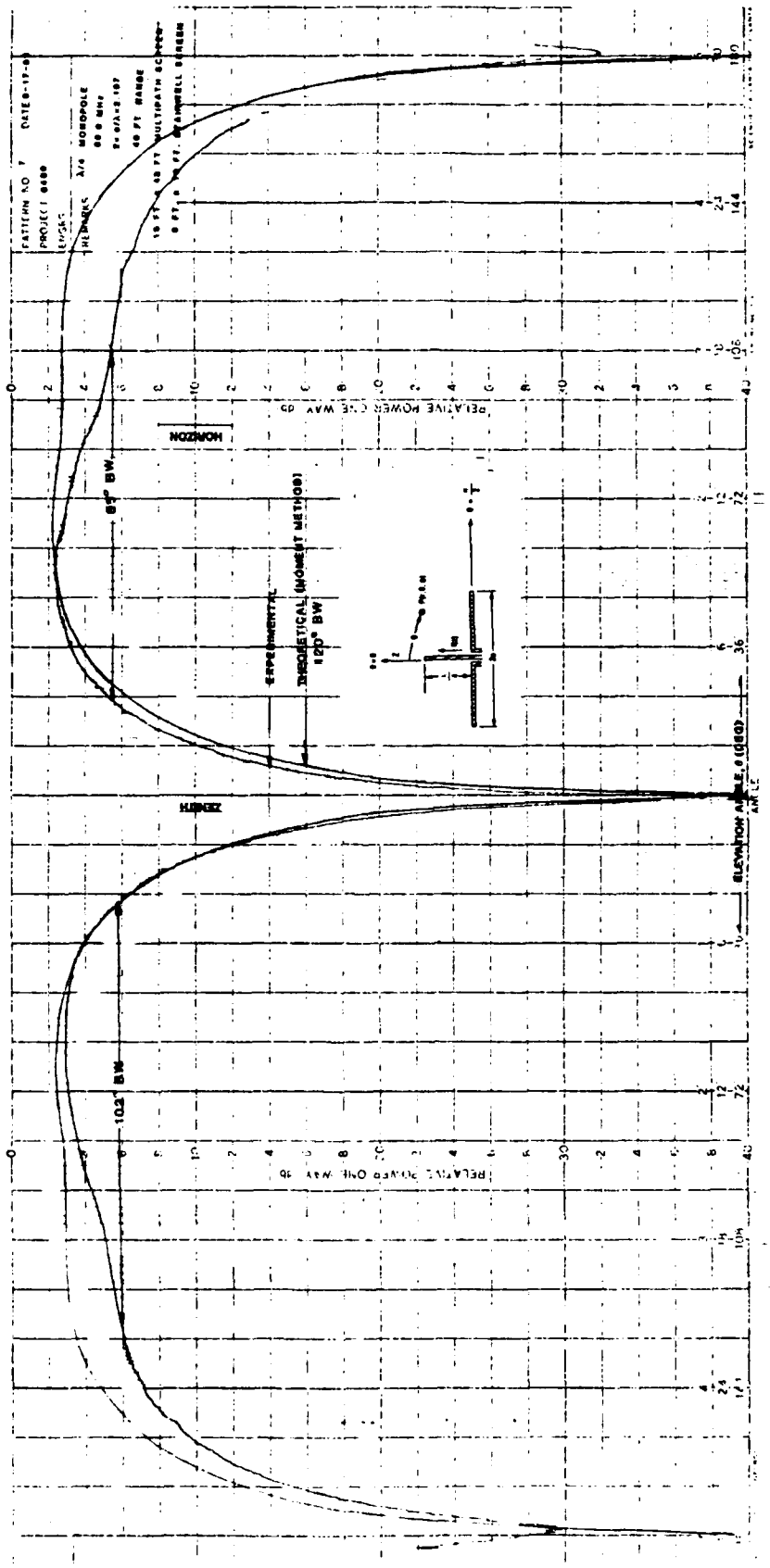

Figure 27. Measured and Theoretical Elevation Patterns, 86 MHz
($h/\lambda = 0.2366$, $b/\lambda = 18.22 \times 10^{-4}$, ka = 2.197)

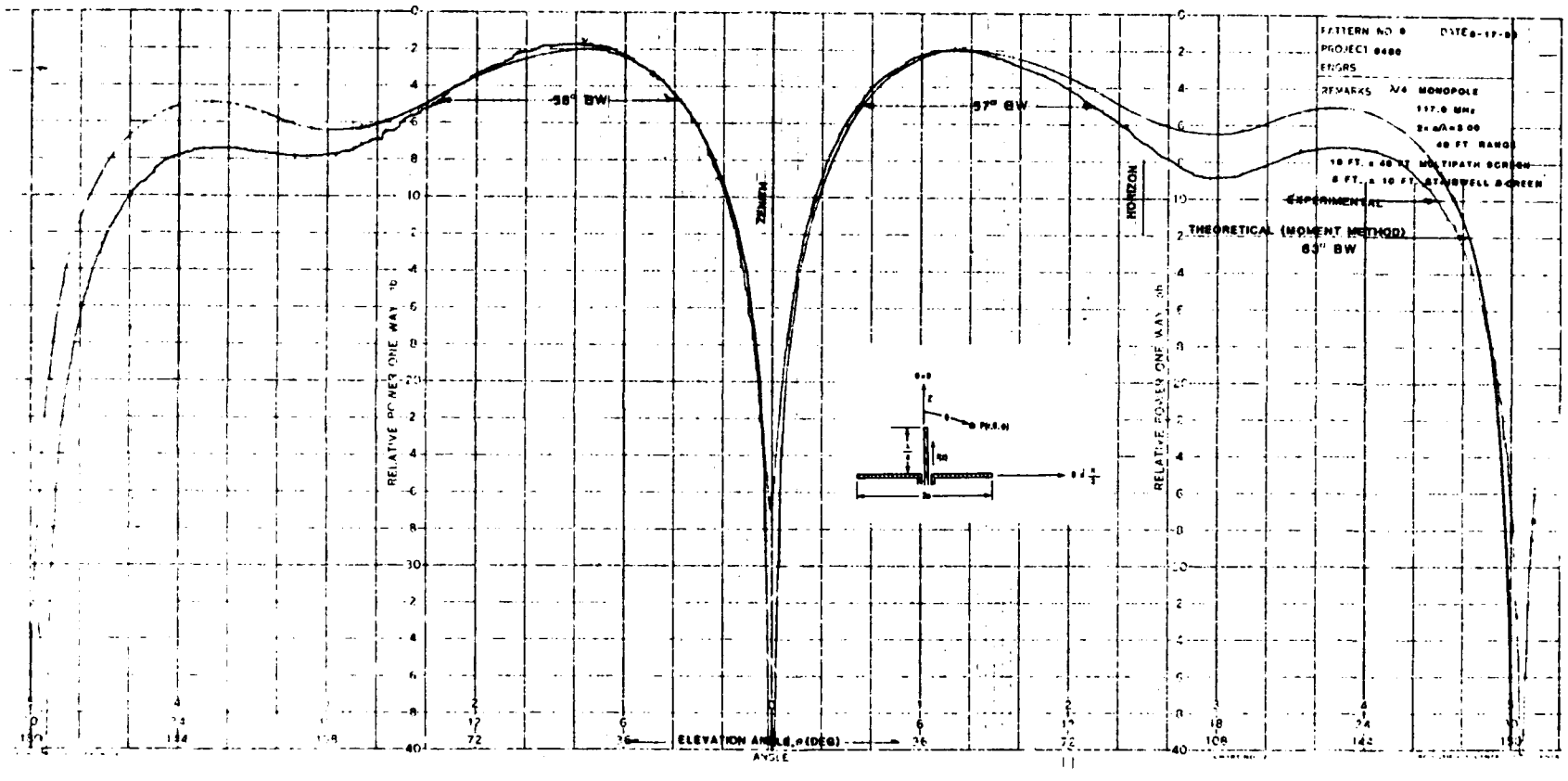

Figure 28. Measured and Theoretical Elevation Patterns, 117 MHz ($h/\lambda = 0.2355$, $b/\lambda = -24.78 \times 10^{-4}$, $ka = 3.000$)

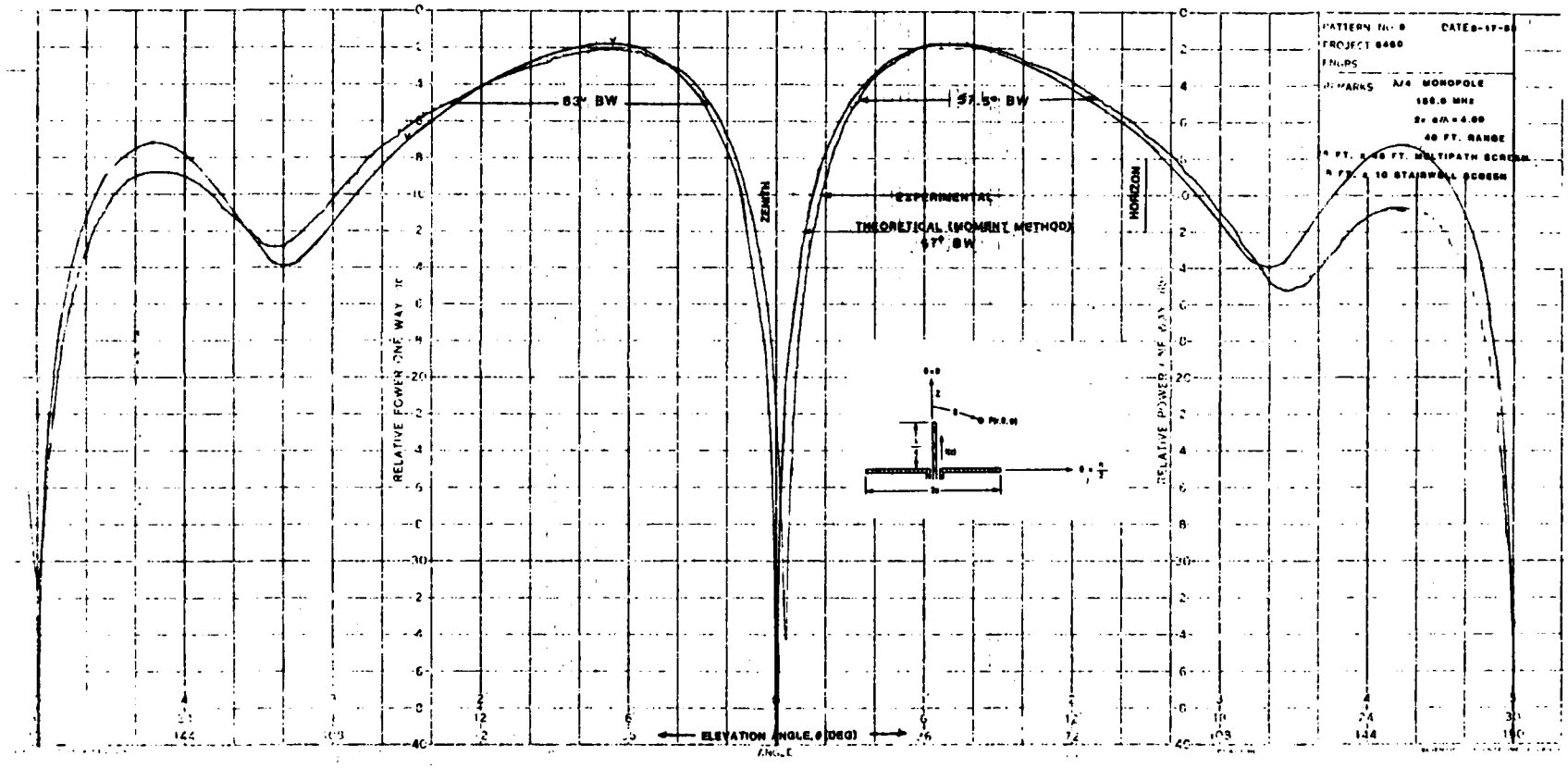

Figure 29. Measured and Theoretical Elevation Patterns, 156 MHz (h/λ =0.2346, b/λ =33.04 x 10^{-4}, ka = 4.000)

REFERENCES

1. J. Bardeen, "The Diffraction of a Circularly Symmetrical Electromagnetic Wave by a Co-axial Circular Disc of Infinite Conductivity," Physical Review, Vol. 36, pp. 1482-1488, November 1930.

2. J.H. Richmond, "Monopole Antenna on Circular Disk," Technical Report 711639-1, Electro Science Laboratory, Ohio State University, July 1979. See also IEEE Transactions on Antennas and Propagation, Vol. AP-32, No. 12, pp. 1282-1287, December 1984.

3. A. Leitner and R.D. Spence, "The Oblate Spheroidal Wave Functions," Franklin Institute Journal, Vol. 249, No. 4, pp. 299-321, April 1950.

4. A. Leitner, "Effect of a Circular Groundplane on Antenna Radiation," Mathematics Research Group, Research Report No. EM-19, New York University, Washington Square College, April 1950.

5. A. Leitner and R.D. Spence, "Effect of a Circular Groundplane on Antenna Radiation," Journal of Applied Physics, Vol. 21, pp. 1001-1006, October 1950.

6. C.L. Tang, "On the Radiation Pattern of a Base-Driven Antenna Over a Circular Conducting Screen," Technical Report No. 301, Cruft Laboratory, Harvard University, May 1959.

7. J.E. Storer, "The Impedance of an Antenna Over a Large Circular Screen," Journal of Applied Physics, Vol. 22, pp. 1058-1066, August 1951. See also Technical Report No. 119, Cruft Laboratory, Harvard Unviersity, November 1950.

8. J.E. Storer, "The Radiation Pattern of an Antenna Over a Circular Ground Screen," Technical Report No. 126, Cruft Laboratory, Harvard University, June 1951.

9. K.H. Awadalla and T.S.M. Maclean, "Input Impedance of a Monopole Antenna at the Center of a Finite Groundplane," IEEE Transactions on Antennas and Propagation, Vol. AP-26, No. 2, pp. 244-248, March 1978.

10. K.H. Awadalla and T.S.M. Maclean, "Monopole Antenna at the Center of a Circular Groundplane: Input Impedance and Radiation Pattern," IEEE Transactions on Antennas and Propagation, Vol. AP-27, No. 2, pp. 151-153, March 1979.

11. G.A. Thiele and T.H. Newhouse, "A Hybrid Technique for Combining Moment Methods with the Geometrical Theory of Diffraction," IEEE Transactions on Antennas and Propagation, Vol. AP-23, No. 1, pp. 62-69, January 1975. In a telephone conversation with M. Weiner on July 28, 1983, G. Thiele reported that his computer program for a monopole on a circular groundplane, which he wrote while at Ohio State, was lost in moving to the University of Dayton.

12. R.F. Harrington, Time-Harmonic Electromagnetic Fields, New York: McGraw-Hill, 1961, pp. 106-112. Please note that the signs of the radial field E_ρ on p. 111 and the magnetic frill M_ϕ on p. 112 differ from those in Eq. (2.4-9) and (2.4-8), respectively, because in Reference [12] the voltage at the outer conductor is positive with respect to that at the inner conductor.

13. R.W.P. King, The Theory of Linear Antennas, Cambridge, MA: Harvard University Press, 1956, p. 87.

14. R.S. Elliot, Antenna Theory and Design, Englewood Cliffs, New Jersey: Prentice-Hall, 1981, pp. 290-291.

15. C.A. Balanis, Antenna Theory: Analysis and Design, New York: Harper and Row, 1982, p. 315.

16. Op. cit. 15., p. 101, Eq. (4-2).

17. L. Brillouin, "Origin of Radiation Resistance," Radioelectricitè, Vol. 3, pp. 147-152, 1922.

18. J.A. Stratton, Electromagnetic Theory, New York: McGraw-Hill, 1941, pp. 454-457.

19. M. Abramowitz and I.A. Stegun, Handbook of Mathematical Functions, New York: Dover Publications, 1972, pp. 231 and 244.

20. Op. cit. 15, p. 292.

21. W. Magnus and F. Oberhettigner, Formulas and Theorems for the Functions of Mathematical Physics, New York: Chelsea Publishing Co., 1954, p. 34.

22. I.S. Gradshteyn and I.M. Ryzhik, Table of Integrals, Series and Products, New York: Academic Press, 1965.

23. J.B. Thomas, An Introduction to Statistical Communication Theory, New York: John Wiley & Sons, Inc., 1969, Appendix B: The Dirac Delta Function.

24. Op. cit. 19, p. 763.

25. Op. cit. 15, pp. 118-126, 133-135, 285-295.

26. Op. cit. 14, p. 29.

27. Op. cit. 15, pp. 502-522, 529-531.

28. W.J. Stutzman and G.A. Thiele, Antenna Theory and Design, New York: John Wiley & Sons, 1981, pp. 489-495, 500-507.